Università degli Studi di Padova

DEPARTMENT OF INFORMATION ENGINEERING
Telecommunication Engineering

Master Thesis

Statistical Analysis of Differential Group Delay in Few-Mode Spun Optical Fibers

Supervisor
Prof. Luca Palmieri

Master Candidate
Gianluca Guerra
Matricola 1106059

Academic Year 2015/2016

Abstract

This thesis proposes a statistical analysis of the differential group delay in few-mode spun optical fibers. In particular, the numerical analysis is performed by an accurate modeling of the propagation and coupling in a few-mode optical fiber, supporting the first 4 LP groups, perturbed by stress birefringence and core ellipticity, and spun using a sinusoidal spin profile. The results show that the spinning process may reduce the overall differential group delay under specific values of modal birefringence and spin amplitude, nevertheless it changes also the underling probability distribution. Finally, the statistical properties of the differential group delay are compared to the ones of the root mean square modal dispersion. The result shows that they are very similar, therefore the latter may be simpler to use in order to find an analytical solution of the problem.

Contents

Chapter 1

Introduction

The development of single mode optical fibers in the last decades has boosted optical communications to the point that nowadays they underpin the whole Internet backbone. In particular, the capacity improvement has always met the traffic demand, thanks to the implementation of multiplexing techniques and advanced modulation schemes. However, the capacity of single mode optical fibers is limited by nonlinear effects, and the exponential traffic grow expected for the next years, could be unmanageable by the current systems. In this sense, space-division multiplexing (SDM) over multimode fibers could be the key to meet the incoming traffic demand. In particular, SDM systems can be implemented using strong-coupled fibers and thus effective techniques to induce coupling among modes must be developed. The analogy of the problem with the polarization mode dispersion (PMD) in the single mode fiber suggests that spun fibers can be used in this sense.

1.1 Historical Background

Optical signals have always been used for communication, indeed their use dates well before the coming of electric media due to light being partially visible to human beings. The first news about the use of light for free space communication mixes with myths and goes back to the Trojan war, where the information about Troy's fall arrived in Greece from the Aegean islands through a fire pit chain.

Actually, we have to wait until the end of XVIII century to find a more complex system, the semaphore telegraph. It was developed by Claude Chappe and used at first for military communication in France during the Napoleonic era and then in the American Civil War. Semaphore lines were the precursors of electrical telegraphs, where the information were encoded by the position of mechanical elements placed on top of towers and read by the next ones. The main problem of this kind of systems is attenuation, the light propagation in free space is indeed strongly affected by weather. Rain and fog can increase the attenuation up to more than 0.2 dB/m making communication unfeasible. This is one of the reason for which optical telegraphs never were massively used and were quickly substituted by the electrical ones in few years.

A low loss medium with respect to optical waves is required to allow reliable optical communication, but first a question arise: is it actually possible to guide

light? The answer dates back to the mid-nineteenth century from experiments performed by Colladon in Geneva. In particular, he observed that light could get trapped in a flowing water jet. This was one of the first observations of the *total internal reflection*, where the discontinuity surface between water and air behaves like a mirror since the former medium is denser than the latter.

Once the principle to guide light was known, there was still the problem of the attenuation. Even if the idea to use transparent materials as silica glass (SiO_2) was widely known, the question had remained unsolved until the studies of *Charles K. Kao* in 1966. In the Standard Telecommunications Labs of the United Kingdom, Kao showed that the glass produced in the $60s$ was highly impure yielding attenuations in the order of dB/m. However, the intrinsic attenuation of pure glass could have been orders of magnitude lower, close to 20 dB/km. Finally, Kao provided a fiber design idea that still used nowadays.

At the time there was great interest in Kao's work, the opportunity to deal with high frequency optical waves would have secure high bandwidth transmission. For this reason a lot of companies tried to realized what had been suggested by Kao, amongst these the Corning Glass was the first to produce the step index optical fiber. The company had0 already focused in special glass manufacturing and was the quickest to develop a reliable production technique. In particular the process, that is still use today, was based on *chemical vapor decomposition* (CVD). Thanks to this method the obtained preforms are by far more purer than the used reagents. This resulted in an optical fiber made by very pure silica with an attenuation of about 17 db/km, much lower than the best coaxial cables in the market.

The further development of optical sources as led and laser and the refinement of fiber production allowed the installation of the firsts optical links. At the beginning, the transmission focused on the I window ($\sim$ 850 nm) yielding an attenuation of about 4 dB/km, but with the improvement of both fibers and sources it switched to more interesting regions, as the II window ($\sim$ 1330 nm) and the III window ($\sim$ 1550nm), where the attenuation drops to 0.2 dB/km.

Although the attenuation in correspondence of the working wavelengths is the lowest possible according to the optical properties of pure silica, optical systems are still affected by losses that need to be compensated using amplifiers. In this sense the early systems were highly inefficient due the use of electrical amplifiers that required optical-electro-optical conversions, moreover the amplifiers constrained the whole system to use fixed modulation and bit rate. The solution to these drawbacks has been the development of optical amplifiers, these have the advantage to make amplification on photon level, regardless modulation and bit rate. In particular, the most popular are the *Erbium Doped Fiber Amplifiers* (EDFA) that uses fibers doped with erbium to exploit the population inversion amplification through a 3-level pumping system.

It is important to note that without this kind of amplifiers long range optical links would not have been possible and telecommunication would be very different from how they are now. At the beginning of 2008 more than one billion kilometers of optical fiber has been placed, and in the later six years this number has doubled exceeding two billions, the equivalent of more than one times the Sun-Jupiter round trip distance, moreover optical links have been brought closer to the users by means of FFTB (*Fiber To The Building*) and FTTH (*Fiber To The Home*) projects. Also many efforts have been done in order to maximize the bit rate, exploiting all the useful bandwidth and reaching the actual single

mode fiber capacity.

Today, optical telecommunication systems constitute the Internet backbone, allowing the global, ubiquitous and persistent network that we know. Despite this, the trend forecast for the next years shows that there will be a tremendous growth in terms of data produced by mobile, IoT devices, video streaming applications etc., that could saturate all the available single mode fiber bandwidth. This grim scenario has spurred to look for possible alternative solutions, one of the most promising involves *spatial division multiplexing* (SDM) in few-mode optical fibers.

1.2 The Capacity Crunch

The development of systems able to handle high bit-rates in term of traffic are fundamentals from a telecommunication point of view. In this sense, the Shannon's theorem presented in 1948 states that a communication, in order to be reliable, must transmit with a bit-rate lower than the capacity of the used channel. Given this result, many efforts have been put in order to develop channels with higher and higher capacity. Indeed, this concept is closely related to the notion of mutual information. Anyway, for channels with linear additive noise, it can be written as [MS01]

$$C = B \log_2(1 + \Gamma), \tag{1.1}$$

where the capacity C scales linearly with the transmission bandwidth B and logarithmically with respect to the signal-to-noise ratio (SNR) Γ.

In the past, transmission over single mode optical fibers have managed to meet the global demand in term of capacity. However, it may not be sufficient due to the exponential grow in term of traffic expected in the next years, that is going to hang over the single mode paradigm.

Up to now, multiplexing over all possible single mode fiber degrees of freedom have been implemented, namely time-division multiplexing (TDM), polarization multiplexing (PolMUX) and wavelength-division multiplexing (WDM). In particular, the last has allowed to increase the capacity of two orders of magnitude [Gui+14] by exploiting a considerable portion of the transmission bandwidth. Indeed, it would be impractical to modulate all the available optical bandwidth at once, due to electronics limitations. Then, in order to achieve the maximum capacity, the whole spectrum is split as disjoint channels modulated separately. Theoretically speaking, silica limits the bandwidth suitable for communication to a maximum of 50 THz [MS01]. However, even if today the bandwidth can be further increased beyond the C and L windows, the improvement would be lower than one order of magnitude and the lack of commercial amplifiers working at those frequencies make this choice unattractive [Gui+14].

Once the bandwidth has been maximized, a further way to increase the capacity is to improve the spectral efficiency of the transmission, that is the bit-rate per unit of bandwidth. In this sense, concepts from radio frequency communication have been adopted. In particular, coherent detection, advanced modulation techniques and digital signal processing have boosted the spectral efficiency and allowed polarization multiplexing [Gui+14].

Owing to these improvements, today's commercial systems transmit up to 10 Tb/s at 100 Gb/s per WDM channels [Win12]. Nevertheless, the only way

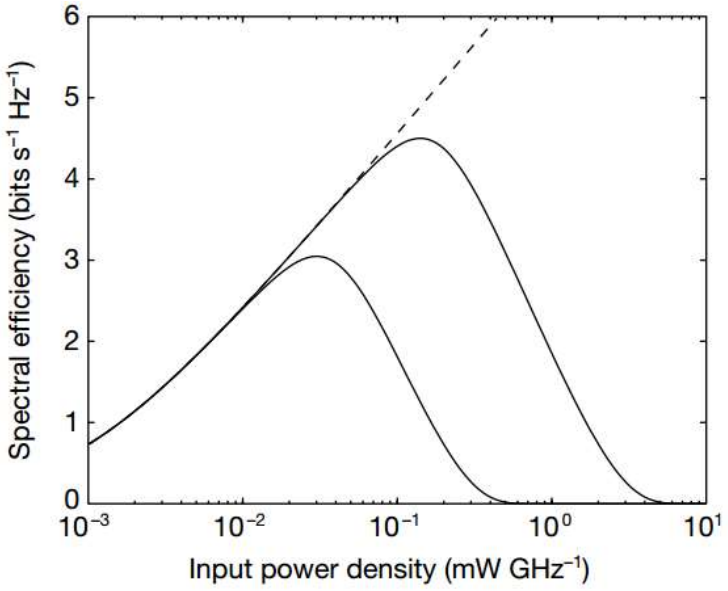

Figure 1.1: Spectral efficiencies curves for channels with multiplicative noise (solid lines) and additive noise (dashed one) [MS01].

to further improve the capacity in single mode fibers seems the one to increase the signal power. However, this choice is not viable because it would enhance nonlinear effects in the medium. Indeed, expression (1.1) holds when the noise is additive but this happens only if the transmission occurs under the so-called low power regime of the fiber. In particular, [MS01] shown how non linear effects impose a saturation and a decline of the spectral efficiency with respect to the increasing of the signal power. Indeed, the real qualitative picture represented with solid lines in Figure 1.1 are quite different to the ideal case of additive noise (dashed one) for high input powers. In particular, this behavior is caused by a non linear cross-phase modulation term due to other WDM channel transmissions that origin in a non additive but multiplicative noise.

Because of this limit, to avoid the so-called capacity crunch, space-division multiplexing by means of multimode/multicore fibers has attracted much attention in the past five years.

1.3 Space-Division Multiplexing

Space-division multiplexing uses the multiplicity of space channels to increase capacity in optical communication [Gui+14]. In particular, it can be implemented by using multimode (or few-mode) fibers or multicore fibers. During the transmission, both of them are affected by coupling caused by perturbations acting along the fiber that break its symmetry inducing interactions among different propagating modes. In particular, multimode fibers are the ones in which

different modes propagate in the very same core, inducing coupling among all of them. In the special case, where only few modes propagate then it is called few-mode fiber. Instead, multicore fibers may be less affected by coupling since the modes are split in many cores. However in this case, it has to be considered a further type of coupling, that occurs among different cores. Moreover, even if a limited number of cores can be inserted in a single fiber, the great advantage of this solution is that the matrix representing the propagation can be considered sparse.

Given this scenario, the propagation both for multimode and multicore fibers can occur in two regimes: the low-coupling regime and the strong-coupling one. Between the two, the first is surely more intuitively to understand. Indeed because of coupling, each spacial channel is affected by the information transmitted in the other ones, this effect clearly leads to a decreasing of the signal-to-noise ratio. In this sense, advanced modulation formats as QPSK or 64-QAM require a minimum SNR level to be implemented, that can be achieved by using special fibers designed to mitigate the effect of perturbations, with an accurate design of the index profile. Indeed, the demodulation of the signal must exploit the orthonormality of the propagating modes in order to achieve spacial multiplexing. Propagation in waveguides able to keep the orthonormal property occurs in the so-called low-coupling regime [Win12]. If the coupling rises to levels where the transmission become infeasible, multiple-input multiple-output (MIMO) techniques can be used in order to counteract the effect of the perturbations and retrieve the original information.

In the majority of cases, orthogonality of modes can be maintained for a very short distance. In this case we talk about strong-coupling regime and MIMO digital signal processing becomes fundamental in order to achieve spacial-division multiplexing. In particular, MIMO equalization techniques can be implemented in two fashions. The first is based on time domain equalization, where fiber is seen as a linear channel. Therefore, the input-output relation can be represented as

$$y(t) = T(t) * x(t), \tag{1.2}$$

where $x(t)$ and $y(t)$ represent the input and output signals respectively and $T(t)$ is the transmission channel matrix. To retrieve the original signal, the MIMO equalizer must invert matrix $T(t)$ that is time dependent, since the perturbations along the fiber can be modeled as a random process. In particular, the inversion of the matrix is achieved using a set of FIR filters adapted by using the least-square method (LMS). It can be shown [Gui+14] that the complexity of this system, neglecting the chromatic dispersion compensation, is proportional to

$$C_{\mathrm{T}} = N(R_s + 1)\Delta\tau LB, \tag{1.3}$$

where N is the number of propagating modes, R_s is the sampling rate, $\Delta\tau$ is the *differential group delay* (DGD), L is the length of the fiber and B is the symbol rate of the transmission.

The second solution is the one to exploit MIMO equalization in the frequency domain. In particular, this approach results to be more efficient, since it exploits multiplications instead of convolutions by means of (inverse) fast Fourier transforms in the MIMO system. As a matter of fact, this type of equalization results in a much lower complexity. Specifically, it can be expressed as

$$C_{\mathrm{F}} = (4 + 2N)\log_2(R_s\Delta\tau LB) + 4N. \tag{1.4}$$

From a strictly optical point of view, the complexity expressions in (1.3) and (1.4) depend on the differential group delay $\Delta\tau$. That is the maximum spread among propagating group delays. Thus, it is critical to design optical fibers with proper modal dispersion properties. In this sense, the most promising solutions are:

- Design fibers with small DGD by using an accurate index profile, e.g., graded index fibers.
- DGD compensation by introducing sections of special fiber with negative dispersion properties. This solution is very similar to the the well known chromatic dispersion compensation.
- Using multicore fibers, that have also the advantage to make the transmission matrix $T(t)$ sparse.
- Using strongly coupled multimode fibers.

Indeed, the last solution is quite counterintuitive, since it is exactly the coupling among modes to make the MIMO equalization necessary. Nevertheless, this approach is one of the most promising and can reduce significantly the dispersion. The basic idea under this type of solution is that each independent data stream has equal probability to travel on the fast or slow modes, making each stream to have a similar amount of delay [Gui+14]. Moreover, this solution can be jointly implemented with the use of graded index fibers, ensuring even lower DGD values.

Actually, efficient methods to introduce coupling must be envisaged. In particular, offset splicing and grating couplers can be used but with the introduction of excess losses, that would make the transmission infeasible. In this sense, there is an open question if the process of spinning the fiber during the drawing, used in single mode transmission to mitigate the polarization mode dispersion, could help to increase the coupling among modes. The following work presents the overall theory that underpins propagation in multimode fibers, and proposes a numerical analysis in order to discover whether the spin can be effective in reducing the fiber differential group delay.

Chapter 2

Modal Theory in Ideal Optical Fibers

The electromagnetic field that propagates in an optical fiber strongly depends on the structure of the medium. However, in the most general case it can be written as a linear combination of particular solutions of the Maxwell's equations. These solutions are called modes of the waveguide and, at least for the classical fibers, two groups of them can be distinguished, namely they are guided and the irradiated modes. Amongst the two groups, the guided modes are by far the most important since they propagate in the core along the longitudinal direction carrying active power to the receiver. Conversely, irradiates modes are much less important from a telecommunications point of view since they are particular solutions that irradiate the cladding. Thus in this chapter only guided modes are taken into account. Moreover, the theory will be investigated referring to isotropic step index fibers with ideal cylindrical symmetry, keeping for the next chapter the more intricate case in which perturbations occur.

Even if the analysis has been restricted to guided modes in ideal optical fibers, the strictly solution of the Maxwell's equations is still cumbersome. Indeed, it includes four types of *hybrid modes*, that are $\mathrm{TE}_{0,p}$, $\mathrm{TM}_{0,p}$, $\mathrm{HE}_{m,p}$ and $\mathrm{EH}_{m,p}$. Nevertheless, under the assumption of *weakly guiding fiber*, i.e., $n_{\mathrm{co}} \simeq n_{\mathrm{cl}}$, an approximated theory can be carried out using *linearly polarized* $\mathrm{LP}_{n,m}$ "modes". Although the solutions are not exact, the approximation is very good and LP modes can be used to describe propagation in optical fibers. Finally, further considerations on the difference between hybrid and linearly polarized modes will be presented at the end of this chapter.

2.1 Linearly Polarized Modes

Considering an ideal optical fiber of core radius a and a reference cylindrical frame oriented with the $\hat{\boldsymbol{z}}$ axis along its longitudinal direction. The LP modes will be derived using an approximated solution of the Maxwell's equations [Pal15b]. In particular we are looking for guided modes, that are propagating solutions along the longitudinal axis of the fiber. In these settings, the

wave can be written as

$$\boldsymbol{E}(x,y,z) = \left(\boldsymbol{\mathcal{E}}_t(x,y) + \mathcal{E}_z(x,y)\hat{\boldsymbol{z}}\right) e^{-j\beta z}, \tag{2.1}$$

$$\boldsymbol{H}(x,y,z) = \left(\boldsymbol{\mathcal{H}}_t(x,y) + \mathcal{H}_z(x,y)\hat{\boldsymbol{z}}\right) e^{-j\beta z}, \tag{2.2}$$

where β is the propagation constant, subscript $_t$ indicates the transversal components of the field and $_z$ the longitudinal one. Note that, at least for the moment, Cartesian coordinates have been used. Moreover, the Maxwell's equations for the particular problem (no free charges or surface currents) yields

$$\begin{cases} \nabla \times \boldsymbol{E} = -j\omega\mu_0 \boldsymbol{H} \\ \nabla \times \boldsymbol{H} = j\omega\epsilon \boldsymbol{E} \end{cases}, \tag{2.3}$$

$$\begin{cases} \nabla \cdot \boldsymbol{E} = 0 \\ \nabla \cdot \boldsymbol{H} = 0 \end{cases}. \tag{2.4}$$

Inserting the desired forms of the fields (2.1)-(2.2) in the equations (2.3)-(2.4) and splitting the longitudinal from the transversal components lays the set of equations

$$\nabla^2 \boldsymbol{\mathcal{E}}_t - \left(\beta^2 - k^2\right)\boldsymbol{\mathcal{E}}_t = 0, \tag{2.5}$$

$$j\beta\mathcal{E}_z = \nabla \cdot \boldsymbol{\mathcal{E}}_t, \tag{2.6}$$

$$j\omega\mu_0 \boldsymbol{\mathcal{H}}_t = \hat{\boldsymbol{z}} \times \left(\nabla\mathcal{E}_z + j\beta\boldsymbol{\mathcal{E}}_t\right), \tag{2.7}$$

$$j\beta\mathcal{H}_z = \nabla \cdot \boldsymbol{\mathcal{H}}_t, \tag{2.8}$$

where k is the phase constant, either for the core ($k_{\text{co}}^2 = \omega^2\mu_0\epsilon_{\text{co}}$) or the cladding ($k_{\text{cl}}^2 = \omega^2\mu_0\epsilon_{\text{cl}}$). Looking at the set of equations (2.5)-(2.6)-(2.7)-(2.8) it is evident that once the solution of (2.5) is found the other unknowns are trivially extracted from the other three equations. In particular, equation (2.5) is called *Helmholtz's equation* and must be solved both in the core and in the cladding. It is worth noting that the left side of the equation is function of $\boldsymbol{\mathcal{E}}_t$ and β. Indeed also β is an unknown of the problem and it must take a value between the two phase constants k_{cl} and k_{co}, i.e.,

$$k_{\text{cl}} \leq \beta \leq k_{\text{co}}. \tag{2.9}$$

At this point, it is useful to split the Helmholtz's equation in two scalar ones, namely

$$\begin{cases} \nabla^2\mathcal{E}_x - \left(\beta^2 - k^2\right)\mathcal{E}_x = 0 \\ \nabla^2\mathcal{E}_y - \left(\beta^2 - k^2\right)\mathcal{E}_y = 0 \end{cases}. \tag{2.10}$$

Furthermore, under the hypothesis of weakly waveguide it is reasonable to assume that the polarization is maintained along the fiber, indeed if the core and cladding refractive indices were the same then it would propagate a planar wave. Then the polarization can be arbitrary assumed linear along the $\hat{\boldsymbol{y}}$ direction, i.e., $\mathcal{E}_x(x,y) = 0$.

To tackle the first equation of (2.10) the separation of variable solving method can be used. In particular, it requires an additional assumption on the

form of $\mathcal{E}$ that will have to be verified at the end. Specifically using cylindrical coordinates, we suppose that

$$\mathcal{E}_y(r,\phi) = f(r)g(\phi), \tag{2.11}$$

and therefore, under this hypothesis equation (2.10) can be rewritten in polar coordinates as

$$\frac{r}{f(r)}\frac{\mathrm{d}^2 f}{\mathrm{d}r^2} + \frac{r}{f(r)}\frac{\mathrm{d}f}{\mathrm{d}r} + r^2\chi^2 = -\frac{1}{g(\phi)}\frac{\mathrm{d}^2 g}{\mathrm{d}\phi^2}, \tag{2.12}$$

where it has been placed $\chi^2 = k^2 - \beta^2$. Noting that the left and the right side of the equation depend only from r and ϕ respectively, it is possible to state that both the terms must be equal to a constant value ν^2. Then, it yields

$$\frac{\mathrm{d}^2 g}{\mathrm{d}\phi^2} + \nu^2 g(\phi) = 0, \tag{2.13}$$

$$\frac{\mathrm{d}^2 f}{\mathrm{d}r^2} + \frac{1}{r}\frac{\mathrm{d}f}{\mathrm{d}r} + \left(\chi^2 - \frac{\nu^2}{r^2}\right) f = 0. \tag{2.14}$$

The above result is positive since it allows to calculate the expressions for g and f by solving two separate equations. In particular for g, equations (2.13) represents the differential equation for an Harmonic oscillator. Then, the solution is a sinusoidal function with azimuthal order ν. In particular, for both core and cladding the expressions are given by

$$g(\phi) = \begin{cases} c_{\mathrm{co,n}}\,\cos(n\phi + \phi_{\mathrm{co,n}}) & \text{in the core} \\ c_{\mathrm{cl,m}}\,\cos(m\phi + \phi_{\mathrm{cl,m}}) & \text{in the cladding} \end{cases}, \tag{2.15}$$

where it has been places $\nu = n$ in the core and $\nu = m$ in the cladding. The quantities $c_{\mathrm{co,n}}$, $c_{\mathrm{cl,m}}$, $\phi_{\mathrm{co,n}}$, and $\phi_{\mathrm{cl,m}}$ are integration constants. Moreover, g is periodic of period 2π since it is a function of the azimuthal coordinate ϕ, then n and m must be integers and can be considered positive quantities.

Instead, to find a solution of equation (2.14) it is necessary to formally split the case whether r refers to a point in the core or in the cladding. In particular, if the point is in the core then the quantity $\chi^2 = \chi^2_{\mathrm{co}} = k^2_{\mathrm{co}} - \beta^2$ is greater than zero because of (2.9), then the solutions of (2.14) are first kind and second kind Bessel functions. However, the lasts are not suitable to represent a possible state of the field since they go to infinity for $r = 0$. Finally, taking into account that $\nu = n$, the solution of f in the core is given by

$$f(r) = b\,J_n(\chi_{\mathrm{co}}\,r) \qquad 0 \le r \le a, \tag{2.16}$$

where b is an integration constant. Similarly for the core, but considering $\nu = m$ and $\chi^2 = \chi^2_{\mathrm{cl}} = k^2_{\mathrm{cl}} - \beta^2 \le 0$, the solutions in the cladding are modified Bessel functions of the first and second kind. Also in this case the second kind ones are not feasible since they would force an infinity intensity field in the cladding. Then, function f in the cladding can be written as

$$f(r) = d\,K_m(\tilde{\chi}_{\mathrm{cl}}\,r) \qquad r \ge a, \tag{2.17}$$

where d is an integration constant and $\tilde{\chi}_{\mathrm{cl}}$ is such that $\tilde{\chi}^2_{\mathrm{cl}} = \beta^2 - k^2_{\mathrm{cl}}$.

Summing up the results in (2.15), (2.16), and (2.17), the y-polarized electric field can be described in the core and in the cladding as

$$\mathcal{E}_{\mathrm{y,co}}(r,\phi) = q_{\mathrm{co}} J_n(\chi_{\mathrm{co}}\, r)\, \cos(n\phi + \phi_{\mathrm{co}}), \tag{2.18}$$

$$\mathcal{E}_{\mathrm{y,cl}}(r,\phi) = q_{\mathrm{cl}} K_m(\tilde{\chi}_{\mathrm{cl}}\, r)\, \cos(m\phi + \phi_{\mathrm{cl}}), \tag{2.19}$$

where the integration constants must be determined forcing the boundary conditions for the transversal field between the core and the cladding. In particular they lays

$$\boldsymbol{\mathcal{E}}_{\mathrm{tan,co}}(a,\phi) = \boldsymbol{\mathcal{E}}_{\mathrm{tan,cl}}(a,\phi), \tag{2.20}$$

$$\boldsymbol{\mathcal{D}}_{\mathrm{norm,co}}(a,\phi) = \boldsymbol{\mathcal{D}}_{\mathrm{norm,cl}}(a,\phi), \tag{2.21}$$

where the first is the boundary condition for the tangent component of the electrical field, while the second one imposes the consistency of the normal component of the displacement field. Specifically, forcing condition (2.20) yields $m = n$ and $\phi_{\mathrm{co}} = \phi_{\mathrm{cl}}$ since it must hold for every ϕ. Then, $\mathcal{E}_{\mathrm{y}}(a,\phi)$ satisfies the relation

$$\frac{q_{\mathrm{co}}}{q_{\mathrm{cl}}} = \frac{K_n(\tilde{\chi}_{\mathrm{cl}}\, a)}{J_n(\chi_{\mathrm{co}}\, a)}. \tag{2.22}$$

Instead, the constitutive equation (2.21) can be rewritten as

$$\epsilon_{\mathrm{co}}\, \boldsymbol{\mathcal{E}}_{\mathrm{norm,co}}(a,\phi) = \epsilon_{\mathrm{cl}}\, \boldsymbol{\mathcal{E}}_{\mathrm{norm,cl}}(a,\phi), \tag{2.23}$$

that leads to a similar relation of (2.22), namely

$$\frac{q_{\mathrm{co}}}{q_{\mathrm{cl}}} = \frac{\epsilon_{\mathrm{cl}}}{\epsilon_{\mathrm{co}}} \frac{K_n(\tilde{\chi}_{\mathrm{cl}}\, a)}{J_n(\chi_{\mathrm{co}}\, a)}. \tag{2.24}$$

Obviously, (2.22) and (2.24) can't be satisfied together, this is indeed because of the linearly polarization assumption, that is not strictly true in a real case where $\epsilon_{\mathrm{co}} \simeq \epsilon_{\mathrm{cl}}$. However, if we are still assuming $\epsilon_{\mathrm{co}} \simeq \epsilon_{\mathrm{cl}}$ then the two conditions are consistent and the transversal electric field is

$$\boldsymbol{\mathcal{E}}_t(r,\phi) = \begin{cases} q\, \frac{J_n(\chi_{\mathrm{co}}\, r)}{J_n(\chi_{\mathrm{co}}\, a)}\, \cos(n\phi + \phi_0)\hat{\boldsymbol{y}} & \text{in the core} \\ q\, \frac{K_n(\tilde{\chi}_{\mathrm{cl}}\, r)}{K_n(\tilde{\chi}_{\mathrm{cl}}\, a)}\, \cos(n\phi + \phi_0)\hat{\boldsymbol{y}} & \text{in the cladding} \end{cases}. \tag{2.25}$$

The next step consists of calculating the longitudinal component of the field, namely $\mathcal{E}_z(r,\phi)$. Actually, the expression for $\mathcal{E}_z(r,\phi)$ can be easily calculated by transforming (2.6) in polar notation. Specifically, it yields

$$\mathcal{E}_z(r,\phi) = \frac{1}{j\beta}\big(\sin\phi \frac{\partial \mathcal{E}_y}{\partial r} + \frac{1}{r}\cos\phi \frac{\partial \mathcal{E}_y}{\partial \phi}\big). \tag{2.26}$$

The resulting field is much lower than the one along the transversal direction because of the weakly waveguide assumption. Nevertheless the expression of $\mathcal{E}_z(r,\phi)$ is fundamental to force the last boundary condition that will allow to find an expression for the mode propagation constant β. In particular, it must be such that

$$\mathcal{E}_{\mathrm{z,co}}(a,\phi) = \mathcal{E}_{\mathrm{z,cl}}(a,\phi), \tag{2.27}$$

for every possible value of the azimuthal coordinate ϕ since the longitudinal field is always tangent to the boundary between the core and the cladding. Then, exploiting (2.26) with (2.27) leads to the *characteristic equation*

$$\chi_{\mathrm{co}} a \, \frac{J_{\mathrm{n}+1}(\chi_{\mathrm{co}} a)}{J_{\mathrm{n}}(\chi_{\mathrm{co}} a)} = \tilde{\chi}_{\mathrm{cl}} a \, \frac{K_{\mathrm{n}+1}(\tilde{\chi}_{\mathrm{cl}} a)}{K_{\mathrm{n}}(\tilde{\chi}_{\mathrm{cl}} a)} \tag{2.28}$$

The equation (2.28) is also called *dispersion equation* because the only unknowns are the values of β and therefore it sets the modal dispersions properties of the fiber. In particular, each guided mode has a cutoff frequency under which it stops to exist. From a physical point of view this happens whenever β reaches its lower bound, i.e. $\beta = k_{\mathrm{cl}}$. At that point, the mode is no more guided and starts to invade the cladding becoming an irradiating mode. Specifically for the characteristic equation, this occurs when $\tilde{\chi}_{\mathrm{cl}} = 0$ or equivalently when $\chi_{\mathrm{co}} = (\omega/c_0)(n_{\mathrm{co}}^2 - n_{\mathrm{cl}}^2)^{1/2}$, where c_0 is the speed of light in vacuum. Moreover since $\tilde{\chi}_{\mathrm{cl}}$ is zero, then the right side of the dispersion equation can be shown to be equal to $2n$. Therefore the cutoff frequencies can be found exploiting the above considerations to (2.28), that is by solving the equation

$$\frac{\omega \, a}{c_0} (n_{\mathrm{co}}^2 - n_{\mathrm{cl}}^2)^{1/2} \, \frac{J_{n+1}\Big(\frac{\omega \, a}{c_o}(n_{\mathrm{co}}^2 - n_{\mathrm{cl}}^2)^{1/2}\Big)}{J_n\Big(\frac{\omega \, a}{c_o}(n_{\mathrm{co}}^2 - n_{\mathrm{cl}}^2)^{1/2}\Big)} = 2n \tag{2.29}$$

where $(n_{\mathrm{co}}^2 - n_{\mathrm{cl}}^2)^{1/2}$ is the numerical aperture of the fiber. The above equation exhibits a countable infinity set of solutions, where at each of them corresponds an LP mode. Thus an LP mode is labeled by means of two indices, the first represents the azimuthal order n while the second is called p and is the solution number of (2.29).

To study (2.28) and (2.29) it is more convenient to introduce a normalized version of them. In particular, it useful to define a *normalized frequency* v and a *normalized propagation constant* b, such that

$$v = (u^2 + w^2)^{1/2} = \frac{2\pi}{\lambda} a \, \mathrm{NA}, \tag{2.30}$$

$$b = \frac{\beta^2 - k_{\mathrm{cl}}^2}{k_{\mathrm{co}}^2 - k_{\mathrm{cl}}^2} = \frac{w^2}{v^2} = 1 - \frac{u^2}{v^2}, \tag{2.31}$$

where $u = a \, \chi_{\mathrm{co}}$ and $w = a \, \tilde{\chi}_{\mathrm{cl}}$ are normalized quantities [KW12]. Then, owing to definitions (2.30) and (2.31) equations (2.28) and (2.29) become respectively

$$\frac{J_n(u)}{u \, J_{n+1}(u)} = \frac{J_n(w)}{w \, J_{n+1}(w)}, \tag{2.32}$$

$$v \, \frac{J_{n+1}(v)}{J_n(v)} - 2n = 0. \tag{2.33}$$

Equations (2.31) and (2.32) describe the dispersion and the cutoff equations using normalized quantities. Solving the equations using numerical tools leads to a global picture of the modal dispersion. In this sense, Figure 2.1 shows the behaviors of the propagation constants for the first six LP modes. In particular, the single mode propagation is assured using a normalized working frequency

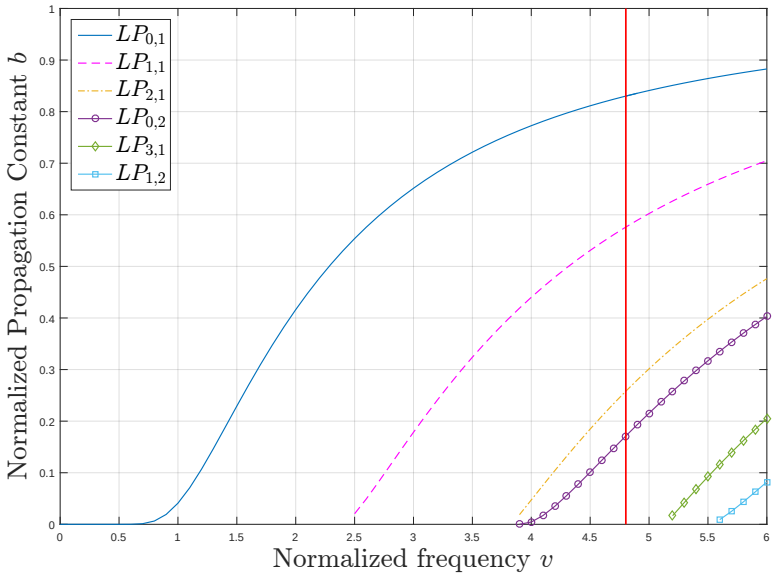

Figure 2.1: Normalized propagation constants as a function of the normalized frequency for the first 4 LP groups.

spanning from 0 to 2.405. Instead, considering propagation in a multimode optical fiber with $n_{\text{co}} = 1.4660$, $n_{\text{cl}} = 1.4585$ and radius $a = 8\mu$m yields to a normalized frequency $v = 4.80$ working at a central wavelength of 1550nm (vertical red line in Figure 2.1). Therefore there is the propagation of 4 LP modes, namely $\text{LP}_{0,1}$, $\text{LP}_{1,1}$, $\text{LP}_{2,1}$ and $\text{LP}_{0,2}$. In this case the dispersion of the transmitted signal is evident since each mode has a different propagation constant and thus propagates with different group velocity.

Up to this point the analysis has been carried out using two arbitrary decisions. The first is the polarization of $\boldsymbol{\mathcal{E}}_t(r,\phi)$, that has been assumed y-polarized. However this is a completely arbitrary choice and the analysis could have been done assuming the transversal field x-polarized. Indeed the two types of mode, $\text{LP}^y_{n,p}$ and $\text{LP}^x_{n,p}$ respectively, are equally valid and share the same dispersion equation since the particular polarization choice doesn't appear in it. This behavior spurs from the ideal symmetry of the fiber and therefore the two modes are called degenerate. Moreover, the second arbitrary decision involves the form of the Harmonic function for g. Indeed it has been written as $g(\phi) = \cos(n\phi + \phi_0)$, where the integration constant ϕ_0 hides a further type of degeneracy. This can be formally caught by observing that $g(\phi) = \cos(n\phi + \phi_0) = q_1 \cos(n\phi) + q_2 \sin(n\phi)$. Actually, the original mode is a superposition of two further ones, an even and an odd mode where a cosine and a sine function appear respectively. Finally, it is worth to note that the last type of degeneration exists only for azimuthal order grater than 0. Therefore each $\text{LP}_{n,p}$ is actually a group of degenerate modes, in particular groups of the type $\text{LP}_{0,p}$ are 2-fold degenerate ($\text{LP}^x_{0,p}$ and $\text{LP}^y_{0,p}$) while the others are 4-

fold degenerate ($\mathrm{LP}_{n,p}^{(x,e)}$, $\mathrm{LP}_{n,p}^{(y,e)}$, $\mathrm{LP}_{n,p}^{(x,o)}$ and $\mathrm{LP}_{n,p}^{(y,o)}$). However the degeneracy holds only under the hypothesis of ideal fiber, in the case of perturbations the LP groups detune and each mode within a group propagates with a different velocity. This effect is more evident in "single" mode propagation, where the detuning of the $\mathrm{LP}_{0,1}$ group forces a bimodal transmission causing the so called polarization mode dispersion (PMD).

To conclude the analysis with respect to the LP modes it is worth to note the property of orthogonality among non-degenerate modes, namely

$$\frac{\beta_\mu}{2\omega\mu_0}\iint_S \boldsymbol{\mathcal{E}}_{t,\mu}\times\boldsymbol{\mathcal{H}}^*_{t,\nu}\cdot\hat{\boldsymbol{z}}\,\mathrm{d}s=\delta_{\mu,\nu}, \tag{2.34}$$

where μ and ν represent two LP modes, S is the fiber cross-section and $\boldsymbol{\mathcal{H}}_t$ is the transversal component of the magnetic field calculated using (2.7).

2.2 Hybrid Modes and Modal Birefringence

In general LP modes don't represent true modes of the waveguide, although in practice the weakly guide approximation is reasonably in communication optical fibers and LP modes manage to grasp the global picture of the propagation properties. In particular, defining the quantity

$$\Delta=\frac{n_{\mathrm{co}}^2-n_{\mathrm{cl}}^2}{2\,n_{\mathrm{co}}^2}, \tag{2.35}$$

it is considered negligible under the weakly guide approximation. However it is not, otherwise there wouldn't have been the guide at all, and it must be taken into account if we want a finer description of the modes propagating in the fiber.

Under weak-guide approximation, LP modes are linear combination of the true ones, called *hybrid modes* [PG16]. However, whenever $\Delta\neq 0$ the last ones exhibit different propagation constants, causing dispersion even considering a single LP mode in an ideal fiber. This phenomenon is called *modal birefringence* [KW12] and should be taken into account in the propagation analysis when it is comparable to the birefringence induced by perturbations [PG]. Then, modal birefringence changes the spacial pattern of the single LP mode, that regains the original one after a modal beat length. Finally, it is worth to note that this effect is almost negligible if compared with the dispersion among different LP groups.

In general, a mode in a $\mathrm{LP}_{n,p}$ group can be written as a combination of 4 types of hybrid mode, namely $\mathrm{TE}_{0,p}$, $\mathrm{TM}_{0,p}$, $\mathrm{HE}_{n+1,p}$ and $\mathrm{EH}_{n-1,p}$, where they are characterized respectively by $\mathcal{H}_z=0$, $\mathcal{E}_z=0$, $0\neq\mathcal{H}_z<\mathcal{E}_z$ and $0\neq\mathcal{E}_z<\mathcal{H}_z$. These modes have in general different propagation constants with respect to the one of the LP group, since their dispersion equation depends on Δ. In particular, for the $\mathrm{TE}_{0,p}$, $\mathrm{TM}_{0,p}$, $\mathrm{HE}_{n+1,p}$ and $\mathrm{EH}_{n-1,p}$ respectively the normalized characteristic equations are [KW12]

$$\frac{J_1(u)}{u\,J_0(u)}=-\frac{K_1(w)}{w\,K_0(w)}, \tag{2.36}$$

$$\frac{J_1(u)}{u\,J_0(u)}=-\frac{K_1(w)}{w\,K_0(w)}(1-2\Delta), \tag{2.37}$$

$$\frac{J_n(u)}{u\,J_{n-1}(u)} = -\frac{K_n(w)}{w\,K_{n-1}(w)}(1-\Delta), \tag{2.38}$$

$$\frac{J_n(u)}{u\,J_{n+1}(u)} = \frac{K_n(w)}{w\,K_{n+1}(w)}(1-\Delta), \tag{2.39}$$

where u and w are normalized quantities defined as in the previous section. In particular it can be shown that (2.36) represents an exact relation and it is equivalent to the dispersion equation for the $\mathrm{LP}_{1,p}$ modes in (2.32). Thus mode $\mathrm{TE}_{0,p}$ shares the same cutoff frequency and propagation constant of the $\mathrm{LP}_{1,p}$ group. Instead, equation (2.37) for the $\mathrm{TM}_{0,p}$ still is an exact relation but it is different from the LP one, nevertheless they share the very same zeros when $J_0(u) = 0$, meaning that (2.37) has the same cutoff frequency of the $\mathrm{LP}_{1,p}$ group [KW12]. Regarding equations (2.38) and (2.39), they are first order approximations of their corresponding dispersion equations and they have in general different solutions and cutoff frequencies.

Also the hybrid modes $\mathrm{HE}_{n+1,p}$ and $\mathrm{EH}_{n-1,p}$ represent a group of degenerate modes for the ideal symmetry case. Specifically, they both are 2-fold degenerate with an even and an odd mode for each, namely $\mathrm{HE}^{e}_{n+1,p}$, $\mathrm{HE}^{o}_{n+1,p}$ and $\mathrm{EH}^{e}_{n-1,p}$, $\mathrm{EH}^{e}_{n-1,p}$. If we want to write each possible LP mode as a combination of hybrid modes it is convenient to distinguish three cases.

- The LP modes within the $\mathrm{LP}_{0,p}$ groups can be expressed in terms of the following hybrid modes:
  - $\mathrm{LP}_{0,p} \longrightarrow \mathrm{HE}^{e}_{1,p}$.
  - $\mathrm{LP}_{0,p} \longrightarrow \mathrm{HE}^{o}_{1,p}$.

  In this particular case there is not modal birefringence, indeed the degenerate LP groups are mapped in degenerate hybrid modes.

- The LP modes within the $\mathrm{LP}_{1,p}$ groups can be expressed in terms of the following hybrid modes:
  - $\mathrm{LP}^{x,e}_{1,p} \longrightarrow \mathrm{HE}^{e}_{2,p}$ and $\mathrm{TM}_{0,p}$.
  - $\mathrm{LP}^{y,e}_{1,p} \longrightarrow \mathrm{HE}^{o}_{2,p}$ and $\mathrm{TE}_{0,p}$.
  - $\mathrm{LP}^{x,o}_{1,p} \longrightarrow \mathrm{HE}^{e}_{2,p}$ and $\mathrm{TE}_{0,p}$.
  - $\mathrm{LP}^{y,o}_{1,p} \longrightarrow \mathrm{HE}^{o}_{2,p}$ and $\mathrm{TM}_{0,p}$.

  In this case the four degenerate modes of the $\mathrm{LP}_{1,p}$ groups can be written using three non-degenerate hybrid mode types. Then, within this family of LP groups there is modal birefringence caused by the three different propagation constants of the hybrid modes.

- The LP modes within the $\mathrm{LP}_{n,p}$ (n>1) groups can be expressed in terms of the following hybrid modes:
  - $\mathrm{LP}^{x,e}_{n,p} \longrightarrow \mathrm{HE}^{e}_{n+1,p}$ and $\mathrm{EH}^{e}_{n-1,p}$.
  - $\mathrm{LP}^{y,e}_{n,p} \longrightarrow \mathrm{HE}^{o}_{n+1,p}$ and $\mathrm{EH}^{o}_{n-1,p}$.
  - $\mathrm{LP}^{x,o}_{n,p} \longrightarrow \mathrm{HE}^{e}_{n+1,p}$ and $\mathrm{EH}^{o}_{n-1,p}$.
  - $\mathrm{LP}^{y,o}_{n,p} \longrightarrow \mathrm{HE}^{o}_{n+1,p}$ and $\mathrm{EH}^{e}_{n-1,p}$.

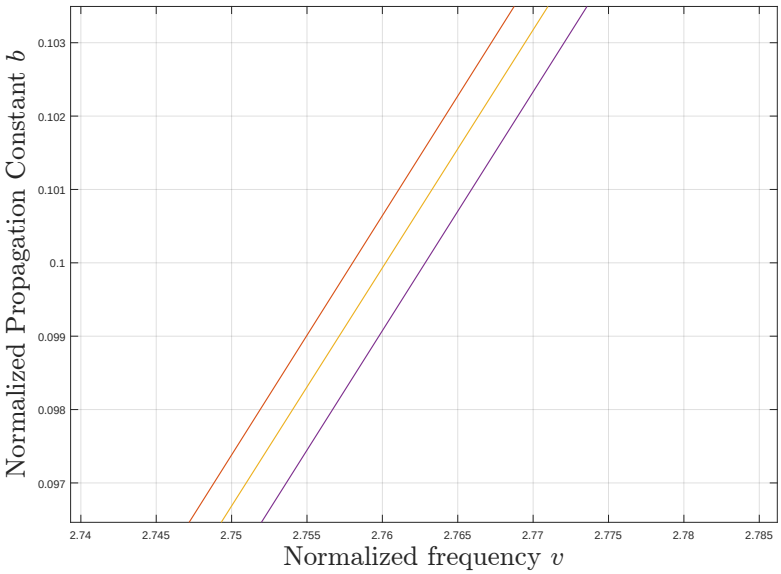

Figure 2.2: A close view of the modal birefringence in the $\mathrm{LP}_{1,1}$ group.

In this last case, the degenerate group LP can be expressed using two non-degenerate hybrid modes. Therefore, also in this case there is modal birefringence due to the two different propagation constants of $\mathrm{HE}_{n+1,p}$ and $\mathrm{HE}_{n-1,p}$.

In Figure 2.2 and Figure 2.3 the effect of the modal birefringence on the normalized propagation constant is represented within the $\mathrm{LP}_{1,1}$ and $\mathrm{LP}_{2,1}$ group respectively. In particular using the same fiber of Figure 2.1, it is possible to appreciate how this effect is risible with respect to the propagation constant difference among non-degenerate LP modes.

Finally the conversion matrices from the hybrid modes to the LP ones are reported below. In particular, for the $\mathrm{LP}_{0,p}$, $\mathrm{LP}_{1,p}$ and $\mathrm{LP}_{n,p}$ $(n > 1)$ groups it yields respectively:

$$\begin{pmatrix} \mathrm{LP}^{x}_{0,p} \\ \mathrm{LP}^{y}_{0,p} \end{pmatrix} = \begin{pmatrix} 1 & 0 \\ 0 & 1 \end{pmatrix} \begin{pmatrix} \mathrm{HE}^{e}_{1,p} \\ \mathrm{HE}^{o}_{1,p} \end{pmatrix}, \tag{2.40}$$

$$\begin{pmatrix} \mathrm{LP}^{x,e}_{1,p} \\ \mathrm{LP}^{y,e}_{1,p} \\ \mathrm{LP}^{x,o}_{1,p} \\ \mathrm{LP}^{y,o}_{1,p} \end{pmatrix} = \frac{1}{\sqrt{2}} \begin{pmatrix} 1 & 0 & -1 & 0 \\ 0 & 1 & 0 & 1 \\ 0 & 1 & 0 & -1 \\ -1 & 0 & -1 & 0 \end{pmatrix} \begin{pmatrix} \mathrm{HE}^{e}_{2,p} \\ \mathrm{HE}^{o}_{2,p} \\ \mathrm{TM}_{0,p} \\ \mathrm{TE}_{0,p} \end{pmatrix}, \tag{2.41}$$

$$\begin{pmatrix} \mathrm{LP}^{x,e}_{1,p} \\ \mathrm{LP}^{y,e}_{1,p} \\ \mathrm{LP}^{x,o}_{1,p} \\ \mathrm{LP}^{y,o}_{1,p} \end{pmatrix} = \frac{1}{\sqrt{2}} \begin{pmatrix} 1 & 0 & -1 & 0 \\ 0 & 1 & 0 & 1 \\ 0 & 1 & 0 & -1 \\ -1 & 0 & -1 & 0 \end{pmatrix} \begin{pmatrix} \mathrm{HE}^{e}_{n+1,p} \\ \mathrm{HE}^{o}_{n+1,p} \\ \mathrm{EH}^{e}_{n-1,p} \\ \mathrm{EH}^{o}_{n-1,p} \end{pmatrix}, \tag{2.42}$$

where $1/\sqrt{2}$ is a normalization factor to have the right intensity of the field.

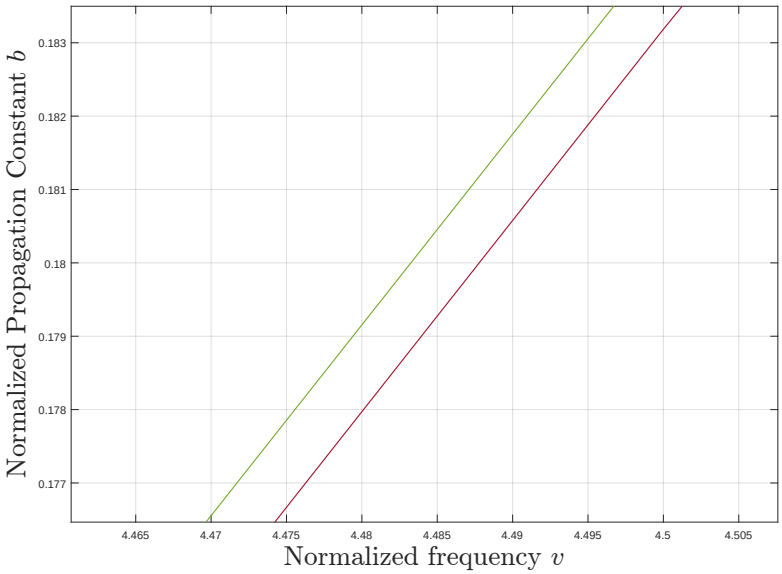

Figure 2.3: A close view of the modal birefringence in the $LP_{2,1}$ group.

Chapter 3

Mode-Coupling in Optical Fibers

The modal theory analyzed in Section 2 is a nice tool to describe the propagation in ideal fibers. However, in a more real scenario the ideal symmetry is broken by several perturbations that act simultaneously along the fiber. Thus, it is necessary a more general theory that describes these effects as coupling among the ideal modes of the fiber. In this chapter it will be explained the general *coupled-mode theory* for anisotropic dielectric media [Mar74] and then it will be applied to the case of optical fibers , considering different types of perturbations [Pal14][GM05][Cho00][PG14].

3.1 The Coupled-Mode Theory

The coupling mechanism in optical fibers can be effectively described by a more general results about the coupling in dielectric waveguides. The following analysis is a special case of the one proposed by *D. Marcuse* in [Mar74] for anisotropic media, specifically only coupling among guided modes that propagate along the $\hat{\boldsymbol{z}}$ direction has been considered.

3.1.1 Field Equations in Anisotropic Media

The electromagnetic behavior of a linear, time invariant, not dispersive and isotropic medium can be described by two quantities, the dielectric permittivity ϵ and the magnetic permeability μ, that are in general space dependent functions, that is $\epsilon = \epsilon(x, y, z)$ and $\mu = \mu(x, y, z)$. In particular, they measure how the field affects the medium by means of the constitutive equations: $\boldsymbol{D} = \epsilon \boldsymbol{E}$ and $\boldsymbol{B} = \mu \boldsymbol{H}$. This is indeed the case of silica glass, however, perturbations that act along the fiber make the waveguide anisotropic with respect to the dielectric permittivity. In a strictly mathematical sense, anisotropy means that vectors $\boldsymbol{D}$ and $\boldsymbol{E}$ are no more parallel, making the propagation of light directional dependent from a physical point of view. The constitutive equations for these kind of media become

$$\boldsymbol{D} = \boldsymbol{\epsilon} \cdot \boldsymbol{E}, \tag{3.1}$$

and

$$\boldsymbol{B} = \mu \boldsymbol{H}, \tag{3.2}$$

where $\boldsymbol{\epsilon}$ is a space-dependent tensor, and $\mu = \mu_0$ is assumed constant and equals to the vacuum permeability. Therefore, in the considered case, $\boldsymbol{\epsilon}$ is a rank-2 tensor, completely defined by its real components, namely

$$\boldsymbol{\epsilon} = \begin{pmatrix} \epsilon_{xx} & \epsilon_{xy} & \epsilon_{xz} \\ \epsilon_{yx} & \epsilon_{yy} & \epsilon_{yz} \\ \epsilon_{zx} & \epsilon_{zy} & \epsilon_{zz} \end{pmatrix}. \tag{3.3}$$

Moreover, since we assume the propagation in a lossless medium, the expression for the dielectric permittivity can be further simplified considering a symmetric tensor, i.e., $\boldsymbol{\epsilon} = \boldsymbol{\epsilon}^T$.

In these settings, the Maxwell's equations for the electric and magnetic fields yields

$$\nabla \times \boldsymbol{H} = j\omega \boldsymbol{\epsilon} \cdot \boldsymbol{E}, \tag{3.4}$$

$$\nabla \times \boldsymbol{E} = -j\omega \mu \, \boldsymbol{H}, \tag{3.5}$$

where (3.5) is the classic differential equation for isotropic media, while (3.4) involves a rank-2 tensor. As for the derivation of the LP modes, it is convenient to separate the transversal field from the longitudinal one, where we recall that the longitudinal direction is the co-propagating one, i.e., $\hat{\boldsymbol{z}}$. In order to do this we redefine the fields as

$$\boldsymbol{E} = \boldsymbol{E}_t + E_z \, \hat{\boldsymbol{z}}, \tag{3.6}$$

$$\boldsymbol{H} = \boldsymbol{H}_t + H_z \, \hat{\boldsymbol{z}}, \tag{3.7}$$

and the gradient operator as

$$\nabla = \nabla_t + \frac{\partial}{\partial z} \hat{\boldsymbol{z}}, \tag{3.8}$$

where $\boldsymbol{E}_t = (E_x, E_y, 0)^T$, $\boldsymbol{H}_t = (H_x, H_y, 0)^T$ and $\nabla_t = (\frac{\partial}{\partial x}, \frac{\partial}{\partial y}, 0)^T$. Finally, following the same principle, the transversal components can be highlighted also for the dielectric tensor:

$$\boldsymbol{\epsilon}_t = \begin{bmatrix} \boldsymbol{\epsilon}_x \\ \boldsymbol{\epsilon}_y \\ 0 \end{bmatrix} = \begin{bmatrix} \epsilon_{xx} & \epsilon_{xy} & \epsilon_{xz} \\ \epsilon_{yx} & \epsilon_{yy} & \epsilon_{yz} \\ 0 & 0 & 0 \end{bmatrix}. \tag{3.9}$$

Thus, the Maxwell's equations are split in two sets, the first is for the transversal components, and lays

$$\nabla_t \times H_z \, \hat{\boldsymbol{z}} + \hat{\boldsymbol{z}} \times \frac{\partial \, \boldsymbol{H}_t}{\partial z} = j\omega \boldsymbol{\epsilon}_t \cdot \boldsymbol{E}, \tag{3.10}$$

$$\nabla_t \times E_z \, \hat{\boldsymbol{z}} + \hat{\boldsymbol{z}} \times \frac{\partial \, \boldsymbol{E}_t}{\partial z} = -j\omega \mu_0 \boldsymbol{H}_t, \tag{3.11}$$

while the second is for the longitudinal one, yielding

$$\nabla_t \times \boldsymbol{H}_t = j\omega \, (\boldsymbol{\epsilon}_z \cdot \boldsymbol{E}_t + \epsilon_{zz} E_z \, \hat{\boldsymbol{z}}), \tag{3.12}$$

$$\nabla_t \times \boldsymbol{E}_t = -j\omega \mu_0 H_z \, \hat{\boldsymbol{z}}). \tag{3.13}$$

In particular, it is possible to express the longitudinal fields as a function of the transversal ones using equations (3.12) and (3.13), yielding

$$E_z\,\hat{\boldsymbol{z}} = \frac{1}{j\omega\epsilon_{zz}}\nabla_t \times \boldsymbol{H}_t - \frac{1}{\epsilon_{zz}}\boldsymbol{\epsilon}_z \cdot \boldsymbol{E}_t, \tag{3.14}$$

$$H_z\,\hat{\boldsymbol{z}} = -\frac{1}{j\omega\mu_0}\nabla_t \times \boldsymbol{E}_t. \tag{3.15}$$

Substituting (3.14) and (3.15) in (3.10) (3.11) brings to the final set of equations

$$-\frac{1}{j\omega\mu_0}\nabla_t \times (\nabla_t \times \boldsymbol{E}_t) + \hat{\boldsymbol{z}} \times \frac{\partial \boldsymbol{H}_t}{\partial z} = j\omega\boldsymbol{\epsilon}_t \cdot \boldsymbol{E}_t - \frac{j\omega}{\epsilon_{zz}}\boldsymbol{\epsilon_t} \cdot \boldsymbol{\epsilon}_z \cdot \boldsymbol{E}_t + \frac{1}{\epsilon_{zz}}\boldsymbol{\epsilon}_t \cdot (\nabla_t \times \boldsymbol{H}_t), \tag{3.16}$$

$$\nabla_t \times \Big[\frac{1}{j\omega\epsilon_{zz}}\nabla_t \times \boldsymbol{H}_t - \frac{1}{\epsilon_{zz}}\boldsymbol{\epsilon}_z \cdot \boldsymbol{E}_t\Big] + \hat{\boldsymbol{z}} \times \frac{\partial \boldsymbol{E}_t}{\partial z} = -j\omega\mu_0\boldsymbol{H}_t. \tag{3.17}$$

These two are the equivalent Maxwell's equations with respect to the transversal component, where the number of scalar equations have decreased from 6 of the original problem (3.4)-(3.5) to 4. As stated before, in our analysis we are only interested in the coupling among guided modes, from a mathematical point of view these modes can be described as

$$\boldsymbol{E}^\nu(x,y,z) = \Big(\boldsymbol{\mathcal{E}}_t^\nu(x,y) + \mathcal{E}_z^\nu(x,y)\hat{\boldsymbol{z}}\Big)\,e^{-j\beta_\nu z}, \tag{3.18}$$

$$\boldsymbol{H}^\nu(x,y,z) = \Big(\boldsymbol{\mathcal{H}}_t^\nu(x,y) + \mathcal{H}_z^\nu(x,y)\hat{\boldsymbol{z}}\Big)\,e^{-j\beta_\nu z}, \tag{3.19}$$

where the only z dependence is in $e^{j\beta_\nu z}$ and β_ν is a real propagation constant, $\beta_\nu \in \mathbb{R}$. However, it is possible to show that a solution such (3.18)-(3.19) is not feasible with respect to the system of equations in (3.16)-(3.17). The main reason is that the dielectric tensor is a function of z, that is it changes along the longitudinal axis. To proceed in the analysis we introduce a similar dielectric tensor that is not dependent from z, i.e., $\boldsymbol{\epsilon} = \boldsymbol{\epsilon}(x,y,z) \simeq \bar{\boldsymbol{\epsilon}}(x,y) = \bar{\boldsymbol{\epsilon}}$. Introducing the new ideal tensor $\bar{\boldsymbol{\epsilon}}$ and equations (3.18)-(3.19) in (3.16)-(3.17) yields

$$-\frac{1}{j\omega\mu_0}\nabla_t \times (\nabla_t \times \boldsymbol{\mathcal{E}}_t) - j\beta\hat{\boldsymbol{z}} \times \boldsymbol{\mathcal{H}}_t = j\omega\bar{\boldsymbol{\epsilon}}_t \cdot \boldsymbol{\mathcal{E}}_t - \frac{j\omega}{\bar{\epsilon}_{zz}}\bar{\boldsymbol{\epsilon}}_{\boldsymbol{t}} \cdot \bar{\boldsymbol{\epsilon}}_z \cdot \boldsymbol{\mathcal{E}}_t + \frac{1}{\bar{\epsilon}_{zz}}\bar{\boldsymbol{\epsilon}}_t \cdot (\nabla_t \times \boldsymbol{\mathcal{H}}_t), \tag{3.20}$$

$$\nabla_t \times \Big[\frac{1}{j\omega\bar{\epsilon}_{zz}}\nabla_t \times \boldsymbol{\mathcal{H}}_t - \frac{1}{\bar{\epsilon}_{zz}}\bar{\boldsymbol{\epsilon}}_z \cdot \boldsymbol{\mathcal{E}}_t\Big] - j\beta\hat{\boldsymbol{z}} \times \boldsymbol{\mathcal{E}}_t = -j\omega\mu_0\boldsymbol{\mathcal{H}}_t. \tag{3.21}$$

Equations (3.20)-(3.21) constitute a linear system with 5 unknowns in 4 scalar equations. Therefore there are an infinity number of solutions, that are called modes, of the type ($\boldsymbol{\mathcal{E}}^\nu$,$\boldsymbol{\mathcal{H}}^\nu$,$\beta_\nu$), in particular they must be countable since β_ν has been chosen real.

3.1.2 The Orthogonality Relationship

Considering now two different guided modes, namely ν and μ, such that

$$\nu : \begin{cases} \boldsymbol{E}^\nu(x,y,z) = \boldsymbol{\mathcal{E}}^{\boldsymbol{\nu}}(x,y)e^{-j\beta_\nu z} \\ \boldsymbol{H}^\nu(x,y,z) = \boldsymbol{\mathcal{H}}^{\boldsymbol{\nu}}(x,y)e^{-j\beta_\nu z} \end{cases}, \tag{3.22}$$

$$\mu : \begin{cases} \boldsymbol{E}^{\mu}(x,y,z) = \boldsymbol{\mathcal{E}}^{\boldsymbol{\mu}}(x,y)e^{-j\beta_{\mu}z} \\ \boldsymbol{H}^{\mu}(x,y,z) = \boldsymbol{\mathcal{H}}^{\boldsymbol{\mu}}(x,y)e^{-j\beta_{\mu}z} \end{cases} . \tag{3.23}$$

Using them in the original Maxwell's equations, specifically ν in (3.4) and μ in (3.5), lays

$$\nabla_t \times \boldsymbol{\mathcal{H}}^{\nu} - j\beta_{\nu}\hat{\boldsymbol{z}} \times \boldsymbol{\mathcal{H}}^{\nu} = j\omega\bar{\epsilon} \cdot \boldsymbol{\mathcal{E}}^{\nu}, \tag{3.24}$$

$$\nabla_t \times \boldsymbol{\mathcal{E}}^{\mu} - j\beta_{\mu}\hat{\boldsymbol{z}} \times \boldsymbol{\mathcal{E}}^{\mu} = j\omega\mu_0\boldsymbol{\mathcal{H}}^{\mu}. \tag{3.25}$$

Then, taking the integral over the waveguide cross-section S of the complex conjugate of (3.24) pre-multiplied by $\boldsymbol{\mathcal{E}}^{\mu}$ and added to (3.25) pre-multiplied by $\boldsymbol{\mathcal{H}}^{\nu\,*}$, i.e., $\boldsymbol{\mathcal{E}}^{\mu} \cdot (3.24)^{*} + \boldsymbol{\mathcal{H}}^{\nu\,*} \cdot (3.25)$, yields

$$\begin{aligned} &\iint_S \Big(\boldsymbol{\mathcal{E}}^{\mu} \cdot \nabla_t \times \boldsymbol{\mathcal{H}}^{\nu\,*} - \boldsymbol{\mathcal{H}}^{\nu\,*} \cdot \nabla_t \times \boldsymbol{\mathcal{E}}^{\mu} \\ &\qquad + j\beta_{\nu}\boldsymbol{\mathcal{E}}^{\mu} \cdot \hat{\boldsymbol{z}} \times \boldsymbol{\mathcal{H}}^{\nu\,*} + j\beta_{\mu}\boldsymbol{\mathcal{H}}^{\nu\,*} \cdot \hat{\boldsymbol{z}} \times \boldsymbol{\mathcal{E}}^{\mu} \Big) \mathrm{d}x\,\mathrm{d}y. \\ &= -j\omega \iint_S \Big(\boldsymbol{\mathcal{E}}^{\mu} \cdot \bar{\boldsymbol{\epsilon}} \cdot \boldsymbol{\mathcal{E}}^{\nu\,*} - \mu_0 \boldsymbol{\mathcal{H}}^{\nu\,*} \cdot \boldsymbol{\mathcal{H}}^{\mu} \Big) \mathrm{d}x\,\mathrm{d}y \end{aligned} \tag{3.26}$$

Equation (3.26) can be heavily simplified, in particular the vector identity $\nabla \cdot (\boldsymbol{A} \times \boldsymbol{B}) = (\nabla \times \boldsymbol{A}) \cdot \boldsymbol{B} - \boldsymbol{A} \cdot (\nabla \times \boldsymbol{B})$ simplifies the first term of the integral into $-\nabla_t \cdot (\boldsymbol{\mathcal{E}}^{\boldsymbol{\mu}} \times \boldsymbol{\mathcal{H}}^{\nu\,*})$, for which the divergence theorem lays

$$-\iint_S \nabla_t \cdot (\boldsymbol{\mathcal{E}}^{\mu} \times \boldsymbol{\mathcal{H}}^{\nu\,*}) \mathrm{d}x\,\mathrm{d}y = \oint_{S_l} (\boldsymbol{\mathcal{E}}^{\mu} \times \boldsymbol{\mathcal{H}}^{\nu\,*}) \cdot \hat{\boldsymbol{n}}\,\mathrm{d}l, \tag{3.27}$$

where $\hat{\boldsymbol{n}}$ is the outward normal direction of S. Moreover, the latter integral is equal to zero, since the cross-section is ideally infinitely extended. Therefore the line S_l corresponds to an infinite circle where the fields of the guided mode must be zero. Instead, the second term becomes $j(\beta_{\mu} - \beta_{\nu})[\hat{\boldsymbol{z}} \cdot (\boldsymbol{\mathcal{E}}^{\mu} \times \boldsymbol{\mathcal{H}}^{\mu\,*})]$ by noting that $\hat{\boldsymbol{z}} \times \boldsymbol{\mathcal{H}}^{\nu\,*} = -\boldsymbol{\mathcal{H}}^{\nu\,*} \times \hat{\boldsymbol{z}}$ and using a further vector identity, namely $\boldsymbol{A} \cdot (\boldsymbol{B} \times \boldsymbol{C}) = \boldsymbol{C} \cdot (\boldsymbol{A} \times \boldsymbol{B}) = \boldsymbol{B} \cdot (\boldsymbol{C} \times \boldsymbol{A})$. According to these considerations, relation (3.26) can be rewritten as

$$\begin{aligned} &(\beta_{\mu} - \beta_{\nu}) \iint_S \hat{\boldsymbol{z}} \cdot (\boldsymbol{\mathcal{E}}^{\mu} \times \boldsymbol{\mathcal{H}}^{\mu\,*}) \mathrm{d}x\,\mathrm{d}y \\ &\qquad = -\omega \iint_S \Big(\boldsymbol{\mathcal{E}}^{\mu} \cdot \bar{\boldsymbol{\epsilon}} \cdot \boldsymbol{\mathcal{E}}^{\nu\,*} - \mu_0 \boldsymbol{\mathcal{H}}^{\nu\,*} \cdot \boldsymbol{\mathcal{H}}^{\mu} \Big) \mathrm{d}x\,\mathrm{d}y \end{aligned} . \tag{3.28}$$

It is remarkably to note that the role of μ and ν can be switched since they are completely arbitrary guided modes. Therefore, a similar expression of (3.28) with μ and ν exchanged must hold. In particular, subtracting the complex conjugate of the mentioned expression to (3.28) and recalling that $\bar{\boldsymbol{\epsilon}}$ is symmetric yields to *the orthogonality relationship*, namely

$$(\beta_{\mu} - \beta_{\nu}) \iint_S \hat{\boldsymbol{z}} \cdot \Big(\boldsymbol{\mathcal{E}}^{\mu} \times \boldsymbol{\mathcal{H}}^{\nu\,*} + \boldsymbol{\mathcal{E}}^{\nu\,*} \times \boldsymbol{\mathcal{H}}^{\mu} \Big) \mathrm{d}x\,\mathrm{d}y = 0. \tag{3.29}$$

Equation (3.29) is fundamental and states that guided modes in anisotropic waveguide are mutually orthogonal. In particular it shows how there couldn't be any power transfer between different modes towards the propagating direction, in fact β_{ν} and β_{μ} would be different and the integral will go to zero.

Conversely, the integral has the meaning of power flow across S in the case of equal modes, that is $\nu = \mu$. Indeed, in the latter case the term in the integral can be rewritten as $\hat{\boldsymbol{z}} \cdot 2\,\mathrm{Re}\{\boldsymbol{\mathcal{E}} \times \boldsymbol{\mathcal{H}}^*\} = 4\hat{\boldsymbol{z}} \cdot \boldsymbol{P}$, where $\boldsymbol{P} = \frac{1}{2}(\boldsymbol{\mathcal{E}} \times \boldsymbol{\mathcal{H}}^*)$ is the Poynting vector. Finally, the integral in (3.29) can be rewritten in terms of transversal components because of the internal product with respect to $\hat{\boldsymbol{z}}$:

$$\iint_S \hat{\boldsymbol{z}} \cdot \left(\boldsymbol{\mathcal{E}}_t^{\mu} \times \boldsymbol{\mathcal{H}}_{\boldsymbol{t}}^{\boldsymbol{\nu}\,*} + \boldsymbol{\mathcal{E}}_t^{\nu\,*} \times \boldsymbol{\mathcal{H}}_t^{\mu}\right) \mathrm{d}x\,\mathrm{d}y = 4P\,\delta_{\mu,\nu}, \tag{3.30}$$

where P is the power carried by the mode along the $\hat{\boldsymbol{z}}$ direction.

3.1.3 The Coupling Equations

In general, an arbitrary field in a dielectric waveguide can be represented as a linear combination of radiating and guided modes, where these modes are calculated using the ideal waveguide characterized by $\bar{\boldsymbol{\epsilon}}$. However, the presence of radiating modes can be safely neglected in optical fibers and thus also in this analysis. In particular, using the definition of guided modes in (3.18)-(3.19), the actual field can be described with a finite linear combination of those, as

$$\boldsymbol{E}(x,y,z) = \sum_{\nu} c_\nu(z)\boldsymbol{\mathcal{E}}^{\nu}(x,y), \tag{3.31}$$

$$\boldsymbol{H}(x,y,z) = \sum_{\nu} c_\nu(z)\boldsymbol{\mathcal{H}}^{\nu}(x,y), \tag{3.32}$$

where ν represents a guided mode and c_ν is the corresponding complex coefficient of the combination, also called amplitude. It is worth to note that in each term of the sum the only z dependence is on the coefficient c_ν, while $\boldsymbol{\mathcal{H}}_\nu$ and $\boldsymbol{\mathcal{E}}_\nu$ depend on the transversal coordinate. Therefore the $e^{j\beta_\nu z}$ behavior in (3.18)-(3.19) is included in c_ν, as all the perturbations acting along the waveguide. Consequently, similar expressions of (3.31) and (3.32) hold for the transversal components of the actual fields $\boldsymbol{E}_t$ and $\boldsymbol{H}_t$, namely

$$\boldsymbol{E}_t(x,y,z) = \sum_{\nu} c_\nu(z)\boldsymbol{\mathcal{E}}_t^{\nu}(x,y), \tag{3.33}$$

$$\boldsymbol{H}_t(x,y,z) = \sum_{\nu} c_\nu(z)\boldsymbol{\mathcal{H}}_t^{\nu}(x,y). \tag{3.34}$$

Specifically, for these fields, affected by the real $\boldsymbol{\epsilon}$, the Maxwell's equations for the transversal components in the form of (3.16)-(3.17) still hold. Moreover, using equations (3.20) and (3.21) for guided modes, taking the scalar product with $-\boldsymbol{\mathcal{E}}_t^{\mu\,*}$ and $\boldsymbol{\mathcal{H}}_t^{\mu\,*}$ respectively, summing the two contributions, integrating over section S and exploiting the orthogonality relation in (3.30) yields to the differential equation that describes the evolution of c_μ,

$$\frac{\mathrm{d}c_\mu}{\mathrm{d}z} = -j\left(\beta_\mu c_\mu + \sum_{\nu} K_{\mu\nu} c_\nu\right), \tag{3.35}$$

where $K_{\mu\nu}$ is the coupling rate between mode μ and ν. In terms of longitudinal and transversal components of the electric field $\boldsymbol{\mathcal{E}}$ it is defined as

$$\begin{aligned} K_{\mu\nu} = -\frac{\omega}{4P} \iint_S \Big\{ & \boldsymbol{\mathcal{E}}_t^{\mu\,*} \cdot \Big[\Big(\frac{\boldsymbol{\epsilon}_t \cdot \boldsymbol{\epsilon_z}}{\epsilon_{zz}} - \frac{\bar{\boldsymbol{\epsilon}}_t \cdot \bar{\boldsymbol{\epsilon}}_{\boldsymbol{z}}}{\bar{\epsilon}_{zz}} \Big) - \Big(\boldsymbol{\epsilon}_t - \bar{\boldsymbol{\epsilon}}_t \Big) \Big] \cdot \boldsymbol{\mathcal{E}}_t^{\nu} \\ & - \boldsymbol{\mathcal{E}}_t^{\mu\,*} \cdot \Big(\frac{\bar{\epsilon}_{zz}}{\epsilon_{zz}} \boldsymbol{\epsilon}_t - \bar{\boldsymbol{\epsilon}}_t \Big) \cdot \Big(\frac{\bar{\boldsymbol{\epsilon}}_z}{\bar{\epsilon}_{zz}} \cdot \boldsymbol{\mathcal{E}}_t^{\nu} + \boldsymbol{\mathcal{E}}_z^{\nu} \Big) \\ & + \Big(\bar{\boldsymbol{\epsilon}}_z \cdot \boldsymbol{\mathcal{E}}_t^{\mu\,*} + \bar{\epsilon}_{zz} \boldsymbol{\mathcal{E}}_z^{\mu\,*} \Big) \cdot \Big[\Big(\frac{\bar{\epsilon}_{zz}}{\epsilon_{zz}} - 1 \Big) \Big(\frac{\bar{\boldsymbol{\epsilon}}_z}{\bar{\epsilon}_{zz}} \cdot \boldsymbol{\mathcal{E}}_t^{\nu} + \boldsymbol{\mathcal{E}}_z^{\nu} \Big) \\ & - \Big(\frac{\boldsymbol{\epsilon}_z}{\epsilon_{zz}} - \frac{\bar{\boldsymbol{\epsilon}}_z}{\bar{\epsilon}_{zz}} \Big) \cdot \boldsymbol{\mathcal{E}}_t^{\nu} \Big] \Big\} \, \mathrm{d}x \, \mathrm{d}y \end{aligned} \tag{3.36}$$

In the general case, coupling rate among modes has a very complicated expression. However it can be simplified in the case of slight anisotropy and small difference between $\boldsymbol{\epsilon}$ and $\bar{\boldsymbol{\epsilon}}$, i.e., the actual dielectric tensor is close to the ideal one used to calculated the propagating modes. In this case the coupling rate can be approximated in

$$K_{\mu\nu} = \frac{\omega}{4P} \iint_S \boldsymbol{\mathcal{E}}^{\mu\,*} \cdot \big(\boldsymbol{\epsilon} - \bar{\boldsymbol{\epsilon}} \big) \cdot \boldsymbol{\mathcal{E}}^{\nu} \mathrm{d}x \, \mathrm{d}y. \tag{3.37}$$

3.2 Coupling Mechanisms in Optical Fibers

When it comes to analyze mode coupling in optical fibers different types of perturbations must taken into account. In fact, mode coupling is caused by all the effects that break the cylindrical shape or isotropicity of the ideal fiber. In particular, perturbations can be of two types [GM05]: intrinsic or extrinsic. The former one is due to all the imperfections that occur in the manufacturing, either during the preform production or the drawing. In turn, intrinsic perturbations give raise to two main effects: stress birefringence and geometrical asymmetries. It is important to note that the two come together, in fact a geometrical asymmetry induces intrinsic stress birefringence [Cho00]. Usually the perturbations that causes stress birefringence are core eccentricity, core ellipticity and cladding ellipticity. Where core eccentricity is the displacement of the center of the core with respect to the cladding. While the cladding and core ellipticity measure the departure from roundness for the core and the cladding respectively. The geometrical asymmetries are instead caused only by core ellipticity. Instead, the extrinsic perturbations act when the fiber is spooled in the ground. Examples of those are *twist*, *bend* and subjection to *magnetic field*, however this latter effect is of little interest in optical communications.

Coupling mechanisms in optical fibers can be effectively described by the coupled-mode theory. In particular, given the cylindrical form of the waveguide it is convenient to introduce a cylindrical coordinate system, identified by the triplet $\hat{\boldsymbol{r}}$, $\hat{\boldsymbol{\phi}}$, $\hat{\boldsymbol{z}}$, where $\hat{\boldsymbol{r}}$ represents the radial axis, $\hat{\boldsymbol{\phi}}$ the azimuthal axis and $\hat{\boldsymbol{z}}$ the longitudinal one. Moreover, we consider N modes propagating in a multimode fiber, where these modes can be approximated using the LP modes. Once this assuption has been made, coupling can occur within the same LP group or both within and among different LP groups, the first case is called *weak coupling regime*, while in the latter one we talk about *strong coupling regime*

[PG16][Pal14]. In these settings, assuming slight perturbations in the dielectric tensor, we can recall the approximated result (3.35) of the coupled-mode theory

$$\frac{\mathrm{d}\boldsymbol{c}}{\mathrm{d}z} = -j(\boldsymbol{D} + \boldsymbol{K}) \cdot \boldsymbol{c}, \tag{3.38}$$

where $\boldsymbol{c}(z)$ is the N-dimensional vector of the complex amplitudes, $\boldsymbol{D}$ is the diagonal matrix with the mode propagation constants of the considered modes,

$$\boldsymbol{D} = \begin{pmatrix} \beta_1 & & & \\ & \beta_2 & & \\ & & \ddots & \\ & & & \beta_N \end{pmatrix}, \tag{3.39}$$

and $\boldsymbol{K}(z)$ is the NxN coupling rate matrix, such that

$$\boldsymbol{K} = \begin{pmatrix} K_{1,1} & K_{1,2} & \dots & K_{1,N} \\ K_{2,1} & K_{2,2} & \dots & K_{2,N} \\ \vdots & & \ddots & \vdots \\ K_{N,1} & K_{N,2} & \dots & K_{N,N} \end{pmatrix}. \tag{3.40}$$

In particular, $\boldsymbol{c}$ represents the cumulative coupling along the fiber. In this sense the effect of matrix K is to enhance the coupling, while $\boldsymbol{D}$ counteracts it since is diagonal. This means that coupling within the very same LP group (or manifold) is usually much stronger since their share similar propagation constants according to the modal birefringence analysis of Chapter 2. Matrix $\boldsymbol{K}$ elements are functions of z and their values are given by equation (3.37). In particular, it can be revised using polar coordinates as

$$K_{\mu\nu} = \frac{\omega}{4P} \int_0^{\infty} \int_0^{2\pi} r \boldsymbol{\mathcal{E}}^{\mu\,*} \cdot \tilde{\boldsymbol{\epsilon}} \cdot \boldsymbol{\mathcal{E}}^{\nu} \mathrm{d}\phi\, \mathrm{d}r, \tag{3.41}$$

where $\tilde{\boldsymbol{\epsilon}} = \boldsymbol{\epsilon} - \bar{\boldsymbol{\epsilon}}$. Moreover, the tensor $\tilde{\boldsymbol{\epsilon}}$ represents the perturbation in the dielectric since it is defined as the difference between the actual tensor $\boldsymbol{\epsilon}$ and the ideal one $\bar{\boldsymbol{\epsilon}}$. In particular, $\bar{\boldsymbol{\epsilon}} = \epsilon\, \boldsymbol{I}$, where $\boldsymbol{I}$ is the rank-2 identity tensor and ϵ is the dielectric permittivity either of the core or the cladding. This is simply because LP modes are derived from an ideal isotropic fiber. It is remarkable to note that since $\tilde{\boldsymbol{\epsilon}}$ is symmetric then there is no losses and matrix $\boldsymbol{K}(z)$ is Hermitian.

Recalling the modal theory from Chapter 2, a generic $LP_{n,p}$ mode has the electric field $\boldsymbol{\mathcal{E}}^{n,p}$ that can be written as $\boldsymbol{\mathcal{E}}^{n,p} = \boldsymbol{\mathcal{E}}_t^{n,p} + \mathcal{E}_z^{n,p}\hat{\boldsymbol{z}}$. Specifically

$$\boldsymbol{\mathcal{E}}_t^{n,p}(r,\phi) = f_{n,p}(r) g_n(\phi)\, \hat{\boldsymbol{e}}, \tag{3.42}$$

and

$$\begin{aligned} \mathcal{E}_z^{n,p}(r,\phi) &= -\frac{j}{\beta_{n,p}} \nabla_t \cdot \boldsymbol{\mathcal{E}}_t^{n,p}(r,\phi) \\ &= u_{n,p}(r)\, \nu_n(\phi), \end{aligned} \tag{3.43}$$

where, for the transversal field, $f_{n,p}(r)$ is a Bessel function, $g_n(\phi)$ can be either $\cos(n\phi)$ or $\sin(n\phi)$ and $\hat{\boldsymbol{e}}$ represents the linear polarization of the field, i.e.,

$\hat{\boldsymbol{e}} = \hat{\boldsymbol{x}}$ or $\hat{\boldsymbol{e}} = \hat{\boldsymbol{y}}$. For the longitudinal component, $u_{n,p}(r)$ consists in a linear combination of Bessel functions, while $\nu_n(\phi)$ in a linear combination of sinusoidal terms of argument $(n \pm 1)\phi$. Finally, the power constant P can be set to an unitary value ($P = 1$), since the Poynting vector is equal to

$$\boldsymbol{P} \simeq \frac{\beta_\mu}{2\omega\mu_0} |\boldsymbol{\mathcal{E}}_t^\mu|^2 \, \hat{\boldsymbol{z}}, \tag{3.44}$$

then, the power flow towards $\hat{\boldsymbol{z}}$ is

$$P = \iint_S \boldsymbol{P} \cdot \hat{\boldsymbol{z}} \, \mathrm{d}s, \tag{3.45}$$

and the orthogonality property for LP modes states

$$\frac{\beta_\mu}{2\omega\mu_0} \iint_S \boldsymbol{\mathcal{E}}_t^{\mu\,*} \cdot \boldsymbol{\mathcal{E}}_t^\nu \, \mathrm{d}s = \delta_{\mu\nu}. \tag{3.46}$$

The solution of the integral (3.41) is quite cumbersome. However, to optimize its evaluation it is convenient to introduce a necessary condition for the modes to couple. In order to do so, it is useful to note that coupling can occur between different field components, namely, transversal-transversal coupling, transversal-longitudinal coupling and the longitudinal-longitudinal one. Moreover, the perturbation of the dielectric tensor, expressed in term or cylindrical coordinates, must be periodic with respect to the azimuth variable ϕ, i.e., $\tilde{\boldsymbol{\epsilon}}(r, \phi) = \tilde{\boldsymbol{\epsilon}}(r, \phi + 2\pi)$. Due to this observation, in the most general case, $\tilde{\boldsymbol{\epsilon}}$ is a linear combination of sinusoidal functions with angular frequency $k \in \mathbb{Z}$. Therefore, considering two LP modes defined as (3.42)-(3.43), namely $LP_{n,p}$ and $LP_{m,r}$, there will be coupling if and only if integral (3.41) is different from zero. In particular, this is surely true if at least one of these relations holds [Pal14]:

$$n \pm k \pm m = 0, \tag{3.47}$$

$$n \pm k \pm (m \pm 1) = 0, \tag{3.48}$$

$$(n \pm 1) \pm k \pm (m \pm 1) = 0, \tag{3.49}$$

where they account respectively for coupling among transversal-transversal, transversal-longitudinal, and longitudinal-longitudinal components. These relationships descend from the sinusoidal periodicity with respect of ϕ for both electric fields and perturbations. Therefore, the overall integrating term in (3.41) is also periodic with respect to ϕ, and it can be expressed as a sum of sinusoidal terms which angular frequencies are combinations of n, k and m, that are both integers. Then, the period must be a multiple of 2π, meaning that the integral for ϕ over $[\,0\ 2\pi\,]$ won't vanishes if one among (3.47), (3.48) or (3.49) holds. It is remarkable to point out that this is only a necessary condition to have coupling, theoretically speaking, the value of (3.41) can still go to zero after integration over r, although this is not common. Finally, we note that transverse-transverse coupling is the stronger one since the the longitudinal components are much smaller.

In the next sections different perturbation types have been analyzed, where particular effort has been put in the description of coupling due to the intrinsic perturbations. This choice is justified by the fact that fiber spinning mainly

affects this type of coupling, and it is almost negligible for the extrinsic one. Moreover, all the perturbations in the dielectric tensor have been considered aligned with the reference coordinates of the fiber. The general case will be extended later in the analysis.

3.2.1 Stress Birefringence

Intrinsic perturbation over the fiber can result in a slightly birefringence, this is equivalent to have an anisotropic dielectric. Therefore the perturbation of the dielectric tensor is given by

$$\tilde{\boldsymbol{\epsilon}} = \frac{\delta_\epsilon}{2} \begin{pmatrix} 1 & 0 & 0 \\ 0 & -1 & 0 \\ 0 & 0 & 0 \end{pmatrix}, \tag{3.50}$$

where δ_ϵ represents the strength of the perturbation. From the form of (3.50) and equation (3.41), it follows that coupling can occur only among transversal components. Moreover, the azimuthal order k of (3.50) is zero, therefore the necessary condition in (3.47) allows coupling only among LP modes with the same azimuthal order, namely $n = m$. Exploiting these observations, (3.41) becomes

$$\frac{\omega\delta_\epsilon}{8} \int_0^\infty \int_0^{2\pi} r\left[\left(\mathcal{E}_x^{n,p\,*}\,\mathcal{E}_x^{n,r}\right) - \left(\mathcal{E}_y^{n,p\,*}\,\mathcal{E}_y^{n,r}\right)\right] \mathrm{d}\phi\,\mathrm{d}r. \tag{3.51}$$

Furthermore, the orthogonal conditions for LP modes in (3.46) allows coupling if and only if $p = r$. Then, coupling can occur only among modes within the same LP group and it doesn't affect propagation among different manifolds. Figure 3.1 [Pal14] shows the schematic situation about coupling for the first 4 groups. Where the solid circles represents coupling among transverse components. In particular, looking within each manifolds, i.e., considering also $p = r$, yields

$$\frac{\omega\delta_\epsilon}{8} \iint_S \left(|\mathcal{E}_x^{n,p}|^2 - |\mathcal{E}_y^{n,p}|^2\right)\mathrm{d}s. \tag{3.52}$$

In the case where both the degenerate modes have transversal fields $\hat{\boldsymbol{x}}$ polarized the term $|\mathcal{E}_y^{n,p}|^2$ in (3.52) vanishes and it is possible to exploit the orthogonality property in (3.46). Thus the coupling rate is

$$K_{n,p}^{xx} = \frac{\omega\mu_0\delta_\epsilon}{4\beta_{n,p}} = d, \tag{3.53}$$

where d is called detuning factor. Instead, if the degenerate modes have transversal fields $\hat{\boldsymbol{y}}$ polarized, $|\mathcal{E}_x^{n,p}|^2$ is zero and the coupling rate is $K_{n,p}^{yy} = -d$. Finally, the last two cases are symmetric and involve discordant polarizations, in this scenario the two contributions in the integral are zero and there is no coupling. To summarize, birefringence affects coupling only within each manifolds, and only among transversal component with the same polarization. This leads to the detuning of the y- and x-polarized modes within each LP group. Moreover, if we assume weak birefringence, i.e., $\delta_\epsilon \ll 1$, the detuning factor can be approximates by

$$d \simeq \frac{n_{\mathrm{av}}\pi\Delta n}{n_{\mathrm{eff}}\lambda}, \tag{3.54}$$

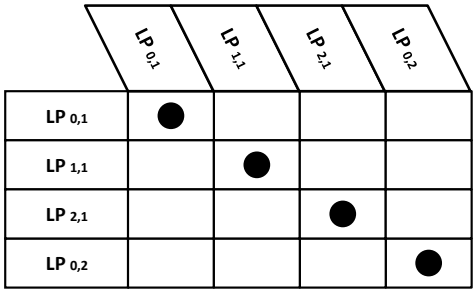

Figure 3.1: Schematic representation of coupling due to stress birefringence for the first 4 LP groups.

where, n_{av} and n_{eff} are respectively the mean and the effective refractive index, λ the wavelength in vacuum and Δn the differences in refractive index birefringence axis. Then, the effect of the birefringence in mode coupling is similar for every LP groups since ratio $n_{\text{av}}/n_{\text{eff}}$ is close to 1 for all the manifolds. Finally, considering the first 4 LP groups ($LP^{0,1}$, $LP^{1,1}$, $LP^{2,1}$ and $LP^{0,2}$) for a total of 12 degenerate modes, the birefringence coupling rate matrix is given by

$$\boldsymbol{K} = \begin{pmatrix}
d & 0 & \dots & & & & & & & \dots & 0 \\
0 & -d & 0 & \dots & & & & & & & \vdots \\
\vdots & 0 & d & 0 & \vdots & & & & & & \\
 & \vdots & 0 & -d & 0 & \vdots & & & & & \\
 & & \vdots & 0 & d & 0 & \vdots & & & & \\
 & & & \vdots & 0 & -d & 0 & \vdots & & & \\
 & & & & \vdots & 0 & d & 0 & \vdots & & \\
 & & & & & \vdots & 0 & -d & 0 & \vdots & \\
 & & & & & & \vdots & 0 & d & 0 & \vdots \\
 & & & & & & & \vdots & 0 & -d & 0 \\
\vdots & & & & & & & \cdots & 0 & d & 0 \\
0 & \dots & & & & & & & \dots & 0 & -d
\end{pmatrix}, \tag{3.55}$$

where the modes are ordered alternating x and y polarization of even modes and then x and y polarizations of odd modes.

3.2.2 Core Ellipticity

A slightly elliptical core represents an intrinsic geometric deformation and it can be represented using a scalar perturbation on the dielectric tensor [Pal14], namely

$$\tilde{\epsilon} = \gamma\, \epsilon\, (n_{\text{co}}^2 - n_{\text{cl}}^2)\, \delta(r-a)\, \cos(2\phi), \tag{3.56}$$

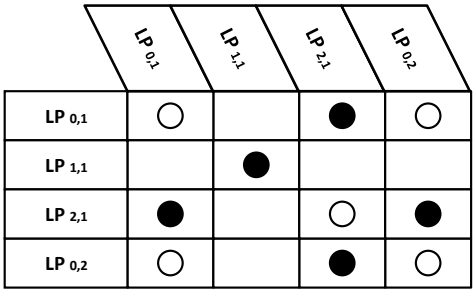

Figure 3.2: Schematic representation of coupling due to core ellipticity for the first 4 LP groups.

where γ is a form factor, ϵ is the isotropic dielectric permittivity, a is the radius of the core, δ is a delta function that becomes 1 whenever $r = a$, $(n_{\text{co}}^2 - n_{\text{cl}}^2)$ is the square of the numerical aperture of the fiber, and n_{co} and n_{cl} are respectively the core and the cladding refractive indeces.

In this case, the coupling could be only between transversal-transversal and longitudinal-longitudinal components since the perturbation is scalar and the modes are linearly polarized. Indeed, the quantity $\boldsymbol{\mathcal{E}}^{n,p\,*} \cdot \tilde{\boldsymbol{\epsilon}} \cdot \boldsymbol{\mathcal{E}}^{m,r}$ in the coupling rate integral (3.41) can be equal to $\tilde{\epsilon}\,(\mathcal{E}_x^{n,p\,*}\,\mathcal{E}_x^{m,r} + \mathcal{E}_z^{n,p\,*}\,\mathcal{E}_z^{m,r})$ or $\tilde{\epsilon}\,(\mathcal{E}_y^{n,p\,*}\,\mathcal{E}_y^{m,r} + \mathcal{E}_z^{n,p\,*}\,\mathcal{E}_z^{m,r})$ or $\tilde{\epsilon}\,\mathcal{E}_z^{n,p\,*}\,\mathcal{E}_z^{m,r}$ depending on the transversal field polarization of the two modes. Owing to this observation, the only necessary conditions that must be checked are those in (3.47) and (3.49). In particular, relation (3.47) yields

$$n = 1, \quad m = 1 \qquad \text{or} \qquad |n - m| = 2, \tag{3.57}$$

and the (3.49) one leads to

$$n = m \qquad \text{or} \qquad |n - m| = 2 \qquad \text{or} \qquad |n - m| = 4, \tag{3.58}$$

This time the orthogonality of LP modes is not useful and thus it is not possible to perform further simplification to solve analytically (3.41). However, before sticking to that, it is useful to observe the situation screened by (3.57) and (3.58) in Figure 3.2 [Pal14], where solid circles and empty circles have been used to represent coupling between transversal and longitudinal components respectively. Observing the figure, it is clear that unlike the stress birefringence perturbation, the coupling occurs both within and among different LP groups. In particular, as we will see in the analytical expressions for the coupling rates, core ellipticity causes both coupling and detuning among degenerate modes in the same group, and coupling among degerate modes in different groups.

The analytical solution of the integral (3.41) is involved. Therefore, it has been reported only the final expression of the coupling rate matrix $\boldsymbol{K}$. Specifically, for the first 12 degenerate modes ordered as in the stress birefringence

case, it yields

$$\boldsymbol{K} = \begin{pmatrix} K_{1,1} & 0 & 0 & 0 & 0 & 0 & K_{1,7} & 0 & 0 & K_{1,10} & K_{1,11} & 0 \\ 0 & K_{2,2} & 0 & 0 & 0 & 0 & 0 & K_{2,8} & K_{2,9} & 0 & 0 & K_{2,12} \\ 0 & 0 & K_{3,3} & 0 & 0 & 0 & 0 & 0 & 0 & 0 & 0 & 0 \\ 0 & 0 & 0 & K_{4,4} & 0 & 0 & 0 & 0 & 0 & 0 & 0 & 0 \\ 0 & 0 & 0 & 0 & K_{5,5} & 0 & 0 & 0 & 0 & 0 & 0 & 0 \\ 0 & 0 & 0 & 0 & 0 & K_{6,6} & 0 & 0 & 0 & 0 & 0 & 0 \\ K_{7,1} & 0 & 0 & 0 & 0 & 0 & K_{7,7} & 0 & 0 & K_{7,10} & K_{7,11} & 0 \\ 0 & K_{8,2} & 0 & 0 & 0 & 0 & 0 & K_{8,8} & K_{8,9} & 0 & 0 & K_{8,12} \\ 0 & K_{9,2} & 0 & 0 & 0 & 0 & 0 & K_{8,9} & K_{9,9} & 0 & 0 & K_{9,12} \\ K_{10,1} & 0 & 0 & 0 & 0 & 0 & K_{10,7} & 0 & 0 & K_{10,10} & K_{10,11} & 0 \\ K_{11,1} & 0 & 0 & 0 & 0 & 0 & K_{11,7} & 0 & 0 & K_{11,10} & K_{11,11} & 0 \\ 0 & K_{12,2} & 0 & 0 & 0 & 0 & 0 & K_{12,8} & K_{12,9} & 0 & 0 & K_{12,12} \end{pmatrix}, \tag{3.59}$$

where the analytical expressions of the coefficients have been computed using a numerical calculus tool and they won't be reported for sake of brevity. A closer look to $\boldsymbol{K}$ and its coefficients shows that there are both intra- and inter-coupling among LP groups. In particular, the intra-coupling are all weak since they involve longitudinal components but for $LP_{1,1}$ where it occurs among transversal ones. Moreover, considering the intra-coupling, it has the same effect of stress birefringence, that is the detuning of the polarizations, but for $LP_{2,1}$ where there is a further cross-coupling among degenerate modes in the manifold.

3.2.3 Twist

Twist is an extrinsic perturbation that effects the permittivity tensor, this is due to the elasto-optical effect of the shear stresses induced by the twist. In this case, the perturbation tensor is

$$\tilde{\boldsymbol{\epsilon}} = g\tau\epsilon n_{\text{av}} r \begin{pmatrix} 0 & 0 & -\sin\phi \\ 0 & 0 & \cos\phi \\ -\sin\phi & \cos\phi & 0 \end{pmatrix}, \tag{3.60}$$

where g ($g \simeq 0.15$) is an elasto-optic coefficient, τ is the twist per unith length, ϵ is the isotropic dielectric permittivity of the ideal fiber and n_{av} is the mean refractive index. Moreover, it should be point out that twist causes an additional physical rotation of the fiber with respect to the reference frame, however this aspect will be treat in a dedicated section.

For the specific composition of the perturbation tensor, coupling can occur only between longitudinal and transversal components. In particular, owing an azimuthal order k equals to 1, the coupling necessary condition in (3.48) yields to

$$n = m \qquad \text{or} \qquad |n - m| = 2, \tag{3.61}$$

that is it occurs among manifolds with the same azimuthal order or with orders differing by 2. The global coupling relationships among LP groups are represented in Figure 3.3, where dashed circles represent coupling between transversal and longitudinal components.

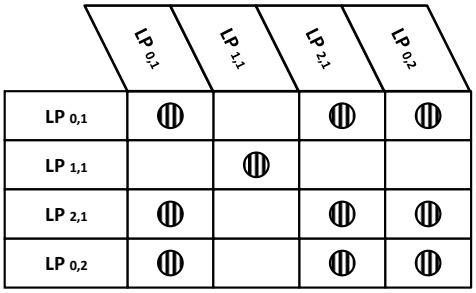

Figure 3.3: Schematic representation of coupling due to twist for the first 4 LP groups.

3.2.4 Bend

Bend is another extrinsic type of perturbation that involves two main physical contributions [UR80]. The first one is a longitudinal stress that stretches the silica in the outer layers of the fiber and compresses it in the inner ones. Instead, the second is a compressive stress exerted from the outer layers to the inner ones but in the direction of the bending radius. In particular, assuming that the bend occurs on the z-y plane, the perturbation of the first contribution on the dielectric tensor is

$$\tilde{\boldsymbol{\epsilon}}_z = -\kappa n_{\text{av}}^4 r \cos\phi \begin{pmatrix} q_1 & 0 & 0 \\ 0 & q_1 & 0 \\ 0 & 0 & q_2 \end{pmatrix}, \tag{3.62}$$

while for the second one it can be approximated as

$$\tilde{\boldsymbol{\epsilon}}_x = \frac{1}{2}\kappa^2 a^2 n_{\text{av}}^4 \begin{pmatrix} q_2 & 0 & 0 \\ 0 & q_1 & 0 \\ 0 & 0 & q_1 \end{pmatrix}, \tag{3.63}$$

where κ is the curvature, i.e., the inverse of the bending radius, n_{av} is the average refractive index and q_1, q_2 are two suitable coefficients. Specifically, their values are given by $q_1 = (1-\nu)p_{1,2} - \nu p_{1,1}$ and $q_2 = p_{1,1} - 2\nu p_{1,2}$, where $\nu = 0.164$ is the Poisson ratio of fused silica and $p_{1,1} = 0.121$, $p_{1,2} = 0.270$ are its elasto-optical coefficients.

Regarding the type of coupling, it can occur only between transversal-transversal and longitudinal-longitudinal components since $\tilde{\boldsymbol{\epsilon}}_z$ and $\tilde{\boldsymbol{\epsilon}}_x$ are both diagonal. However, the necessary condition to couple yields different results for the two contribution. This is because (3.62) and (3.63) have different azimuthal orders ($k_z = 1$ and $k_x = 0$). Applying the necessary conditions (3.47) and (3.48) on (3.62) leads to

$$|n-m| = 1, \tag{3.64}$$

$$|n-m| = 1 \qquad \text{or} \qquad |n-m| = 3, \tag{3.65}$$

for the transverse and the longitudinal coupling respectively. Similarly, the same conditions on (3.63) read

$$n = m, \tag{3.66}$$

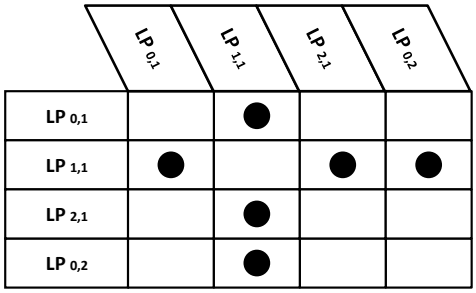

Figure 3.4: Schematic representation of coupling due to bend first contribution for the first 4 LP groups.

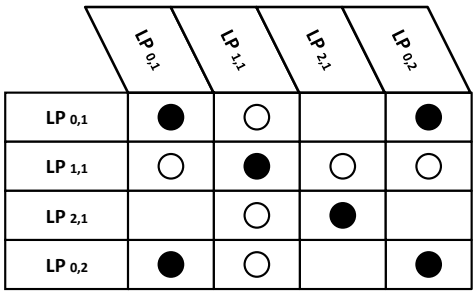

Figure 3.5: Schematic representation of coupling due to bend second contribution for the first 4 LP groups.

$$|n - m| = 1. \tag{3.67}$$

Finally, the relationships highlighted by the two pair of equations are represented in Figure 3.4 and Figure 3.5 respectively.

3.2.5 Magnetic Field

The presence of a magnetic field with a component oriented along the $\hat{\boldsymbol{z}}$ direction causes coupling among modes. Indeed this is an extrinsic type of perturbation that should be taken into account. Although external magnetic fields are not common in optical communication they are intensively used in fiber optic sensing.

Specifically, a polarization rotation occurs whenever an optical fiber is subjected to a magnetic field with a non-negligible component along its longitudinal axis. This is called Faraday's effect and its result can be described by means of

a perturbation of the dielectric tensor. Namely,

$$\tilde{\boldsymbol{\epsilon}} = j\frac{\lambda n_{\text{av}} B_z V}{\pi}\begin{pmatrix} 0 & 1 & 0 \\ -1 & 0 & 0 \\ 0 & 0 & 0 \end{pmatrix}, \tag{3.68}$$

where n_{av} is the mean refractive index, B_z is the magnetic field component involved in the Faraday's effect and $V \simeq 0.6\text{rad/T/m}$ is the Verdet constant. This case is very similar to the one of stress birefringence. Indeed, the coupling relations among LP groups are the ones depicted in Figure 3.1, where coupling occurs only among degenerate manifolds with respect to the transversal components.

3.2.6 Perturbation with Arbitrary Orientation

Until now all the perturbations have been analyzed with a fixed orientation, parallel to the reference frame of the fiber. However, as a general result, the coupling matrices with respect to an arbitrary frame can be derived from the ones of the previous sections [Pal14].

Considering an electromagnetic field propagating in a fiber, it can be represented as a linear combination of LP modes defined with respect to a reference frame $\{\hat{\boldsymbol{x}}', \hat{\boldsymbol{y}}'\}$, let $\boldsymbol{c}'$ be the vector coefficients of such combination. Similarly, the field can be represented through a vector $\boldsymbol{c}$ by using LP modes based on a different reference frame $\{\hat{\boldsymbol{x}}, \hat{\boldsymbol{y}}\}$, where we assume the second reference frame rotated by an angle of θ in a clockwise direction with respect to the first one. In particular, a change in the reference frame cannot modify the physics of the problem, therefore the only possible effect is a shuffle within each LP group since there is no coupling among different manifolds. Owing to these observations and ordering the modes by alternating x and y polarization of even and odd modes, vector $\boldsymbol{c}_{n,p}$ can be derived from $\boldsymbol{c}'_{n,p}$ as

$$\boldsymbol{c}_{n,p} = \boldsymbol{R}_n(\theta)\boldsymbol{c}'_{n,p}, \tag{3.69}$$

where matrix $\boldsymbol{R}_n(\theta)$ assumes different forms depending on the value of the azimuthal order n. In particular, for a 2-fold-degenerate mode as $LP_{0,p}$ matrix $\boldsymbol{R}_0(\theta)$ is

$$\boldsymbol{R}_0(\theta) = \begin{pmatrix} \cos\theta & -\sin\theta \\ \sin\theta & \cos\theta \end{pmatrix}. \tag{3.70}$$

Instead, considering the case of 4-fold-degenerate group, i.e., $n \geq 1$, $\boldsymbol{R}_n(\theta)$ can be written as the product of two matrices,

$$\begin{aligned} \boldsymbol{R}_n(\theta) = &\begin{pmatrix} \cos\theta & -\sin\theta & 0 & 0 \\ \sin\theta & \cos\theta & 0 & 0 \\ 0 & 0 & \cos\theta & -\sin\theta \\ 0 & 0 & \sin\theta & \cos\theta \end{pmatrix} \\ &\begin{pmatrix} \cos(n\theta) & 0 & -\sin(n\theta) & 0 \\ 0 & \cos(n\theta) & 0 & -\sin(n\theta) \\ \sin(n\theta) & 0 & \cos(n\theta) & 0 \\ 0 & \sin(n\theta) & 0 & \cos(n\theta) \end{pmatrix}. \end{aligned} \tag{3.71}$$

Specifically, equation (3.70) represents a rotation in polarization within the manifold of the $LP_{0,p}$ modes, and similarly, the first term of (3.71) is a rotation

in polarization with respect to even and odd modes sub-manifolds. Conversely, the second term in (3.71) represents the rotation of the field pattern with respect to the azimuthal order n. Therefore the matrices $\boldsymbol{R}_0(\theta)$ and $\boldsymbol{R}_n(\theta)$ can be seen as a rigid rotation by an angle θ of a 2-fold-degenerate and a 4-fold-degenerate group respectively. Finally, we observe that both the two types of matrix are orthogonal.

Vectors $\boldsymbol{c}'$ and $\boldsymbol{c}$ will be the concatenation of all the $\boldsymbol{c}'_{n,p}$ and $\boldsymbol{c}_{n,p}$ vectors respectively. For example, considering the first 4 LP groups: $\boldsymbol{c} = (\boldsymbol{c}_{0,1}, \boldsymbol{c}_{1,1}, \boldsymbol{c}_{1,2}, \boldsymbol{c}_{0,2})$ and $\boldsymbol{c}' = (\boldsymbol{c}'_{0,1}, \boldsymbol{c}'_{1,1}, \boldsymbol{c}'_{1,2}, \boldsymbol{c}'_{0,2})$. Thus, it is possible to introduce a similar expression of (3.69), namely

$$\boldsymbol{c} = \boldsymbol{R}(\theta)\boldsymbol{c}', \tag{3.72}$$

where $\boldsymbol{R}(\theta) = \mathrm{diag}(\boldsymbol{R}_{i_1}(\theta), \boldsymbol{R}_{i_2}(\theta), \ldots, \boldsymbol{R}_{i_N}(\theta))$ is a block diagonal matrix with i_j the azimuthal orders of the considered LP groups. In particular, its expression descends from (3.70) and (3.71) considering the fact that a change of reference frame cannot cause coupling among non-degenerate modes. Keeping on the example with the first 4 LP groups, the overall matrix will be $\boldsymbol{R}(\theta) = \mathrm{diag}(\boldsymbol{R}_0(\theta), \boldsymbol{R}_1(\theta), \boldsymbol{R}_1(\theta), \boldsymbol{R}_0(\theta))$.

Finally, it is possible to find the relationship between a coupling rate matrix $\boldsymbol{K}'$, referred to the reference frame $\{\hat{\boldsymbol{x}}', \hat{\boldsymbol{y}}'\}$, and the same one $\boldsymbol{K}$ but derived using another reference frame $\{\hat{\boldsymbol{x}}, \hat{\boldsymbol{y}}\}$. The relation simply follows from the differential equation in (3.38) considered with $\boldsymbol{c}$ as in (3.72). In particular, it lays

$$\boldsymbol{K} = \boldsymbol{R}^T(\theta)\, \boldsymbol{K}'\, \boldsymbol{R}(\theta). \tag{3.73}$$

Therefore, all the previous coupling rate matrices $\boldsymbol{K}'$ calculated with respect to a perturbation aligned with the fiber reference frame are consistent and can be easily adapted for every orientation of the perturbation.

3.2.7 Combined Perturbations

Up to now it has been analyzed the effect of different types of perturbation when they act alone. However, in a more realistic scenario they are concurrently present along the fiber. To treat the general case, it is sufficient to note that for the equations provided by the coupled-mode theory in (3.38) and (3.41) the superposition of effects holds. Therefore it is sufficient to consider the sum of each coupling rate matrix calculated as they would act individually.

However, a special situation occurs in the case of twist. In fact this effect causes also a physical rotation with respect to the reference frame that is not caught by its coupling rate matrix. In particular, let $\boldsymbol{K}_{\mathrm{u}}(z)$ the untwisted coupling rate matrix, where the dependency over z allows evolution for the orientation of the perturbations along the fiber. Then, if the fiber is also affected by twist the overall coupling rate matrix will read

$$\boldsymbol{K}(z) = \boldsymbol{R}^T(\alpha(z))\, \boldsymbol{K}_{\mathrm{u}}(z)\, \boldsymbol{R}(\alpha(z)) + \boldsymbol{K}_{\mathrm{twist}}(z), \tag{3.74}$$

where $\alpha(z) = \int_0^z \tau(s)\,\mathrm{d}s$ and $\tau(z)$ is the twist rate.

Chapter 4

Propagation in Multimode Fibers

Once that the modal-coupled theory has been disentangled, it is possible to describe the propagation in multimode fibers. In this sense, specific field patterns of the generalized Jones space exist and they are called principal modes of propagation [FK05]. In particular, they are states that propagate undistorted and set the dispersion properties of the fiber through an $N \times N$ Hermitian matrix $\boldsymbol{Q}$. The evolution of this matrix is ruled by a differential relation called *dynamic equation* that depends on the coupling conditions [AM12]. Moreover the dispersion can be defined in terms of DGD or root-mean square modal dispersion [PG16]. Finally, all the above relations can be expressed using an isomorphic space, the so-called generalized Stokes space [AM12].

4.1 Principal States and Modal Dispersion

We consider a narrow band signal, centered in ω_0 and propagating in a multimode optical fiber by means of N modes (each degenerate mode counted independently). Let $\boldsymbol{E}(x, y, z)$ be the electromagnetic field in the medium, then it can be expressed as a superposition of the N guided modes where its complex amplitudes are the components of the *state vector* $|c(z)\rangle \in \mathbb{C}^N$, that represents the excitation of each different mode. In particular, it is given by

$$|c(z)\rangle = \begin{pmatrix} c_1(z) \\ c_2(z) \\ \vdots \\ c_N(z) \end{pmatrix}. \tag{4.1}$$

Then, the state vector describes the field in the so-called *generalized Jones space*, that extends the concept of Jones vector of single mode propagation [AM12][GK00]. For convenience, at the input of the fiber, $|c(z_0)\rangle$ can be assumed normalized, that is

$$\langle c(z_0)|c(z_0)\rangle = 1, \tag{4.2}$$

where $\langle c(z)| = |c(z)\rangle^H$ and ^{H} represents the Hermitian conjugate operation.

Let's now assume that from the input of the fiber a field $|c(z_0)\rangle$ propagates along the z direction, with amplitude $\mathcal{A}(z,\omega)$ that represents the spectral information along the fiber. The propagation along the fiber can be associated with a complex $N \times N$ linear operator $\boldsymbol{T}$ since optical fibers act like linear systems under the assumption of lower power transmission. In general, matrix $\boldsymbol{T}$ is function of space and frequency: $\boldsymbol{T}(z,\omega)$. The relation between an input field $\mathcal{A}(z_0,\omega)\,|c(z_0)\rangle$ and the output one $\mathcal{A}(z,\omega)\,|c(z)\rangle$ is given by

$$\mathcal{A}(z,\omega)\,|c(z)\rangle = \boldsymbol{T}(z,\omega)\mathcal{A}(z_0,\omega)\,|c(z_0)\rangle\,, \tag{4.3}$$

where $\boldsymbol{T}(z,\omega)$ describes the propagation and the coupling effects from point z_0 to z along the fiber. Neglecting medium and mode-dependent losses, matrix $\boldsymbol{T}$ can be represented as

$$\boldsymbol{T}(z,\omega) = e^{-j\kappa(z,\omega)}\,\boldsymbol{U}(z,\omega), \tag{4.4}$$

where the $e^{-j\kappa(z,\omega)}$ is a scalar representing a common phase change and $\boldsymbol{U}$ is a $N \times N$ Jones matrix representing the interactions among modes during the propagation. Then, the overall input-output relation becomes

$$\mathcal{A}(z,\omega)\,|c(z)\rangle = e^{-j\kappa(z,\omega)}\,\boldsymbol{U}(z,\omega)\mathcal{A}(z_0,\omega)\,|c(z_0)\rangle\,. \tag{4.5}$$

Moreover, $\boldsymbol{U}(z,\omega)$ can be considered unitary since we are neglecting propagation losses in the fiber, that is $\boldsymbol{U}^H\boldsymbol{U} = \boldsymbol{U}\boldsymbol{U}^H = \boldsymbol{I}\ \forall\,\omega$. In fact given the conservation of energy and exploiting (4.5) yields

$$\begin{aligned} |\mathcal{A}(z,\omega)|^2 &= \langle c(z)|\mathcal{A}^*(z,\omega)\mathcal{A}(z,\omega)|c(z)\rangle \\ &= \langle c(z_0)|\mathcal{A}^*(z_0,\omega)\boldsymbol{U}^H(z,\omega)\boldsymbol{U}(z,\omega)\mathcal{A}(z_0,\omega)|c(z_0)\rangle \\ &= \langle c(z_0)|\mathcal{A}^*(z_0,\omega)\mathcal{A}(z_0,\omega)|c(z_0)\rangle = |\mathcal{A}(z_0,\omega)|^2. \end{aligned} \tag{4.6}$$

In such scenario, a special propagation modes called *principal modes* can be defined [FK05]. In particular, the principal modes of the fiber are special field states $|\Psi_i\rangle$ such that given in input $|\Psi_i(z_0)\rangle$ the corresponding output principal state $|\Psi_i(z)\rangle$ is independent from frequency at the first order, that is

$$\frac{\partial\,|\Psi_i\rangle}{\partial\omega} = 0. \tag{4.7}$$

Then, principal states of propagation are fundamentals to describe the dispersion properties of the transmission. Considering the input-output relation in (4.5) for a principal state $|\Psi\rangle$ and taking the derivative with respect to ω lays

$$\frac{\partial\mathcal{A}(z,\omega)}{\partial\omega}\,|\Psi_i(z)\rangle = e^{-j\kappa(z,\omega)}\Big(-j\frac{\partial\kappa}{\partial\omega}\,\boldsymbol{U} + \frac{\partial\boldsymbol{U}}{\partial\omega}\Big)\,|\Psi_i(z_0)\rangle \tag{4.8}$$

where it has been assumed $\mathcal{A}(z_0,\omega) = 1$. Furthermore, expressing $|\Psi_i(z_0)\rangle$ as a function of $|\Psi_i(z)\rangle$ by using (4.5) yields

$$|\Psi_i(z_0)\rangle = \mathcal{A}(z,\omega)\boldsymbol{U}^H(z,\omega)e^{j\kappa(z,\omega)}\,|\Psi_i(z)\rangle\,, \tag{4.9}$$

substituting this expression in (4.8) leads to

$$j\frac{\partial\boldsymbol{U}}{\partial\omega}\,\boldsymbol{U}^H\,|\Psi_i(z)\rangle = j\Big(\frac{1}{\mathcal{A}(z,\omega)}\frac{\partial\mathcal{A}(z,\omega)}{\partial\omega} + j\frac{\partial\kappa}{\partial\omega}\Big)\,|\Psi_i(z)\rangle\,. \tag{4.10}$$

Equation (4.10) represents an eigenvalue-eigenvector relation, in fact, defining $\boldsymbol{Q}(z,\omega)$ and $\tau_i(z,\omega)$ as

$$\boldsymbol{Q}(z,\omega) = j\frac{\partial \boldsymbol{U}}{\partial \omega}\boldsymbol{U}^H(z,\omega), \tag{4.11}$$

$$\tau_i(z,\omega) = j\Big(\frac{1}{\mathcal{A}(z,\omega)}\frac{\partial \mathcal{A}(z,\omega)}{\partial \omega} + j\frac{\partial \kappa}{\partial \omega}\Big), \tag{4.12}$$

we have the meaningful relation

$$\boldsymbol{Q}(\omega,z)\,|\Psi_i(z)\rangle = \tau(z,\omega)\,|\Psi_i(z)\rangle\,. \tag{4.13}$$

In particular, $\tau_i(z,\omega)$ is a scalar quantity and represents an eigenvalue of matrix $\boldsymbol{Q}(z,\omega)$, while the principal state $|\Psi_i(z)\rangle$ is the corresponding eigenvector. Moreover is it possible to show that the eigenvectors τ_i are real quantities since matrix $\boldsymbol{Q}$ is Hermitian. This is directly related to the unitarity of $\boldsymbol{U}$, in fact, since must be $\boldsymbol{U}\boldsymbol{U}^H = \boldsymbol{I}$ then

$$\frac{\partial(\boldsymbol{U}\boldsymbol{U}^H)}{\partial \omega} = 0 \quad \Longrightarrow \quad j\frac{\partial \boldsymbol{U}}{\partial \omega}\boldsymbol{U}^H = -j\boldsymbol{U}\frac{\partial \boldsymbol{U}^H}{\partial \omega}, \tag{4.14}$$

and these relations yield trivially to $\boldsymbol{Q} = \boldsymbol{Q}^H$ by using (4.11). As a consequence, the eigenvectors $|\Psi_i(z)\rangle$, that represent principal states, form an orthonormal basis. Therefore each possible pattern fields $|c(z)\rangle$ can be expressed as a linear combination of these principal states. Moreover matrix $\boldsymbol{Q}(z,\omega)$ expressed as (4.11) completely defines the evolution of the $\boldsymbol{U}$ operator over frequency, by means of the differential equation

$$\frac{\partial \boldsymbol{U}}{\partial \omega} = -j\boldsymbol{Q}(z,\omega)\boldsymbol{U}(z,\omega), \tag{4.15}$$

then all the modal dispersion properties are enclosed in $\boldsymbol{Q}$ and, in particular, its eigenvalues τ_i assume the meaning of group delays.

4.1.1 Example

To show that the last statement is indeed true, it is proposed a simplified example of propagation in a multimode fiber. In particular, let's consider the propagation of an narrow band pulse shape identified by its complex envelope $\boldsymbol{A}(z_0,t)$, as input of a fiber with length L. The propagation from the beginning to the end of the fiber is ruled by matrix $\boldsymbol{U}(L,\omega)$. That, in turn it is described by matrix $\boldsymbol{Q}(L,\omega)$. Assuming $\boldsymbol{Q}$ approximately constant in frequency, i.e., $\boldsymbol{Q}(\omega) \simeq \boldsymbol{Q}_0$, the expression of the propagation matrix $\boldsymbol{U}$ is straightforward by using (4.15), that is

$$\boldsymbol{U}(L,\omega) = e^{-j\boldsymbol{Q}_0\omega}\,\boldsymbol{U}(L,\omega_0), \tag{4.16}$$

where ω_0 is the central frequency of the narrow band transmitted signal.

In the frequency domain, the complex envelope at the input may be represented as $\mathcal{A}(\omega)$ with state field $|c(z_0)\rangle$, where it is common to assume $|c(z_0)\rangle$ frequency independent. Then, exploiting (4.5) and (4.16) the output spectrum turns out to be

$$\mathcal{A}(\omega)\,e^{j\kappa(L,\omega)}e^{-j\boldsymbol{Q}_0\omega}\,\boldsymbol{U}(L,\omega_0)\,|c(z_0)\rangle\,, \tag{4.17}$$

where $\kappa(L,\omega)$ can be approximated through its Taylor polynomial, stopped at the first order as

$$\kappa(L,\omega) \simeq \kappa(L,\omega_0) + \omega \frac{\partial \kappa}{\partial \omega}\Big|_{w=0} = \kappa_0 + \kappa_1 \omega. \tag{4.18}$$

In the time domain, the output pulse is given by the inverse Fourier transform

$$\boldsymbol{A}(L,t) = \frac{1}{2}\int_{-\infty}^{\infty} \mathcal{A}(\omega) e^{-j(\kappa_0+\kappa_1\omega)} e^{-j\boldsymbol{Q}_0\omega} \boldsymbol{U}(L,\omega_0)\,|c(z_0)\rangle\, e^{j\omega t}\,\mathrm{d}\omega, \tag{4.19}$$

where the term $|c(z_0)\rangle$ is mapped in the output state $|c(L)\rangle$ by $\boldsymbol{U}(L,\omega_0)$. In particular, this last state vector can be expressed using a linear combination of principal states $|\Psi_i(L)\rangle$, namely

$$|c(L)\rangle = \sum_{i=1}^{N} \psi_i\,|\Psi_i(L)\rangle\,. \tag{4.20}$$

Owing these observations, equation (4.21) can be rewritten as

$$\boldsymbol{A}(L,t) = \frac{1}{2} e^{-j\kappa_0} \sum_{i=1}^{N} \psi_i \int_{-\infty}^{\infty} \mathcal{A}(\omega) e^{j(t-\kappa_1)\omega} e^{-j\boldsymbol{Q}_0\omega}\,|\Psi_i(L)\rangle\,\mathrm{d}\omega, \tag{4.21}$$

finally observing that $\Psi_i(L)$ are eigenvectors of $\boldsymbol{Q}_0$, and that for exponential matrices it holds

$$\boldsymbol{Q}_0\,|\Psi_i\rangle = \tau_i\,|\Psi_i\rangle \quad \Longrightarrow \quad e^{\boldsymbol{Q}_0}\,|\Psi_i\rangle = e^{\tau}\,|\Psi_i\rangle\,, \tag{4.22}$$

the output pulse is given by

$$\begin{aligned} \boldsymbol{A}(L,t) &= \frac{1}{2} e^{-j\kappa_0} \sum_{i=1}^{N} \psi_i \int_{-\infty}^{\infty} \mathcal{A}(\omega) e^{j(t-\kappa_1-\tau_i)\omega}\,|\Psi_i(L)\rangle\,\mathrm{d}\omega \\ &= e^{-j\kappa_0} \sum_{i=1}^{N} \psi_i A(t-\kappa_1-\tau_i)\,|\Psi_i(L)\rangle\,. \end{aligned} \tag{4.23}$$

Then at the output, N superposed clones of the signal arrive, each one delayed by τ_i from the temporal center of the pulse $t-\kappa_1$.

Although the example depicts an oversimplified scenario, it captures a fundamental aspect of the real propagation: the modal dispersion of the signal. This parameter is usually measured using the *differential group delay* (DGD), that is defined as

$$\Delta\tau = \max\{\mathrm{eig}(\boldsymbol{Q})\} - \min\{\mathrm{eig}(\boldsymbol{Q})\}. \tag{4.24}$$

In multimode transmission this is a key metric because its value directly affect the length of equalization filter at the MIMO receiver. It is worth to note that the dispersion of the system can be measured using a second parameter, called *root mean square modal dispersion* and defined as

$$\tau = \left(N \sum_i \tau_i^2\right)^{1/2}. \tag{4.25}$$

Even if this last parameter doesn't affect directly the complexity of the SDM system it is much more usable from a theoretically prospective since $\tau^2 = N\,\mathrm{Tr}(\boldsymbol{Q}^2)$. Ultimately, it is possible to note that for $N = 2$, the two parameter $\Delta\tau$ and τ coincide, that happens when only the first manifold propagates affected by PMD.

Also the assumption of $\boldsymbol{Q} \simeq \boldsymbol{Q}_0$ is consistent with the narrow band signal hypothesis, indeed this approximation is enough to capture the analysis of the modal dispersion (MD). Finally the example fails to consider the evolution of matrix $\boldsymbol{Q}$ along the fiber. Indeed it is strongly influenced by the Maxwell's equations and therefore on the physical and geometrical properties of the actual medium. Then in such scenario, coupling effects and modal birefringence will play a key role in the spacial evolution of $\boldsymbol{Q}$.

4.2 The Dynamic Equation

To catch the evolution properties of matrix $\boldsymbol{Q}$ it is necessary to characterized the complex $N \times N$ Jones matrix $\boldsymbol{U}$ also from a spacial point of view. Specifically, its evolution directly descends from the coupled-mode theory. In fact, adapting (3.38) with the generalized Jones vector notation for a pattern field $|c\rangle$ leads to

$$\frac{\partial\,|c\rangle}{\partial z} = -j\,(\boldsymbol{D} + \boldsymbol{K}(z))\,|c(z)\rangle\,, \tag{4.26}$$

where we recall that $\boldsymbol{D}$ is a $N \times N$ diagonal matrix independent form z, with the propagation constants of each mode. $\boldsymbol{K}(z)$ is an Hermitian $N \times N$ coupling matrix whose components represent the coupling rate among modes at position z along the fiber.

Exploiting the linear propagation by using the Jones matrix $\boldsymbol{U}$ as in (4.5) and naming matrix $\boldsymbol{B}$ as $\boldsymbol{B} = \boldsymbol{D} + \boldsymbol{K}$ yields to an expression for the evolution of $\boldsymbol{U}$ with respect to z, namely

$$\frac{\partial \boldsymbol{U}}{\partial z} = -j\,\boldsymbol{B}(z,\omega)\boldsymbol{U}(z,\omega), \tag{4.27}$$

where of course $\boldsymbol{B}(z,\omega)$ is space and frequency dependent. Similarly to the case of $\boldsymbol{Q}$, matrix $\boldsymbol{B}(z,\omega)$ can be defined as

$$\boldsymbol{B}(z,\omega) = j\frac{\partial \boldsymbol{U}}{\partial z}\boldsymbol{U}^H(z,\omega), \tag{4.28}$$

and therefore also $\boldsymbol{B}$ must be Hermitian to preserve the unitarity of $\boldsymbol{U}$. Regarding the differential equation in (4.27), it is useful to define two parameters for $\boldsymbol{D}$ and $\boldsymbol{K}$ to catch the overall behavior of $\boldsymbol{U}(z,\omega)$. In particular, we define the *coupling strength* and the overall *modal birefringence* as

$$\Delta k = \max\{\mathrm{eig}(\boldsymbol{K})\} - \min\{\mathrm{eig}(\boldsymbol{K})\}, \tag{4.29}$$

$$\Delta\beta = \max\{\mathrm{eig}(\boldsymbol{D})\} - \min\{\mathrm{eig}(\boldsymbol{D})\}, \tag{4.30}$$

where the first quantity in (4.29) represents the strength of the coupling and the second one in (4.30) highlights the intrinsic birefringence in mode propagations constants. Moreover, since $\boldsymbol{D}$ is a diagonal matrix its eigenvalues are exactly

in the diagonal. It is important to note that this two quantities are in contrast to each other in the overall coupling effect because of (4.26). Indeed, as noted in Section 3, while $\boldsymbol{K}$ enhances the coupling along the fiber, $\boldsymbol{D}$ emphasize the mode differentiation. Finally, Δk and $\Delta\beta$ can be equivalently defined in term of beat lengths. In particular, the *coupling beat length* is defined as $L_C = 2\pi/\Delta k$ while the *modal beat length* as $L_M = 2\pi/\Delta\beta$.

Equations (4.15) and (4.27) put in relation the evolution of the generalized Jones matrix $\boldsymbol{U}$ in terms of ω and z by means of other two matrices, namely $\boldsymbol{Q}(z,\omega)$ and $\boldsymbol{B}(z,\omega)$. Then, it is possible to analyze how their evolutions both in frequency and space affect each other. First of all, let's consider an ensemble of two concatenated fibers characterized by $\boldsymbol{U}_1$ and $\boldsymbol{U}_2$ respectively, then the matrix describing their concatenation will be $\boldsymbol{U} = \boldsymbol{U}_2\boldsymbol{U}_1$. The definitions of matrices $\boldsymbol{Q}_1$ and $\boldsymbol{Q}_2$ for the two splices are given in equation (4.11). Then, the expression of matrix $\boldsymbol{Q}$ at the end of fiber will be

$$\boldsymbol{Q} = j\frac{\partial \boldsymbol{U}}{\partial \omega}\boldsymbol{U}^H, \tag{4.31}$$

that can be further handled minding the fact that $\partial\boldsymbol{U}/\partial\omega = \partial\boldsymbol{U}_2/\partial\omega\,\boldsymbol{U}_1 + \boldsymbol{U}_2\,\partial\boldsymbol{U}_1/\partial\omega$. Finally, the expression for $\boldsymbol{Q}$ in terms of $\boldsymbol{Q}_1$ and $\boldsymbol{Q}_2$ is given by

$$\boldsymbol{Q} = \boldsymbol{Q}_2 + \boldsymbol{U}_2\boldsymbol{Q}_1\boldsymbol{U}_2^H, \tag{4.32}$$

that is, the value of matrix $\boldsymbol{Q}$ at the end of the fiber is given by the one of the first slice rotated by matrix $\boldsymbol{U}$ and added to the one of the second slice.

Now, we can consider a special case of this concatenation, where a small addition Δz in the length of the fiber is put beside to a first slice of length z, whose propagation is represented by $\boldsymbol{U}(z)$. Then, assuming Δz small enough, $\boldsymbol{U}(z+\Delta z,\omega)$ can be approximated using a first order approximation as

$$\boldsymbol{U}(z+\Delta z) \simeq \boldsymbol{U}(z) + \frac{\partial \boldsymbol{U}}{\partial z}\Delta z, \tag{4.33}$$

where the ω dependency has been omitted for sake of notation. At this point, exploiting in the last equation the differential relation of (4.27) yields to

$$\boldsymbol{U}(z+\Delta z) = (\boldsymbol{I} - j\boldsymbol{B}\Delta z)\boldsymbol{U}(z). \tag{4.34}$$

Furthermore, the total Jones matrix $\boldsymbol{U}(z+\Delta z)$ is given by the matrices product of the two slices, namely

$$\boldsymbol{U}(z+\Delta z) = \Delta\boldsymbol{U}(z)\,\boldsymbol{U}(z), \tag{4.35}$$

where $\boldsymbol{U}(z)$ and $\Delta\boldsymbol{U}(z)$ describe the propagation for both the first slice from 0 to z and the differential second one from z to Δz respectively. Comparison of (4.35) and (4.34) yields an expression for accounting the length addition Δz in term of operator $\boldsymbol{U}$, that is:

$$\Delta\boldsymbol{U}(z) = \boldsymbol{I} - j\boldsymbol{B}\Delta z. \tag{4.36}$$

Finally, exploiting (4.36) in (4.32) leads to the dynamic equation that describes the cause-effect relation between mode coupling and modal dispersion,

represented by matrices $\boldsymbol{B}$ and $\boldsymbol{Q}$ respectively. In particular, for the insertion of a slice of length Δz, it yields

$$\Delta_z \boldsymbol{Q} = \boldsymbol{Q} + j\big(\boldsymbol{QB} - \boldsymbol{BQ}\big)\Delta z + \boldsymbol{BQB}\Delta z^2, \tag{4.37}$$

where $\Delta_z \boldsymbol{Q}$ represents a variation of $\boldsymbol{Q}$ along the z direction. Moreover, it is possible to neglect the last term of the right side of the equation, since it represents an higher order infinitesimal if Δz is small enough. Then, owing to (4.15) and (4.27) it possible to note that matrices $\boldsymbol{Q}$ and $\boldsymbol{B}$ are linked by the relation $\boldsymbol{Q}\,\Delta w = \boldsymbol{B}\,\Delta z$. These observations allow to rewrite (4.37) as

$$\frac{\Delta_z \boldsymbol{Q}}{\Delta z} = \frac{\Delta_\omega \boldsymbol{B}}{\Delta \omega} + j\big(\boldsymbol{QB} - \boldsymbol{BQ}\big). \tag{4.38}$$

Ultimately, taking the limit of $\Delta z \longrightarrow 0$ lays the differential *dynamic equation*

$$\frac{\partial \boldsymbol{Q}}{\partial z} = \frac{\partial \boldsymbol{B}}{\partial \omega} + j\big(\boldsymbol{QB} - \boldsymbol{BQ}\big). \tag{4.39}$$

4.3 The Generalized Stokes Space

All the previous relations can be considered in a space isomorphic to the generalized Jones space of dimension N, the so called *generalized Stokes space*. In particular, this isomorphic space originates as a way to describe $N \times N$ Hermitian matrices, as an extension of the Pauli-matrix formalism used in the polarization mode dispersion [AM12]. Specifically, an $N \times N$ Hermitian matrix $\boldsymbol{H}$, in our case either $\boldsymbol{Q}$ or $\boldsymbol{B}$, is such that $H_{jk} = H^*_{kj}$. This means that the diagonal elements must be real and the others come in complex conjugate pairs, then $\boldsymbol{H}$ is fully defined by using N^2 real number. This observation is useful to describe the matrix as a linear combination of others. In particular, if we consider the linear space of the $N \times N$ Hermitian matrices, its bases are formed by N^2 elements (note that elements in the space are matrices too). From all the possible bases it is convenient to choose one like

$$\left\{\boldsymbol{I}, \quad \boldsymbol{\Lambda_1}, \quad \boldsymbol{\Lambda}_2, \quad \ldots, \quad \boldsymbol{\Lambda}_{N^2-1}\right\}, \tag{4.40}$$

where $\boldsymbol{I}$ is the $N \times N$ identity matrix and $\boldsymbol{\Lambda}_i$ are $N \times N$ complex matrices such that

$$\frac{1}{N}\,\mathrm{Tr}\left(\boldsymbol{\Lambda}_i \boldsymbol{\Lambda}_j\right) = \delta_{ij}, \tag{4.41}$$

$$\mathrm{Tr}\left(\boldsymbol{\Lambda}_i\right) = 0 \quad \forall i. \tag{4.42}$$

Where (4.42) is the traceless property and (4.41) is called trace orthogonality condition, that can be shown to induce an inner product in the linear space of the Hermitian matrices. Now that a basis has been formally defined, each possible $N \times N$ Hermitian matrix $\boldsymbol{H}$ can be expressed as a linear combination of the elements in (4.40). Specifically,

$$\boldsymbol{H} = \frac{1}{N}\Big(\eta_0 \mathbf{1} + \boldsymbol{\eta} \cdot \boldsymbol{\Lambda}\Big), \tag{4.43}$$

where η_0 and $\boldsymbol{\eta}$ are a real valued number and a real vector of $N^2 - 1$ elements respectively, and $\boldsymbol{\Lambda}$ is the vector of matrices defined as

$$\boldsymbol{\Lambda} = \left(\boldsymbol{\Lambda}_1, \quad \boldsymbol{\Lambda}_2, \quad \ldots, \quad \boldsymbol{\Lambda}_{N^2-1}\right). \tag{4.44}$$

Then, the dot product in (4.43) is the readily extension of the classic one, taking into account that elements in $\boldsymbol{\eta}$ and $\boldsymbol{\Lambda}$ are real scalars and complex matrices respectively. Once $\boldsymbol{H}$ has been defined as in (4.43) it is possible to extract the coefficients of the corresponding linear combination as

$$\eta_0 = \mathrm{Tr}\left(\boldsymbol{\Lambda}_i \boldsymbol{H}\right), \tag{4.45}$$

$$\boldsymbol{\eta} = \mathrm{Tr}\left(\boldsymbol{H}\right), \tag{4.46}$$

where for the first relation the linearity of the trace has been simply exploited, while for the second one, the linearity has been joined with the trace orthogonality condition in (4.41).

For matrices $\boldsymbol{Q}$ and $\boldsymbol{B}$ it is possible to exploit the expression in (4.43) leading to two linear combinations, namely

$$\boldsymbol{Q} = \frac{1}{N}\left(\tau_0 \boldsymbol{I} + \boldsymbol{\tau} \cdot \boldsymbol{\Lambda}\right), \tag{4.47}$$

$$\boldsymbol{B} = \frac{1}{N}\left(\beta_0 \boldsymbol{I} + \boldsymbol{\beta} \cdot \boldsymbol{\Lambda}\right), \tag{4.48}$$

where the frequency and the longitudinal dependencies of $\boldsymbol{Q}$, $\boldsymbol{B}$, $\boldsymbol{\tau}$, $\boldsymbol{\beta}$, β_0 and τ_0 have been omitted for shortness of notation. Moreover, it must be $\tau_0 = 0$ and $\beta_0 = 0$ since $\boldsymbol{Q}$ and $\boldsymbol{B}$ are traceless. This property results from the unitarity of the Jones matrix $\boldsymbol{U}$, indeed it is possible to express $\boldsymbol{U}$ as a function of $\boldsymbol{Q}$ or $\boldsymbol{B}$ using a first order approximation. For example using the expression of matrix $\boldsymbol{Q}$ in (4.11) yields

$$\boldsymbol{U} = e^{-j\boldsymbol{Q}_0\omega}\boldsymbol{U}_0, \tag{4.49}$$

where it has been indicated $\boldsymbol{U}(z, \omega_0)$ with $\boldsymbol{U}_0$. Recalling that the property of unitarity can be expressed as $\det \boldsymbol{U} = 1$, and that $\det \boldsymbol{U} = \det(e^{-j\boldsymbol{Q}_0\omega}) \det \boldsymbol{U}_0$, the unitarity condition imposes that

$$\det(e^{-j\boldsymbol{Q}_0\omega}) = 1 \quad \Longrightarrow \quad e^{\mathrm{Tr}(\boldsymbol{Q}_0)} = 1, \tag{4.50}$$

that lays $\mathrm{Tr}(\boldsymbol{Q}_0) = 0$. Observing that a very similar approach can be taken for matrix $\boldsymbol{B}$, the two matrices can be rewritten as

$$\boldsymbol{Q} = \frac{1}{N}\left(\boldsymbol{\tau} \cdot \boldsymbol{\Lambda}\right), \tag{4.51}$$

and

$$\boldsymbol{B} = \frac{1}{N}\left(\boldsymbol{\beta} \cdot \boldsymbol{\Lambda}\right), \tag{4.52}$$

where $\boldsymbol{\tau}$ and $\boldsymbol{\beta}$ uniquely represent matrices $\boldsymbol{Q}$ and $\boldsymbol{B}$ respectively. If they hadn't been traceless they still would have been defined by $\boldsymbol{\tau}$ and $\boldsymbol{\beta}$ but for the addition of a common term τ_0 and β_0 in the diagonal. The close relationship between each matrix and the correspondent vector of dimension $N^2 - 1$ let represent $\boldsymbol{Q}$ and $\boldsymbol{B}$ by means of $\boldsymbol{\tau}$ and $\boldsymbol{\beta}$ in an isomorphic vector space of dimension $D = N^2 - 1$, called *generalized Stokes space*:

$$\begin{aligned} \boldsymbol{Q} &\longrightarrow \boldsymbol{\tau}, \\ \boldsymbol{B} &\longrightarrow \boldsymbol{\beta}. \end{aligned} \tag{4.53}$$

If we want to describe the propagation in an optical fiber using the generalized Stoke space, then we need to represent also the state vectors that define the pattern fields. But is it possible to the represent an arbitrary $|c\rangle$ state field using a generalized Stokes vector? The answer is yes, and the solution is to use the projection operator. A projector for the state vector $|c\rangle$ is a self-adjoint function defined by means of the dyadic operator as $|c\rangle\langle c|$, therefore it is uniquely determined. Since it is self-adjoint it is possible to show that its representative matrix is Hermitian and then can be rewritten using (4.43) as

$$|c\rangle\langle c| = \frac{1}{N}\big(\boldsymbol{I} + \boldsymbol{c}\cdot\Lambda\big), \tag{4.54}$$

where it has been placed $c_0 = 1$ since $|c\rangle\langle c|$ has two types of eigenvalues, 1 with 1-fold degeneracy to which corresponds eigenstate $|c\rangle$ and 0 with (N-1)-fold degeneracy to which corresponds eigenstates orthogonal to $|c\rangle$. However, c_0 is a common value for all the state vectors then it is possible to identify $|c\rangle$ using the generalized Stokes vector $\boldsymbol{c}$:

$$|c\rangle \longrightarrow \boldsymbol{c} \tag{4.55}$$

In particular, in order to switch from $|c\rangle$ to $\boldsymbol{c}$ it can be exploited the relation in (4.46), that yields

$$c_i = \mathrm{Tr}\left(\boldsymbol{\Lambda_i}\,|c\rangle\langle c|\,\right) = \langle c|\boldsymbol{\Lambda_i}|c\rangle\,, \tag{4.56}$$

where c_i is the i-th component of vector $\boldsymbol{c}$ and in the second equality it has been used a well known property of trace. In a more compact vectorial form, equation (4.56) can be rewritten as $\boldsymbol{c} = \langle c|\boldsymbol{\Lambda}|c\rangle$.

Moreover, in order to catch some important relationships between the two spaces it is important to evaluate how the scalar product in the Jones space is mapped in the correspondent Stokes one. Before to do this, it is useful to note that the following relation

$$\frac{1}{N}\,\mathrm{Tr}\left((\boldsymbol{c}\cdot\boldsymbol{\Lambda})(\boldsymbol{a}\cdot\boldsymbol{\Lambda})\right) = \boldsymbol{c}\cdot\boldsymbol{a} \tag{4.57}$$

holds, simply by considering the extended definition of the scalar product explained before, and the trace orthogonality among matrices $\boldsymbol{\Lambda}_i$ defined in (4.41). Then the modulus square of the braket operator between two state vectors in the Jones space is defined as

$$|\,\langle c|a\rangle\,|^2 = \langle c|a\rangle\langle c|a\rangle = \mathrm{Tr}\left(\,|c\rangle\langle c|\,|a\rangle\langle a|\,\right), \tag{4.58}$$

where for the last equality it has been used the same trace property as in (4.56). Then exploiting (4.57) it yields

$$|\,\langle c|a\rangle\,|^2 = \frac{1}{N}\big(1 + \boldsymbol{c}\cdot\boldsymbol{a}\big). \tag{4.59}$$

The above relation is quite powerful and links the braket operator in the Jones spaces to the scalar product in the Stokes one, nevertheless it will be very useful to infer interesting properties between the two space. In particular, four of those are going to be useful in our analysis:

- The first property regards the magnitude of a Stokes vector to which corresponds a state vector in the Jones space. Specifically, considering a normalized state vector $|c\rangle$ and exploiting relation (4.59) we would have

$$1 = |\langle c|c\rangle|^2 = \frac{1}{N}\big(1 + \boldsymbol{c}\cdot\boldsymbol{c}\big), \tag{4.60}$$

that brings to $|\boldsymbol{c}|^2 = N - 1$. This means that all the Stokes vector that have a correspondent Jones vector can be represented in a sphere of radius $(N-1)^{1/2}$. In particular, in the case of $N = 2$, Jones vectors represent the states of polarization (SOP) of the field and it can be represented in a unitary norm sphere, called Poincaré sphere.

- The second property instead is about the relation between two orthogonal state vectors $|c\rangle$ and $|a\rangle$ and their counterpart Stokes ones. Again exploiting property (4.59) yields

$$0 = |\langle c|a\rangle|^2 = \frac{1}{N}\big(1 + \boldsymbol{c}\cdot\boldsymbol{a}\big) \quad \Longrightarrow \quad \boldsymbol{c}\cdot\boldsymbol{a} = -1. \tag{4.61}$$

Then recalling that $\boldsymbol{c}\cdot\boldsymbol{a} = |\boldsymbol{c}||\boldsymbol{a}|\cos\alpha$, where α is the angle between the two vectors, it is possible to find a relation that α must satisfied for the orthogonality of the two state vectors. In particular, (4.61) leads to $\cos\alpha = -1/(N-1)$, and only in the case in which $N = 2$ the two Stokes vector are antipodal in the Poincaré sphere.

- The third property is a direct consequence of the first two ones. In particular, they result in determining a bound for the scalar product $\boldsymbol{c}\cdot\boldsymbol{a}$ whenever the two vectors come from a suitable pair of state vectors $|c\rangle$ and $|a\rangle$. Specifically, they yield

$$0 \leq |\langle c|a\rangle|^2 \leq 1 \quad \Longrightarrow \quad -1 \leq \boldsymbol{c}\cdot\boldsymbol{a} \leq N - 1. \tag{4.62}$$

Then, observing (4.62) it is possible to note that not all the vectors in the Stokes space have a correspondent state vector in the Jones one. By contradiction, if this would be the case then $\boldsymbol{c}\cdot\boldsymbol{a} \geq -1$ for all the possible combinations of $\boldsymbol{c}$ and $\boldsymbol{a}$ in the space. But this is not always true, since for the second property it should be $(N-1)\cos\alpha \geq -1\ \forall\alpha$. Actually this last relation holds only for $N = 2$, that is the only case in which for each vector in the Stokes space corresponds a state vector in the Jones one. To be convinced of that we can take the case in which $\boldsymbol{c}$ and $\boldsymbol{a} = -\boldsymbol{c}$ are considered. In such case $\boldsymbol{c}\cdot\boldsymbol{a} = -N - 1$, that would be grater or equal than -1 only if $N \leq 2$.

- The last property regards the link between a vector $\boldsymbol{s}$ in the Stokes space and the $N\times N$ complex matrix $(\boldsymbol{s}\cdot\boldsymbol{\Lambda})$ in the Jones field. In general, there is not an evident relation as $\boldsymbol{s}$ could even not have a legitimate state vector, but for the case in which $N = 2$, where $\boldsymbol{s}$ and $-\boldsymbol{s}$ are eigenvectors of $(\boldsymbol{s}\cdot\boldsymbol{\Lambda})$ with eigenvalues $|\boldsymbol{s}|$ and $-|\boldsymbol{s}|$ respectively. However, for an arbitrary N it can be outlined some general considerations. In particular, let $|\Psi_i\rangle$ be an eigenstate of matrix $(\boldsymbol{s}\cdot\boldsymbol{\Lambda})$ and θ_i its correspondent eigenvalue, then the eigenvalue equation yields

$$(\boldsymbol{s}\cdot\boldsymbol{\Lambda})\ |\Psi_i\rangle = \theta_i\ |\Psi_i\rangle\,. \tag{4.63}$$

Pre-multiplying equation (4.63) by $\langle\Psi_i|$ and using the relation in (4.56) leads to

$$\boldsymbol{s}\cdot\boldsymbol{\Psi_i}=\theta_i, \tag{4.64}$$

where $\boldsymbol{\Psi_i}$ is the Stokes representation of the Jones state $|\Psi_i\rangle$. Specifically, this relation shows that the eigenstate, which has the Stokes equivalent vector more aligned with vector $\boldsymbol{s}$, corresponds to the higher eigenvalue.

Moreover, a further conclusion can be made in this sense, and it involves the pre-multiplication by $(\boldsymbol{s}\cdot\boldsymbol{\Lambda})$ of the both members in (4.63). In particular, it yields

$$(\boldsymbol{s}\cdot\boldsymbol{\Lambda})^2\ |\Psi_i\rangle=\theta_i^2\ |\Psi_i\rangle\,, \tag{4.65}$$

that is $|\Psi_i\rangle$ is also eigenstate for $(\boldsymbol{s}\cdot\boldsymbol{\Lambda})^2$ with corresponding eigenvalue equals to θ_i^2. Then, noting that the trace of $(\boldsymbol{s}\cdot\boldsymbol{\Lambda})^2$ is the sum of the θ_i^2s, and recalling (4.57) leads to the important relation

$$|\boldsymbol{s}|^2=\frac{1}{N}\sum_{i=1}^{N}\theta_i^2. \tag{4.66}$$

The above properties can be used to infer equivalent relations in the generalized Stokes space with respect to the generalized Jones one. In particular, considering matrix $\boldsymbol{Q}$ as in (4.51) and recalling that $|\Psi_i\rangle$ is a principal state of propagation if (4.13) holds, it can be deducted the following relation between $(\boldsymbol{\tau}\cdot\boldsymbol{\Lambda})$ and $|\Psi_i\rangle$. That is

$$(\boldsymbol{\tau}\cdot\boldsymbol{\Lambda})\ |\Psi_i\rangle=N\tau_i\ |\Psi_i\rangle\,, \tag{4.67}$$

meaning that $|\Psi_i\rangle$ is an eigenstate for $(\boldsymbol{\tau}\cdot\boldsymbol{\Lambda})$ with eigenvalue $N\tau_i$, where τ_i has the sense of group delay as seen before. Then exploiting (4.64) for the Stokes space, it yields

$$\boldsymbol{\tau}\cdot\boldsymbol{\Psi_i}=N\tau_i, \tag{4.68}$$

where $\boldsymbol{\Psi_i}$ is the corresponding Stokes vector of the principal state $|\Psi_i\rangle$. Equation (4.68) highlights how the modal dispersion $\Delta\tau$ depends on the orientations of the vectors $\boldsymbol{\Psi_i}$ that correspond to principal states. Indeed, if all these vectors are similarly aligned then the modal dispersion is limited, conversely if they have very different orientations then $\Delta\tau$ would burst. Moreover, it is also possible to bound the values taken by the group delay τ_i in relation to the magnitude of $\boldsymbol{\tau}$. In fact, using (4.68) and noting that $|\boldsymbol{\Psi_i}|=(N-1)^{1/2}$ leads to

$$-\frac{|\boldsymbol{\tau}|(N-1)^{1/2}}{N}\ \leq\tau_i\leq\ \frac{|\boldsymbol{\tau}|(N-1)^{1/2}}{N}. \tag{4.69}$$

Finally, a last consideration about the group delays can be made in term of root-mean square modal dispersion τ. In particular, by exploiting (4.66) with $\theta_i^2=N^2\tau_i^2$ it yields

$$|\boldsymbol{\tau}|^2=N\sum_{i=1}^{N}\tau_i^2=\tau^2, \tag{4.70}$$

that is the root-mean square modal dispersion τ is equal to the magnitude of the corresponding Stokes vector $\boldsymbol{\tau}$ of the operator $\boldsymbol{Q}$ in the Jones space.

The generalized Stokes space can be used to also to check other relations deduced before. For example, to verify that $\boldsymbol{U}_2\boldsymbol{Q}_1\boldsymbol{U}_2^H$ in (4.32) is actually a rotation it is sufficient to check that the magnitude of the correspondent Stokes vector of the rotated matrix $\boldsymbol{Q}_R$ is equal the one of $\boldsymbol{Q}_1$. Indeed, it becomes very easy exploiting (4.57) and writing

$$|\boldsymbol{\tau}_R|^2 = \frac{1}{N}\operatorname{Tr}\left(\boldsymbol{Q}_R^2\right) = \frac{1}{N}\operatorname{Tr}\left(\boldsymbol{U}_2\boldsymbol{Q}_1^2\boldsymbol{U}_2^H\right) = \frac{1}{N}\operatorname{Tr}\left(\boldsymbol{Q}_1^2\right) = |\boldsymbol{\tau}_1|^2, \tag{4.71}$$

where $\boldsymbol{\tau}_R$ and $\boldsymbol{\tau}_1$ are the Stokes representations for $\boldsymbol{Q}_R$, and $\boldsymbol{Q}_1$ respectively. Note that for the third equality has been used the trace invariance properties with respect to rotations.

Finally, the concept of generalized Stokes space can be expanded by introducing a *cross-product* operator $\times$. In order to do this it is useful to introduce the matrix $j(\boldsymbol{\Lambda}_i\boldsymbol{\Lambda}_j - \boldsymbol{\Lambda}_j\boldsymbol{\Lambda}_i)/2N$ that is also traceless and Hermitian. Therefore, exploiting (4.43) it can be rewritten as $\sum_k f_{i,j,k}\boldsymbol{\Lambda}_{\boldsymbol{k}}$, where $f_{i,j,k}$ has been set as

$$f_{i,j,k} = \frac{j}{N^2}\operatorname{Tr}\left(\boldsymbol{\Lambda}_k(\boldsymbol{\Lambda}_i\boldsymbol{\Lambda}_j - \boldsymbol{\Lambda}_j\boldsymbol{\Lambda}_i)\right). \tag{4.72}$$

Then the generalized cross product can be defined as

$$\boldsymbol{a}\times\boldsymbol{b} = \sum_{i,j,k} f_{i,j,k}a_ib_j\boldsymbol{e}_k. \tag{4.73}$$

Using this notation the dynamic equation in (4.39) can be carried in the context of the Stokes vectors. In particular it yields

$$\frac{\partial\boldsymbol{\tau}}{\partial z} = \frac{\partial\boldsymbol{\beta}}{\partial\omega} + \boldsymbol{\beta}\times\boldsymbol{\tau}, \tag{4.74}$$

where $\boldsymbol{\tau}$ and $\boldsymbol{\beta}$ are the correspondent Stokes vector of the operators $\boldsymbol{Q}$ and $\boldsymbol{B}$ in the Jones space. Ultimately, also the differential relationships in (4.15) and (4.27) can be converted using the cross product as

$$\frac{\partial\boldsymbol{c}}{\partial\omega} = \boldsymbol{\tau}\times\boldsymbol{c}, \tag{4.75}$$

$$\frac{\partial\boldsymbol{c}}{\partial z} = \boldsymbol{\beta}\times\boldsymbol{c}, \tag{4.76}$$

where Stokes vector $\boldsymbol{c}$ is the equivalent of state vector $|c\rangle$ in the Jones space.

Chapter 5

Modal Dispersion in Multimode Spun Fibers

The spinning process consists of rotating the fiber during the drawing to enhance the intrinsic mode coupling effects along the fiber. Spin was widely studied for single mode transmission ($N = 2$) as a way to mitigate Polarization Mode Dispersion (PMD), and now there's an open question about its effectiveness if applied to the context of multimode transmission.

In particular, the spinning is applied during the manufacturing as shown in Figure 5.1 [Pal15a]. A cylindric preform, having the very same structure and refractive indices of the desired fiber to draw, is mounted on top of a drawing tower. Then a furnace heats the preform in such way the silica starts to softer and drops by gravity. During this phase all the suitable coatings are applied and also the desired spin can be forced by means of a spinner. Finally, a bobbin is in charge of taking up the fiber at the bottom of the tower in such a way the desired fiber diameter is achieved. Since the rotation induced by the spinning occurs in the so-called neck down, where the silica still is in a viscous state, in first approximation, spin doesn't apply an additional torsional stress to the fiber. The only effect is just a rotation of it by an angle $A(z)$ [PG16][Pal14]. Specifically, the *spin profile* $A(z)$ is the the angle of which the fiber is rotated at each point and its derivative $\mathrm{d}A/\mathrm{d}z$ is called *spin rate*. It is useful to note that an unspun fiber can be modeled as a spun one with constant profile equals to 0, i.e., $A(z) = 0$. Many are the possible spin profiles, but in general the most commonly used are of two types, the unidirectional profiles and the periodic ones. In the *unidirectional* spin profile the fiber angle of rotation is modeled as

$$A(z) = \frac{2\pi}{P} z, \tag{5.1}$$

where P is called spin pitch. In this case the spin rate is constant and equal to $2\pi/P$. However, the by far most used spun type is the periodic one, characterized by a spin profile such that $A(z) = A(z + P)$, where the period of the spin P is again called spin pitch. In this case the spin rate is no more constant but varies with a shape that depends on $A(z)$. An example of periodic spin profile is the sinusoidal one, defined as

$$A(z) = A_0 \sin\Big(\frac{2\pi}{P} z\Big), \tag{5.2}$$

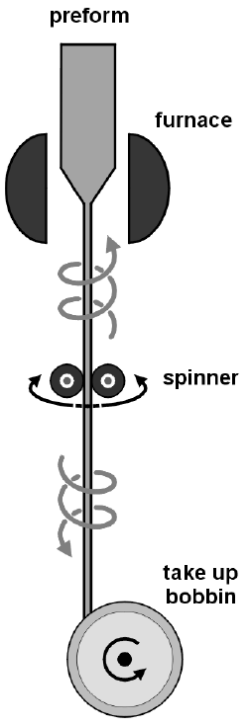

Figure 5.1: The spinning process [Pal15a].

where A is the amplitude of the spin. For this profile, the spin rate is simply given by $2\pi A\cos(2\pi z/P)/P$.

To catch the effect that spinning has in the modal dispersion it is necessary to model the process from a mathematical point of view. According to the coupling theory in Section 3, spin can be modeled as a perturbation in the fiber. However, since it doesn't introduce torsion stresses the coupling rate matrix $\boldsymbol{K}(z)$ remains unchanged but for a rotation of the reference frame of the fiber equals to the spin angle $A(z)$. In particular, considering LP modes and recalling the effect that rotation has on the coupling rate matrix in equation (3.73) it yields [Pal14][PG14]

$$\boldsymbol{K}_s(z) = \boldsymbol{R}^T(A(z))\boldsymbol{K}_u(z)\boldsymbol{R}^T(A(z)), \tag{5.3}$$

where $\boldsymbol{K}_s$ and $\boldsymbol{K}_u$ are the spun and unspun coupling rate matrix respectively and $\boldsymbol{R}$ is the modes rotation matrix as defined in (3.72).

In order to evaluate the effectiveness of the spinning process in term of the dispersion properties of the fiber, it is useful to introduce the *spin-induced reduction factor* (SIRF) defined as the ration between the mean DGD of the fiber and the mean DGD that the fiber would have if it were not spun. Moreover, the SIRF is defined with respect to the mean DGD because of the randomness of perturbations that act on different fibers. Owing to its definition, the parameter can be written as

$$\text{SIRF} = \frac{E[\Delta\tau]}{E[\Delta\tau_{\text{u}}]}, \tag{5.4}$$

where $E[\Delta\tau_{\mathrm{u}}]$ indicates the mean DGD of the unspun fiber. By inspection of (5.4), the spin is effective in reducing the mean DGD of the fiber only if the SIRF < 1. Specifically, lower the SIRF and higher is the effectiveness of the modal dispersion mitigation.

A similar factor can be defined with respect to the root mean square modal dispersion τ, namely

$$\mathrm{SIRF}_{\mathrm{rms}} = \sqrt{\frac{E[\tau^2]}{E[\tau_{\mathrm{u}}^2]}}. \tag{5.5}$$

As for the case of the root mean square modal dispersion, the $\mathrm{SIRF}_{\mathrm{rms}}$ has not a direct physical meaning but it is likely to be more easy to be evaluated considering an analytical solution of the problem.

As stated before, spinning is widely used in single mode fibers to induce a reduction of the DGD $\Delta\tau$. In this case spin forces the x- and y-polarized modes of the $LP_{0,1}$ to couple, recovering "on average" the ideal symmetry of the fiber [PG16]. In particular, the effect of the spin in single mode transmission (N=2) has been analytically resolved [Pal06], thus it is important to briefly review this special case before going into the general one of multimode transmission.

5.1 Polarization Mode Dispersion in Single-Mode Spun Fibers

In case of single mode transmission, $LP_{0,1}$ group is the only one to propagate. In particular, since it is made by two degenerate modes, $LP_{0,1}^x$ and $LP_{0,1}^y$, that eventually will detune because of coupling, the actual number of propagating modes is $N = 2$. Therefore recalling the theory in Chapter 4, the state vector in the Jones space is made by two complex components, and in the particular case in which $N = 2$, it is also called *state of polarization* (SOP) since uniquely describes the polarization of the field along the fiber. In order to understand the evolution of the SOP it is convenient to study the problem in the isomorphic space of the Stokes vectors. In particular, let $\boldsymbol{s}(z,\omega)$ be the three dimensional vector representing the SOP, then $\boldsymbol{s}$ lies in the Poincaré sphere of unit radius.

Moreover, the evolution of $\boldsymbol{s}(z,\omega)$ is described by equation 4.76, namely

$$\frac{\partial \boldsymbol{s}(z,\omega)}{\partial z} = \boldsymbol{\beta}(z,\omega) \times \boldsymbol{s}(z,\omega) \tag{5.6}$$

where $\boldsymbol{\beta}(z,\omega)$ is the three dimensional birefringence vector describing the evolution of the SOP with respect to z in the Stokes space. Moreover, it is customary to assume that there is not circular birefringence in telecommunication fibers, therefore the third component of $\boldsymbol{\beta}$ is zero, i.e., $\beta_3(z,\omega) = 0\ \forall z,\omega$ [Pal06].

In order to grasp the evolution of vector $\boldsymbol{s}$ it is fundamental to characterized the birefringence vector from a statistical point of view. In particular, due to the perturbations acting along the fiber, the birefringence vector $\boldsymbol{\beta}$ can be described as a stochastic process. Thus, it is defined by its correlation matrix

$$\boldsymbol{R}_{\boldsymbol{\beta}}(z,u) = E\big[\boldsymbol{\beta}(z-u)\boldsymbol{\beta}^T(z)\big], \tag{5.7}$$

where the frequency dependence has been omitted for sake of notation. Moreover, further assuming the process wide-sense stationary (WSS) and each component independent and identically distributed (i.i.d.) let the correlation matrix

to be rewritten as

$$\boldsymbol{R}_{\boldsymbol{\beta}}(u) = r_\beta(u)\,\boldsymbol{I}, \tag{5.8}$$

where $r_\beta(u)$ is the autocorrelation function for a single component. Moreover, it is useful to introduce the following quantities to better describe the evolution of $\boldsymbol{s}$ according to the statistics of $\boldsymbol{\beta}$:

- The first parameter is the root-mean square magnitude of $\boldsymbol{\beta}$ and it is defined as

$$\epsilon = \left(E\left[\,|\boldsymbol{\beta}(z)|^2\right]\right)^{1/2} = \sqrt{2\,r_\beta(0)} = \frac{2\pi}{L_B}, \tag{5.9}$$

  where L_B represents the fiber beat length, that is the mean length for the SOP to complete an evolution period. Therefore, greater is L_F and lower will be the evolution of the state of polarization.

- Instead the second quantity is the birefringence correlation length L_F that describes how fast the birefringence vector $\boldsymbol{\beta}$ evolves. It can be written as

$$L_F = \frac{1}{r_\beta(0)} \int_0^\infty r_\beta(u)\,\mathrm{d}u = \frac{1}{\rho}, \tag{5.10}$$

  where ρ is called birefringence decay rate. In particular ρ and L_F describe the scale in which $\boldsymbol{\beta}$ evolves, if ρ is large then L_F is small and the evolution of the birefringence vector will be very fast. Conversely, if ρ is small then L_F is large and the evolution will be on a larger spatial scale.

In the case of spun optical fibers, the decay rate ρ can be shown to be very large $\rho \gg \epsilon$ [Pal06]. Thus we are interested in study equation (5.6) in this particular case. First of all, it is useful to provide a qualitatively picture of the behavior of $\boldsymbol{s}$ by the analysis of equation (5.6). Specifically, assuming the birefringence vector constant, i.e. $\rho = 0$, condition almost met for polarization maintaining fibers, then the state of polarization, that lies on the Poincaré sphere, draws circular paths around the birefringence vector at a speed proportional to ϵ. However this is not the case of spun fibers, indeed since $\rho \gg \epsilon$, while $\boldsymbol{s}(z)$ is rotating around $\boldsymbol{\beta}(z)$ at speed ϵ the latter changes very fast orientation moving along the fiber. Thus, the overall evolution of the SOP will be characterized by small fast oscillations superposed to a slow drift. This result descends from a powerful theorem proved by Papanicolaou and Kohler in [PK74].

Between the two evolutions we are interested only in the slow one. Indeed, it is possible to show that the dispersion dynamics are fully described by this component of $\boldsymbol{s}$. Under these observations, exploiting the Papanicolaou and Kohler theorem, the slow evolution of the SOP can be described with the equivalent relation

$$\frac{\partial \boldsymbol{s}(z,\omega)}{\partial z} = \boldsymbol{\beta}_E(z,\omega) \times \boldsymbol{s}(z,\omega), \tag{5.11}$$

where $\boldsymbol{\beta}_E(z,\omega)$ is the equivalent birefringence vector and in many cases it has a form much simpler than the complete one.

For a spun fiber with negligible circular birefringence, the evolution along z of the birefringence vector can be written as

$$\boldsymbol{\beta}(z) = \begin{pmatrix} \cos\left(2A(z)\right) & -\sin\left(2A(z)\right) & 0 \\ \sin\left(2A(z)\right) & \cos\left(2A(z)\right) & 0 \\ 0 & 0 & 1 \end{pmatrix} \boldsymbol{b}(z), \tag{5.12}$$

where $A(z)$ is the spin profile and $\boldsymbol{b}(z)$ is the intrinsic random birefringence vector of the fiber, which components can be considered WSS and i.i.d.. In particular, in order to proceed with the analysis, it is useful to assume the spin profile $A(z)$ statistically independent from $\boldsymbol{b}$ and such that also $\boldsymbol{\beta}(z)$ is WSS. Actually, this condition is verified by many kind of profiles as the periodic ones. Then, the expression of the correlation matrix in (5.8), for a spun fiber, can be rewritten as

$$\boldsymbol{R}_{\boldsymbol{\beta}}(u) = \begin{pmatrix} c(u) & x(u) & 0 \\ -x(u) & c(u) & 0 \\ 0 & 0 & 0 \end{pmatrix}, \tag{5.13}$$

where $c(u)$ and $x(u)$ are the correlation and cross-correlation functions respectively and their expressions are given by

$$c(u) = r(u)E\big[\cos\big(2\,A(z) - 2A(z-u)\big)\big], \tag{5.14}$$

$$x(u) = r(u)E\big[\sin\big(2\,A(z) - 2A(z-u)\big)\big], \tag{5.15}$$

where $r(u)$ is the autocorrelation function of the intrinsic random birefringence vector components.

At this point, exploiting the Papanicolaou and Kohler theorem leads to the expression for the equivalent birefringence vector

$$\boldsymbol{\beta}_E(z) = \begin{pmatrix} \sqrt{2\mu}\,\xi_1(z) \\ \sqrt{2\mu}\,\xi_2(z) \\ -\gamma \end{pmatrix}, \tag{5.16}$$

where $\xi_1(z)$ and $\xi_2(z)$ are two independent Gaussian white noises with unitary power. While μ and γ are two coefficients defined as

$$\mu = \int_0^\infty c(u)\,\mathrm{d}u, \tag{5.17}$$

$$\gamma = \int_0^\infty x(u)\,\mathrm{d}u. \tag{5.18}$$

It is important to note that, quite strangely, the equivalent birefringence vector has a deterministic circular component that is different form 0 in the general case. This means that the propagation properties of spun fibers are in general different form the unspun ones. Nevertheless, for the spin profiles such that $\gamma = 0$, as the sinusoidal one, the spun fibers behave like the unspun ones but with different dispersion properties. Moreover, it will be useful to note that as μ and γ have been defined in (5.17) and (5.18), μ is always positive and lower than the corresponding value it would have if the fiber were not spun, while γ can be either positive or negative or equal to zero in the case of unspun fibers.

In order to analyze the dispersion properties of the fiber, the equivalent birefringence vector must be characterized also with respect to the frequency domain, in this sense it is common to assume [Pal06]

$$\frac{\partial\boldsymbol{\beta}(z,\omega)}{\partial\omega} = \frac{\boldsymbol{\beta}(z,\omega)}{\omega}. \tag{5.19}$$

Equation (5.19), in these particular settings, leads to $\partial\boldsymbol{b}/\partial\omega = \boldsymbol{b}/\omega$, that is

$$\boldsymbol{b}(z,\omega) = \frac{\omega}{\omega_0}\boldsymbol{b}(z,\omega_0), \tag{5.20}$$

where ω_0 is an integration constant. Therefore, the autocorrelation function $r(u)$ is proportional to ω^2 and so are μ and γ because of their definitions in (5.17) and (5.18) respectively. Finally, the derivative of the equivalent birefringence vector with respect to ω is given by

$$\frac{\partial \boldsymbol{\beta}_E}{\partial \omega} = \left(\frac{\sqrt{2\,\mu}}{\omega} \xi_1(z), \frac{\sqrt{2\,\mu}}{\omega} \xi_2(z), -2\frac{\gamma}{\omega} \right), \tag{5.21}$$

where it has been exploited the fact that white noise functions $\xi_1(z)$ and $\xi_2(z)$ are frequency independent.

In order to evaluate the dispersion properties of spun fibers, it is necessary to recall the Stokes dynamic equation in (4.74), that in the context of single mode propagation it can be rewritten as

$$\frac{\partial \boldsymbol{\Omega}(z,\omega)}{\partial z} = \frac{\partial \boldsymbol{\beta}_E(z,\omega)}{\partial \omega} + \boldsymbol{\beta}_E(z,\omega) \times \boldsymbol{\Omega}(z,\omega), \tag{5.22}$$

where it has been used the equivalent birefringence vector $\boldsymbol{\beta}_E$. Instead, $\boldsymbol{\Omega}(z,\omega)$ is called PMD vector and is the equivalent of the Stokes vector $\boldsymbol{\tau}$ of Chapter 4. Moreover, as pointed out in the previous chapter, for $N = 2$ the differential group delay $\Delta\tau$ is equal to the root mean square modal dispersion τ, that is given by two times the magnitude of the PMD vector, i.e., $\Delta\tau(z,\omega) = \tau(z,\omega) = 2\,|\boldsymbol{\Omega}(z,\omega)|$. In particular, solving (5.22) by using the Kolmogorov backward equation (KBE) leads to [Pal06]

$$E\big[\Delta\tau^2(z)\big] = \frac{4}{\omega^2}\frac{\mu^2+\gamma^2}{\mu} z - \frac{2\gamma^2}{\omega^2\mu^2}\big(1 - e^{-2\mu z}\big). \tag{5.23}$$

Observing equation (5.23), it is possible to note that the mean square DGD $E[\Delta\tau^2]$ increases linearly with the distance z at a rate proportional to $(\mu^2 + \gamma^2)/\mu$ but for a transient that goes exponentially to zero.

In order to evaluate the efficacy of the spin it is possible to use the spin-induced reduction factor (SIRF) [Pal06], that in this case is defined as the ratio between the root square of the incremental rate of $E[\Delta\tau^2]$ and the one that the same fiber would have if it were not spun, namely

$$\text{SIRF} = \sqrt{\frac{\mu^2+\gamma^2}{\mu_0\mu}}, \tag{5.24}$$

where μ_0 refers to the not spun fiber, and it has been set $\gamma_0 = 0$ since there is not circular birefringence in normal fibers. From this definition, it is evident that there would be an improvement by spinning the fiber in term of modal dispersion only if the SIRF is lower than 1. Actually, this condition depends on μ and γ, and therefore also on the spinning profile $A(z)$.

In particular, in the case of $\gamma = 0$, it is possible to note from equation (5.24) that there is surely an improvement by spinning the fiber. Indeed in this case, the SIRF would read $(\mu/\mu_0)^{1/2}$, that is always lower than one since, as noted before, μ is always lower than μ_0. In the remarkably case of periodic spin profile, i.e., $A(z) = A(z+P)$, nice conditions can be found in order to have $\gamma = 0$. Specifically, this occurs when [Pal06] $A(z) = -A(z+P/2)$ or $A(z+q) = A(-z+q)$ for some q.

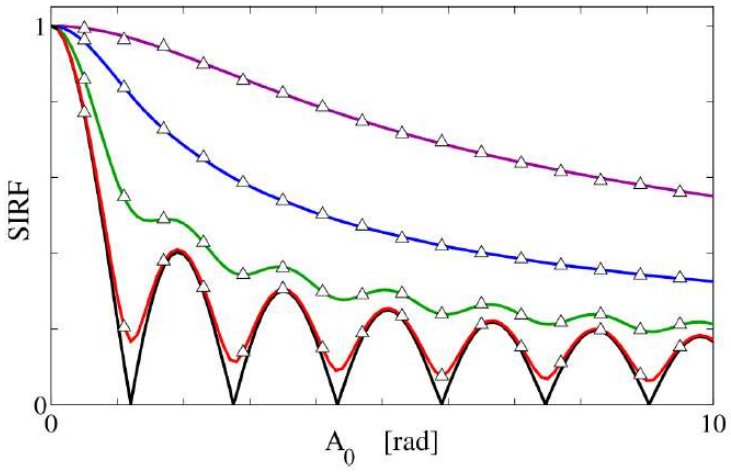

Figure 5.2: SIRF vs spin amplitude A_0 for sinusoidal spin profiles with different spin rates [Pal15a].

Moreover, it should be remembered that the spinning process may actually increase the differential group delay of a single mode fiber rather than decreasing it. However, this occurs only under very specific conditions, namely when the spin profile is asymmetric, close to resonance and the autocorrelation function $r_\beta(u)$ is smooth [GPS08].

Finally, in Figure 5.2 [Pal15a] the SIRF has been represented as a function of the spin amplitude A_0 for a sinusoidal spin profile with different correlation lengths L_F. In this particular case, spinning the fiber induces a decreasing of the differential group delay that improves with the decreasing of L_F. Indeed, it is a reasonable outcome since a too fast random evolution of the birefringence vector would make the spin inefficient. Moreover, it can be observed a peculiar feature of sinusoidal spin profiles, that is optimal values of spin amplitude exist in order to reach minima in term of SIRF.

5.2 Differential Group Delay in Few-Mode Spun Fibers

Motivated by the reduction of the PMD for single mode spun fibers, it sounds reasonable to have a decrease of the DGD also in the multimode propagation. However, at time being a theory describing the properties of multimode spun fibers is missing [PG16]. Indeed, the analytical solution is not trivial since the problem is much more involved than the PMD case. Therefore, in order to evaluate a possible benefit in the spinning process, numerical simulations have been carried out considering the case of few-mode fibers.

To understand the numerical results it is important to describe the mathematical model used to simulate the propagation in such fibers. Specifically,

the dispersion properties have been evaluated with the sinusoidal spin profile in equation (5.2), for different spin amplitudes A_0 and different values of the modal birefringence $\Delta\beta$. Moreover, it has been considered a fix coupling strength $\Delta\kappa$ along the fiber with random orientation of the perturbations. In order to use consistent values for the matrix of the propagation constants $\boldsymbol{D}$ and the coupling one $\boldsymbol{K}$, they have been calculated with respect to a reference fiber of length $L = 1\,\mathrm{km}$, and then scaled according to the proper values of $\Delta\beta$ and $\Delta\kappa$. In particular, the considered few-mode fiber has a step index profile with core and cladding refractive indices equal to $n_{\mathrm{co}} = 1.4660$ and $n_{\mathrm{cl}} = 1.4585$ respectively and radius $a = 8\mu\mathrm{m}$. As depicted in Figure 2.1, at a working wavelength of 1550nm it supports the propagation of the first 4 LP groups. Namely they are $\mathrm{LP}_{0,1}$, $\mathrm{LP}_{1,1}$, $\mathrm{LP}_{2,1}$ and $\mathrm{LP}_{0,2}$, for a total of 12 spatial-polarization modes. Moreover, it has been used a step index profile rather than other fancy ones because this kind of fibers are deeply described in literature.

The analysis has been carried out using hybrid modes rather than the LP ones. The reason, as mentioned before in Section 2.2, is that the intra-modal birefringence in LP groups is not negligible with respect to the order of magnitude of the birefringence induced by perturbations. However, this is not a big deal since LP modes can be written as a linear combination of the hybrid ones, under the weak guide approximation. In particular, we recall that the transformation matrices are given in (2.40), (2.41) and (2.42).

In this sense, the parameter that defines the overall modal birefringence among the propagating modes is $\Delta\beta$, which meaning has been clarified in Section 4.2. In the numerical analysis, the value of $\Delta\beta$ has spanned from $0\,\mathrm{rad/m}$ to about $21\,\mathrm{rad/m}$ according to a non linear scale of variation, that corresponds to a minimum modal beat length of $L_M = 30\,\mathrm{cm}$. It behooves to remind that these values are not appropriate for a step index fiber, where typical modal birefringence spans to higher values. Nevertheless, the case in which $\Delta\beta = 0$ is only an ideal case, where all the propagation constants are equal. However, fibers with particular index profiles as the graded index ones can guarantee to reach modal birefringence values of the same order of the considered ones. A further practical reason to consider this limited range of values is to reduce the burden of simulations. In fact, according to the wave-plate model, the length of a plate should be much smaller than L_M but a too small value would have lead to too complex simulations.

Regarding the coupling occurring along the fiber, only the intrinsic one has been considered, since it is more likely to be affected by the spin. In particular, as seen in Section 3.2, intrinsic coupling involves two types of perturbation, the stress birefringence and the core ellipticity. Moreover, we recall that the stress birefringence is induced by the deformation of the core and the effect of thermal expansion. Therefore its presence is constrained to the core ellipticity one. Despite this, the numerical analysis has been carried out considering five different levels of perturbation that are convex combinations of the two ones, spanning from the case of only stress birefringence to the one with only core ellipticity. Indeed, assuming the two perturbations aligned, the overall coupling rate matrix will be the sum of the two ones, according to the perturbations superposition of Section 3.2.7.

The two coupling rate matrices have been computed using the LP modes, where their values are given in (3.55) and (3.59), for stress birefringence and core ellipticity respectively. Again, considering the LP modes is not an imped-

iment as they can be readily converted in terms of the hybrid ones. Moreover, according to the *fixed modulus model* [WM96] the coupling strength $\Delta\kappa$ is assumed constant along the fiber and the two coupling matrices are scaled with respect to $\Delta\kappa$ and the considered convex combination of the two perturbations. For the numerical simulations a fixed value of coupling strength has been used, i.e., $\Delta\kappa = 0.5$. The value corresponds to a coupling beat length of $L_C = 12.5\,\mathrm{m}$ and it is coherent with the typical measured values of single mode fibers.

Owing to the previous considerations, the perturbation matrix doesn't change along z but for a random orientation. In this sense, the angle of the orientation θ is assumed to be a Wiener process [WM96]. In particular, it is defined such that

$$\frac{\mathrm{d}\theta}{\mathrm{d}z} = -\sigma\eta(z), \tag{5.25}$$

where $\eta(z)$ is a white noise of unitary power and σ influences the correlation of the orientation along the fiber. In particular, a correlation length L_F can be defined as $L_F = 1/\sigma$. For what concern the numerical analysis, the correlation length has been fixed to $L_F = 10\,\mathrm{m}$ according to the experimental results in [Gal+01]. Moreover, the orientation of the perturbation is achieved, as discussed in Section 3.2.6, by applying the rotation matrix $\boldsymbol{R}(\theta(z))$ to $\boldsymbol{K}_\mathrm{b} + \boldsymbol{K}_\mathrm{c}$, where the last quantity is the coupling matrix of the two perturbations superposed and aligned to the reference frame. Then, the randomly oriented coupling matrix $\boldsymbol{K}_\mathrm{u}(z)$, of the unspun fiber, would read

$$\boldsymbol{K}_\mathrm{u}(z) = \boldsymbol{R}^T(\theta(z))\,(\boldsymbol{K}_b + \boldsymbol{K}_c)\,\boldsymbol{R}(\theta(z)). \tag{5.26}$$

Up to this point, the expression in (5.26) accounts only for the intrinsic perturbations and doesn't include the effect of the spinning process. In this sense, as seen at the beginning of this chapter, the spin induces only a rotation of the reference frame, by an angle equivalent to the spin profile. Specifically, exploiting relation (5.3) in (5.26) leads to the coupling matrix of the spun fiber as

$$\begin{aligned}\boldsymbol{K}(z) &= \boldsymbol{R}^T(A(z))\boldsymbol{K}_\mathrm{u}(z)\boldsymbol{R}(A(z)) \\ &= \boldsymbol{R}^T((\theta + A)(z))\,(\boldsymbol{K}_b + \boldsymbol{K}_c)\,\boldsymbol{R}((\theta + A)(z)),\end{aligned} \tag{5.27}$$

where the sinusoidal spin profile $A(z) = A_0 \sin(2\pi z/P)$ has been chosen such that $P = 4\,\mathrm{m}$ and the spin amplitude A_0 spans from $0\,\mathrm{rad}$ to $6\,\mathrm{rad}$. Thus, the maximum spin rate reached in the simulation was about $9.5\,\mathrm{rad/m}$.

Finally, the coupling rate matrix with respect to the hybrid modes has been obtained through the transformation matrix $\boldsymbol{T}$. That is a block diagonal matrix, where at each block corresponds a transformation matrix for a specific LP group. Thus, the coupling rate matrix $\boldsymbol{K}'(z)$, with respect to hybrid modes, can be written as

$$\boldsymbol{K}'(z) = \boldsymbol{T}^T\boldsymbol{K}(z)\boldsymbol{T}, \tag{5.28}$$

Then matrix $\boldsymbol{B}(z)$, that appears in the dynamic equation (4.39), is given by

$$\boldsymbol{B}(z) = \boldsymbol{D} + \boldsymbol{K}'(z). \tag{5.29}$$

Concerning the propagation along the fiber, it has been simulated through the transmission matrix $\boldsymbol{U}$ defined in (4.4). In particular, using the wave-plate

model [GK00], matrix $\boldsymbol{U}$ is calculated as a concatenation of plates $\boldsymbol{W}_i$, that represent sections of fiber of length L_s, where each section is assumed to have constant properties. Therefore, in order for the simulation to be reliable, the section length must be such that

$$L_\mathrm{s} \ll \min\left\{L_M,\, L_C,\, L_F,\, \left(\frac{2\pi\ \max A_0}{P}\right)^{-1}\right\}, \tag{5.30}$$

where among the four terms, the most critical is the last one, that has a value close to 10 cm. Therefore, for the wave-plate model it has been chosen $L_\mathrm{s} = 1\,\mathrm{cm}$, leading to a total number of plates of $M = L/L_\mathrm{s} = 1 \cdot 10^5$.

Then, the transmission matrix $\boldsymbol{U}_m$, that corresponds to the position mL_s along the fiber, is calculated recursively by exploiting the concatenation rule, already seen in Section 4.2. In particular, it yields $\boldsymbol{U}_m = \boldsymbol{W}_m$ where

$$\boldsymbol{W}_m = e^{-j\boldsymbol{B}_m L_\mathrm{s}}\, \boldsymbol{W}_{m-1}, \tag{5.31}$$

and $\boldsymbol{W}_0 = \boldsymbol{I}$.

In order to characterize the fiber from a modal dispersion point of view, it is necessary to evaluate the matrix $\boldsymbol{Q}_m$ for each wave-plate. This is a straightforward operation by exploiting the dynamic equation in (4.39). However, it is remarkable to note that the update of matrix $\boldsymbol{Q}_{m+1}$ from $\boldsymbol{Q}_m$ requires to know $\partial\boldsymbol{B}_m/\partial\omega$. For simplicity, it has been assumed $\partial\boldsymbol{B}_m/\partial\omega = \boldsymbol{B}_m/\omega$ as it is customary in single mode propagation. For this choice to be consistent, it is necessary that this relation holds for both the two coupling rate matrices $\boldsymbol{K}_\mathrm{b}$ and $\boldsymbol{K}_\mathrm{c}$. However, if this approximation is good for the stress birefringence, it is not very accurate for the core ellipticity case [PG16].

Finally, matrix $\boldsymbol{U}$ is calculated at two sufficiently close frequencies ω and $\omega + \delta\omega$, in such a way the mode delays, up to the plate m, can be approximated as

$$\tau_{i,m} = \underline{/\mathrm{eig}}\big(\boldsymbol{U}_m^H(\omega+\delta\omega)\boldsymbol{U}_m(\omega)\big)\Big/\delta\omega. \tag{5.32}$$

Where, the proof of (5.32) is trivial by recalling relations (4.16) and (4.22), and observing that the transformation $\boldsymbol{U}_m^H\, e^{j\boldsymbol{Q}_m\delta\omega}\boldsymbol{U}_m$ doesn't change the eigenvalues of $e^{j\boldsymbol{Q}_m\delta\omega}$.

Before diving in the analysis of the numerical results, a particular case can be solved analytically, and it is the case in which the only acting perturbation is stress birefringence. In particular, owing to the diagonal form of the coupling rate matrix in (3.55), this perturbation causes only the detuning of the x- and y-polarization within each LP groups. Thus, there is not coupling among different groups, and the spin is highly inefficient to mitigate the modal dispersion. This is because it could enhance only the polarization detuning, keeping unchanged the relations among the propagation constants of different LP groups. However, this is not a meaningful case since, as noted before, stress birefringence occurs only jointly with core ellipticity.

5.3 Statistical Analysis of the Numerical Results

The numerical results obtained using the above parameters are presented in this section, where they refer to a statistical ensemble of 600 realizations. In

particular, it has been deeply analyzed the behavior of spun fibers DGD with respect to the aforementioned parameters. Then, it has been correlated to the root-mean square modal dispersion, to understand if it may have sense to try to solve the problem using an analytical approach. Finally, further observations on the evolution of the group delays are presented.

5.3.1 Differential Group Delay Analysis

The most immediate way to check the effectiveness of the spinning process is by analyzing the SIRF factor. Owing to its definition in (5.4), it gives an idea in term of mean about the DGD reduction of the spun fiber with respect to the non-spun one. In particular, it has been chosen to graphically represent its magnitude by distinguishing four types of color: green, yellow, red and white. Specifically, the green one underlines regions in which the spinning process is highly efficient in mitigating the modal dispersion. The yellow one indicates areas where the spin is still effective and results in approximately halving the mean DGD. However, there could be also situations in which spinning the fiber is ineffective on average. This happens where the SIRF is equal to one and it has been graphically represented using the white color. Instead, whenever the spin causes a degradation of the dispersion properties, it has been used the red color.

Moreover, to further characterize the statistical properties of dispersion in spun fibers, it is important to describe the DGD statistics in term of the second central moment. In this sense, a similar definition of the SIRF can be used. Indeed, the *standard deviation ratio* (SDR) is defined as

$$\mathrm{SDR} = \sqrt{\frac{\mathrm{var}(\Delta\tau_{\mathrm{s}})}{\mathrm{var}(\Delta\tau_{\mathrm{u}})}}, \tag{5.33}$$

that is the DGD standard deviation of the spun fiber over the non-spun fiber one. Then, the SDR describes how much the behavior of the dispersion properties of spun fibers vary, with respect to the mean variation of the non-spun case. Owing to the similar definition, the SDR magnitude has been represented using the same colors of the SIRF. In particular, green means that the behavior of the spun fiber DGD is much more deterministic of the non-spun one. The yellow one represents cases in which the spinning process has decreased the variation of the statistics. While, white and red regions highlight situations in which the standard deviation has remained comparable or has increased respectively.

In order to check, whether the spinning process is efficient in the case of only stress birefringence, the SIRF and SDR can be used. In particular, as mentioned before, we expect that spin is completely inefficient to mitigate the modal dispersion of the fiber. In particular, the behaviors of the SIRF and the SDR, as a function of the modal birefringence and the spin amplitude, are represented in Figure 5.3(a) and Figure 5.3(b) respectively. As forecast, the SIRF is equal to 1 for almost all the combined values of spin amplitude and modal birefringence but, for the cases in which the latter is very small. Indeed, these values correspond to the ideal case, in which all the propagating modes are degenerate but for the detuning of the polarizations caused by the perturbation, and recovered by the spinning process. Finally, considering the SDR, it can be

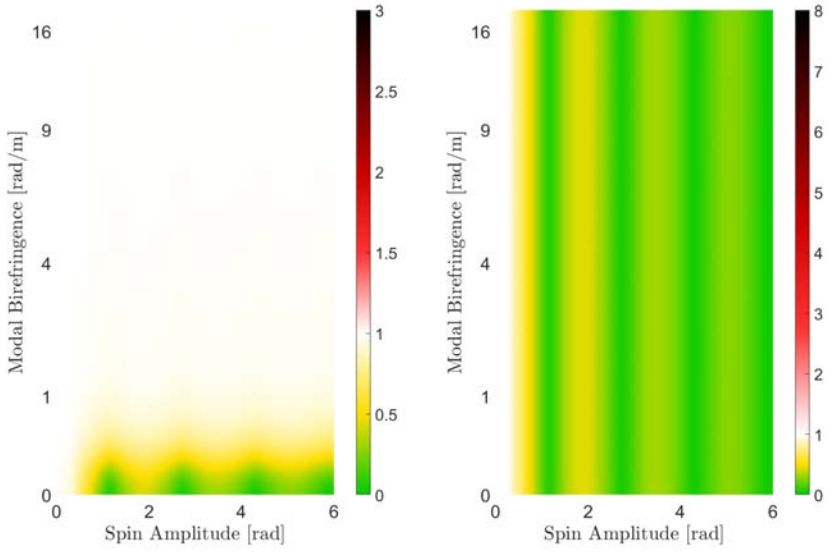

(a) *SIRF*. (b) *SDR*.

Figure 5.3: SIRF and SDR at the end of the fiber, as a function of the modal birefringence and the spin amplitude, in case of only stress birefringence.

observed that, even when the spin is almost ineffective, it makes the statistics of the DGD more deterministic with respect to the non-spun fiber case.

However, the scenario in which stress birefringence is the only perturbation acting along the fiber is not realistic. Indeed, in the most likely case, stress birefringence and core ellipticity are present in similar quantities. This situation is depicted in Figure 5.4, where the SIRF has been represented at a distance of 20 m, 100 m, 500 m and 1000 m. In particular, it can be observed that the effect of the spinning process becomes noticeable after 500 m, where the SIRF values start to stabilize. Yet, the positive effect of spinning the fiber appears much less evident than the single-mode case. Indeed, in most of the cases the SIRF is equal to one (white regions) underlining that spin is non effective in reducing the mean DGD.

As for the only stress birefringence case, the region in which spin is highly effective is the one with low modal birefringence, that corresponds to the ideal case in which all modes are degenerate. However, in this case the core ellipticity induces coupling among different LP groups, as suggested in Figure 3.2. This fact leads to different situations with respect to the previous case. First of all, Figure 5.4(d) presents a clear red zone in which the SIRF is beyond one. In this case, the spin process is not only ineffective but makes the DGD even worst than the non-spun case. It is happening that the spinning process instead of increasing the coupling is actually countering it, then the fiber has dispersion properties similar to the unperturbed one and the mean DGD increases linearly with the distance. It is remarkable to note that this situation is likely to be a resonance effect that occurs only for specific values of the modal birefringence.

That is when the modal beat length is comparable with the coupling one, i.e., $L_M \simeq L_C$. Except for this pathological case, the SIRF exhibits local minima, represented by yellow regions, in correspondence to specific combinations of spin amplitude and modal birefringence. Moreover, observing the figure, we note that as general rule, the spin amplitude required to positively affect the DGD increases with the modal birefringence.

The SDR, for the case of equal intensity of stress birefringence and core ellipticity, is represented in Figure 5.5, at the very same distances used for evaluating the SIRF. In particular, at the beginning of the fiber, the DGD of the spun one has an overall lower variance than the non-spun case, for almost all the spin amplitudes and modal birefringence values. This observation suggests a more deterministic behavior of the statistical properties of the DGD. However, as the propagation continues along the fiber, the SDR increases in correspondence to the yellow SIRF regions of Figure 5.4, until it goes well beyond one on the red and black zones. This means that, whenever the spin effect corresponds to a decreasing of the mean DGD, the latter acquires an higher variability among different realizations of the process. Moreover, an interesting observation is that, even if we are in a case in which spin is ineffective (SIRF $\simeq 1$), the DGD statistics show a lower variability for sufficiently high spin amplitudes. Then, it may be worth to implement a spinning process also in these cases, since the dispersion properties of the spun fiber would be more deterministic. Finally, it behooves to observe that between Figure 5.5(c) and Figure 5.5(d) an asymptotically behavior of the SDR has not been reached yet. Therefore, it should be necessary to analyze longer fibers in order to have a more complete picture.

In order to analyze more deeply the statistical properties of the DGD, it has been considered the estimates of the probability density function (PDF) by using both the histogram method and the built-in MATLAB function *ksdensity*. In particular, this has been done at the end of the fiber, for four noticeable points of spin amplitude and modal birefringence. The first one corresponds to a case in which the spin is highly efficient in mitigating the DGD (SIRF $\ll 1$), one to a case in which the spin increases the DGD (SIRF > 1), another one to the case in which the spin is ineffective (SIRF $\simeq 1$), and the last to a situation in which the mean DGD is almost halved by the spinning process (SIRF $\simeq 0.5$). Note that, in all the figures, the PDF estimate for the DGD of the spun fiber has been represented in light green, while the one for the non-spun case in light red.

- The PDFs of the case in which the SIRF $\ll 1$ are represented in Figure 5.6(a). In particular, it has been chosen the point corresponding to a spin amplitude of 1.2 rad and a modal birefringence of 0.003 rad/m. As it can be seen, the behaviors of the two PDF estimates are consistent with the above observations on SIRF and SDR (Figure 5.4 and Figure 5.5). Specifically, the DGD of the spun fiber presents lower and more deterministic values, while in the DGD of the non-spun fiber they are higher and more variant. However, it must be noted that in terms of absolute values both the mean DGD and the standard deviation of the two distributions are very small. Nevertheless, the considered range of modal birefringence is almost ideal and it doesn't represent a real case.

- The PDFs of the case in which the SIRF > 1 are represented in Figure 5.6(b). In particular, it has been chosen the point corresponding to a

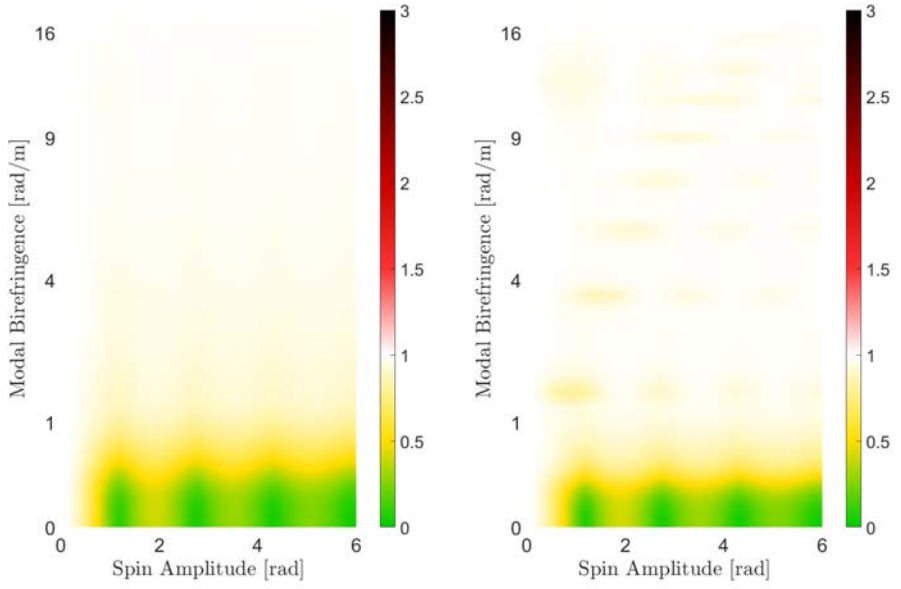

(a) 20 m. (b) 100 m.

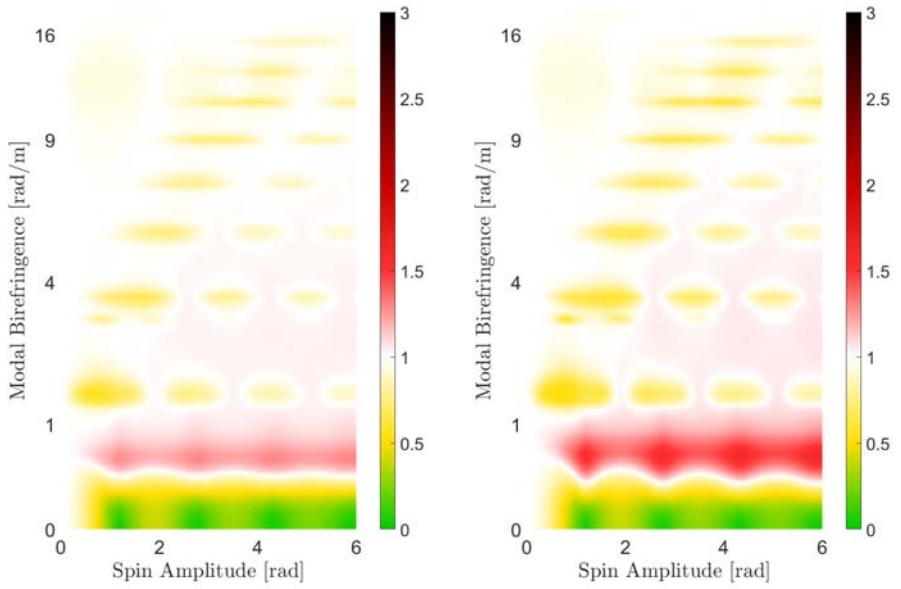

(c) 500 m. (d) 1000 m.

Figure 5.4: SIRF as a function of the modal birefringence and the spin amplitude, in case of equal intensity of stress birefringence and core ellipticity.

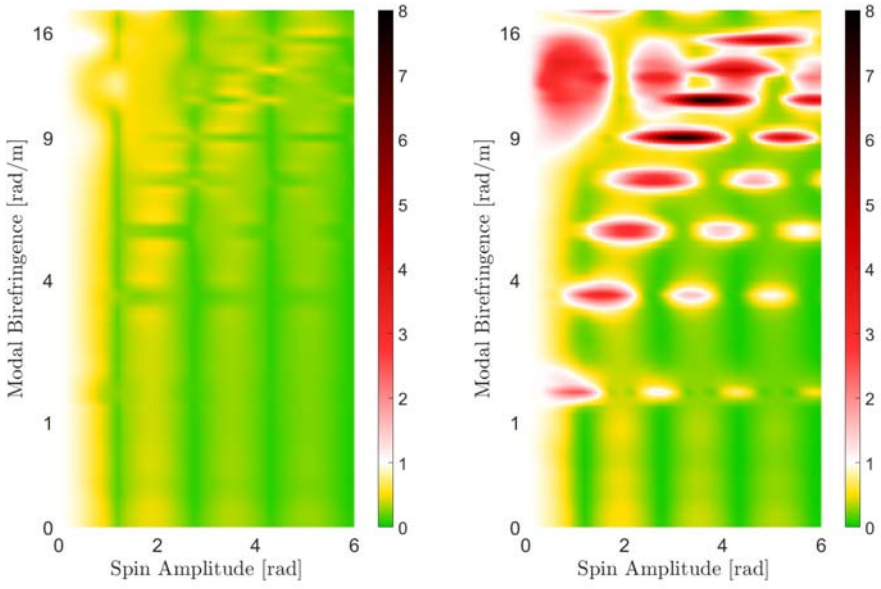

(a) 20 m.

(b) 100 m.

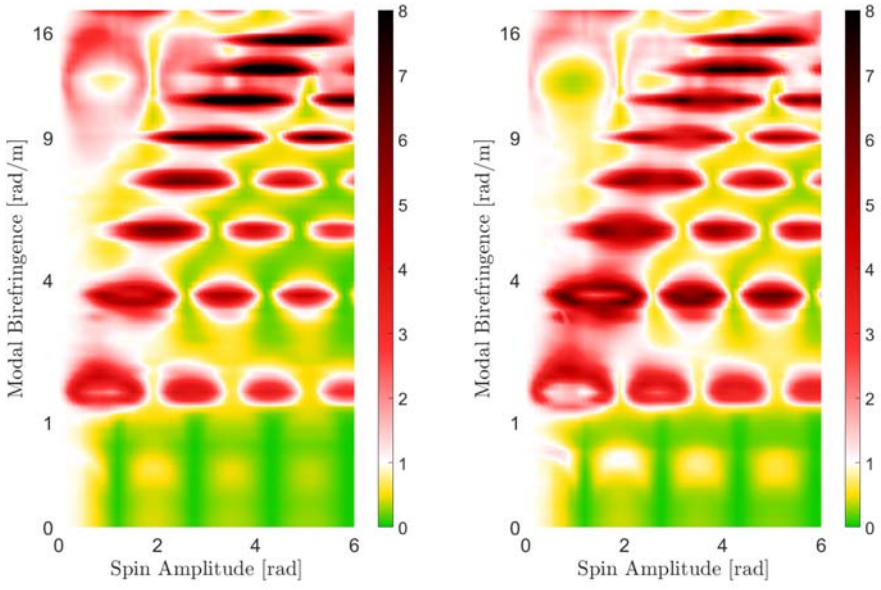

(c) 500 m.

(d) 1000 m.

Figure 5.5: SDR as a function of the modal birefringence and the spin amplitude, in case of equal intensity of stress birefringence and core ellipticity.

spin amplitude of 2.8 rad and a modal birefringence of 0.3 rad/m. In this case the situation is different from the previous one. Indeed, the spun fiber DGD distribution assumes higher values than the non-spun one. However, also in this case, the standard deviation of the spun fiber DGD is lower than the one in the correspondent non-spun case. These two distributions agree with the above ones on the SIRF and the SDR. Also in this case, the considered value of modal birefringence is forbidding, then this probably doesn't represent a case of practical interest.

- Instead, a case of practical interest, it is represented by the situation in which the SIRF $\simeq 1$. The PDFs in this case are represented in Figure 5.7(a), where it has been chosen the point corresponding to a spin amplitude of 5 rad and a modal birefringence of 6 rad/m. In particular, the support of the two PDFs are much closer than the previous cases, this situation highlights the fact that the SIRF is close to one. However, as mentioned before, a source of interest in spinning the fiber may descend from the fact that the spun fiber DGD presents a behavior more deterministic, with respect to the non-spun DGD distribution, as represented also by the SDR in Figure (5.5).

- Finally, maybe the most interesting case, it is when the spin induces a decrement in the DGD for practical modal birefringence values. They are represented by yellow regions in Figure 5.4, where the SIRF is close to 0.5. In particular, the DGD distribution reported in Figure 5.7(b) refers to a point corresponding to a spin amplitude of 4 rad and a modal birefringence of 11 rad/m. Observing the figure, it can be noted that the support of the spun fiber DGD distribution assumes lower values than the other one. Moreover, as observed in the SDR analysis, the spinning process increases the standard deviation of the DGD. However, in this case, this is not a big deal, since the support of the non-spun fiber PDF remains well beyond the one of the spun case.

It is known that for unspun fibers the distribution of the DGD is Maxwellian, and therefore it is characterized by a constant ratio between standard deviation and mean. Moreover, it has been shown that also for single-mode spun fiber the underling distribution is Maxwellian [LCN]. In this sense, it is interesting to check whether this happens also in the multimode case. In Figure 5.8(a) it is represented the ratio between the standard deviation and the mean of the DGD in the spun fiber, as a function of spin amplitude and modal birefringence. In particular, neglecting the region where the birefringence is low, the considered ratio assumes a tight range of values, but for the case in which the SIRF is lower than one and therefore the spin is effective in decreasing the mean DGD. Assuming that the statistics of the DGD, in the case of spun fiber, can be described by using only one parameter, this means that the type of distribution is changing at the varying of spin amplitude and modal birefringence. This observation can be seen also with respect to the underling distribution of the unspun fiber DGD. In particular, normalizing the ratio between the standard deviation and the mean DGD of the spun fiber, with respect to the one of the unspun case, the difference in term of underling distribution is highlighted in Figure 5.8(b). From this figure, it can be observed how the spinning process changes completely the underling statistics of the DGD, this is even more evident where

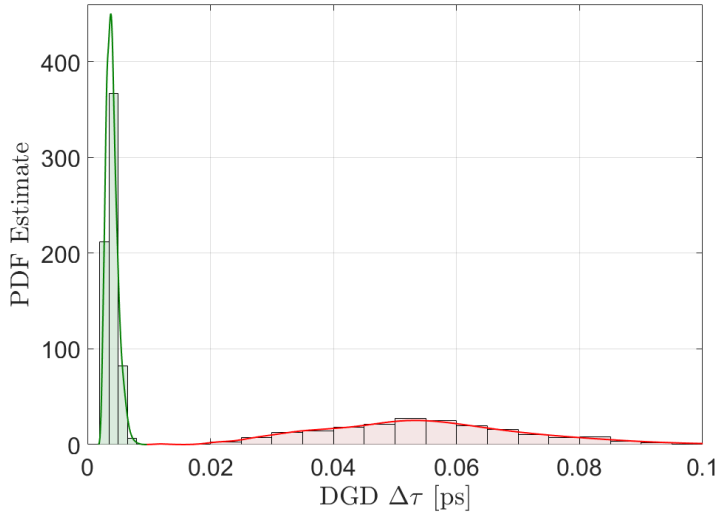

(a) Spin Amp. 1.2 rad, Modal Bire. 0.003 rad/m.

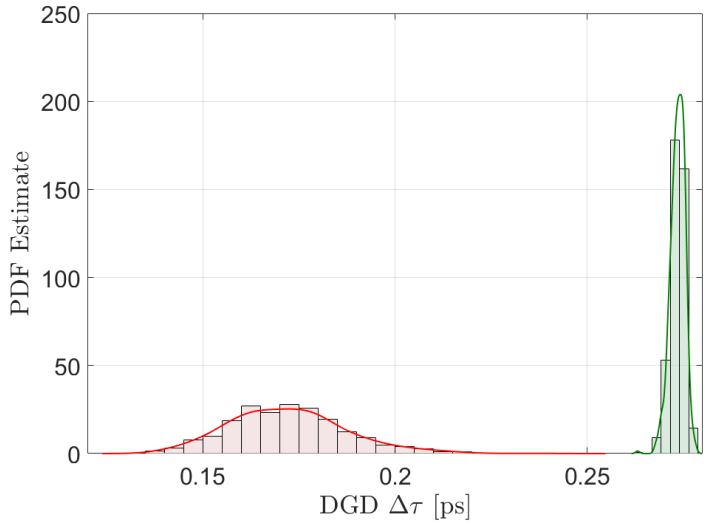

(b) Spin Amp. 2.8 rad, Modal Bire. 0.3 rad/m.

Figure 5.6: PDF estimates of the DGD for the spun (light green) and the non-spun (light red) fiber, computed using histograms and the ksdensity function (solid lines) at the end of the fiber.

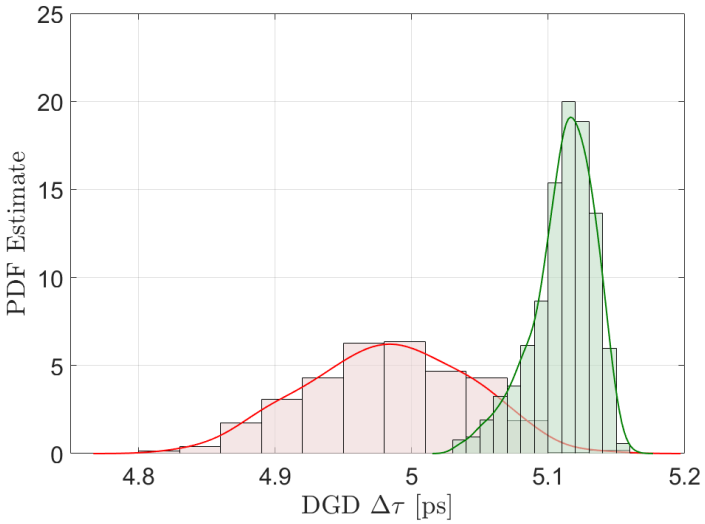

(a) Spin Amp. 5 rad, Modal Bire. 6 rad/m.

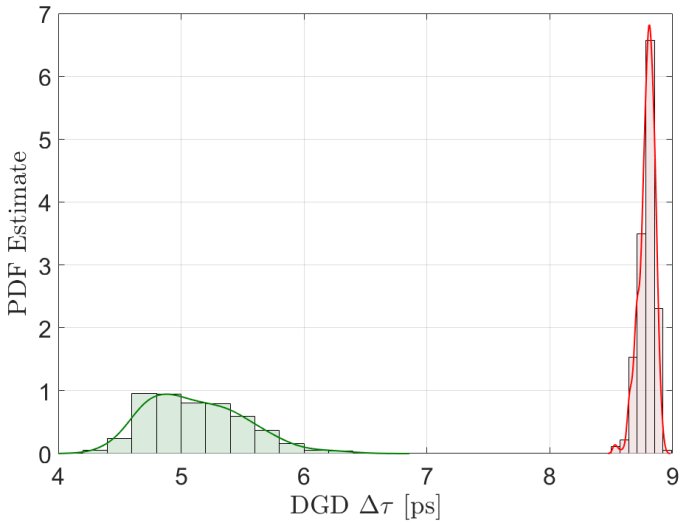

(b) Spin Amp. 4 rad, Modal Bire. 11 rad/m.

Figure 5.7: PDF estimates of the DGD for the spun (light green) and the non-spun (light red) fiber, computed using histograms and the ksdensity function (solid lines) at the end of the fiber.

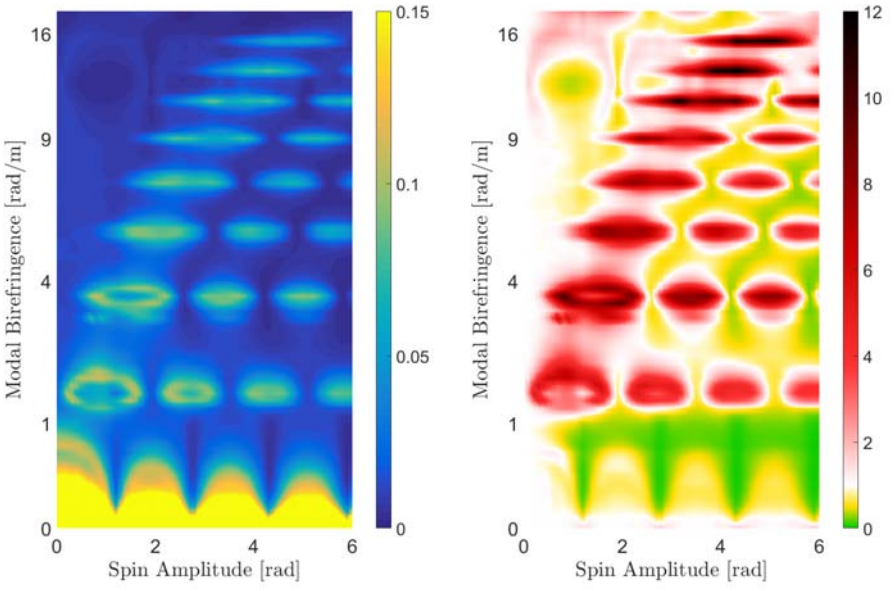

(a) (b)

Figure 5.8: (a): Ratio between the standard deviation and the mean DGD for the spun case. (b): Ratio between the standard deviation and the mean DGD for the spun case normalized with respect to the unspun one.

the spin decreases the dispersion (SIRF < 1). Indeed, if the two distributions were the same, the normalized ratio should be equal to one (white regions in the figure) but this happens only for low values of the spin amplitude.

Recalling the single-mode spun fiber case of Section 5.1 and in particular the Figure 5.2, it is possible to observe that, under a sinusoidal spin profile, the SIRF presents local minima in correspondence to specific values of spin amplitude. In particular, this situation holds also for the multimode case, but for the peculiarity that these minima are wider in term of spin amplitude, with respect to the single mode case. This can be clearly seen in Figure 5.9, where the SIRF at the end of the fiber has been represented as function of the spin amplitude, with respect to different values of modal birefringence. This characteristic would let the correct tuning of the spinning amplitude much more easy to set, from a practical point of view, in order to achieve the best dispersion properties in term of DGD.

Finally, considering the case in which the only perturbation acting is core ellipticity, the SIRF and SDR are graphically represented in Figure 5.10 and Figure 5.11 respectively. In comparison with the SIRF and the SDR of the previous case, the figures highlight an overall emphasis of the spin effect. This is reasonable, since the strength $\Delta\kappa$ is the same for the two cases, but only core ellipticity induces coupling among different LP groups. Then, the fact that there is only core ellipticity makes the LP groups more coupled in this latter case, and the spin unfolds this feature.

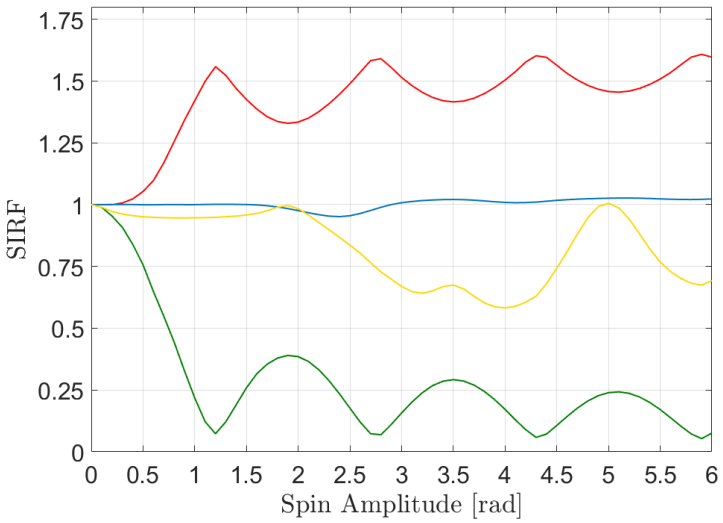

Figure 5.9: SIRF as a function of the spin amplitude for different values of modal birefringence: 0.003 rad/m (green line), 0.3 rad/m (red line), 6 rad/m (blue line) and 11 rad/m (yellow line).

5.3.2 Comparison between the Differential Group Delay and the Root Mean Square Modal Dispersion

In this section, the results obtained for the case of the DGD $\Delta\tau$ are compared to the corresponding ones of the root mean square modal dispersion (rms-MD) τ, which definition is given in (4.25). In particular, the comparison is important in prospecting an analytical analysis of the problem, where the use of the mean square modal dispersion seems much more easy to deal with.

In this sense, similar quantities to the SIRF and the SDR can be defined with respect to the root mean square modal dispersion, namely $\mathrm{SIRF}_{\mathrm{rms}}$ and $\mathrm{SDR}_{\mathrm{rms}}$. In particular, their values at the end of the fiber are graphically represented in Figure 5.12(a) and Figure 5.12(b), where stress birefringence and core ellipticity have been considered with the same intensity.

The comparison between Figure 5.4(d) and Figure 5.12(a), and between Figure 5.5(d) and Figure 5.12(b) for the SIRF and the SDR respectively, shows very similar qualitatively behaviors. Then, it would make sense to carry out an analytical study of the spinning process effect with respect to the mean square modal dispersion.

To further confirm this analysis, the ratio between the standard deviation and the mean of the spun fiber rms-MD is represented if Figure 5.13(a). Moreover, the same quantity but normalized over the unspun one has been reported in Figure 5.13(b). Again, a direct comparison between Figure 5.8(a) and Figure 5.13(a) and between Figure 5.8(b) and Figure 5.13(b) shows a very similar qualitatively behaviors.

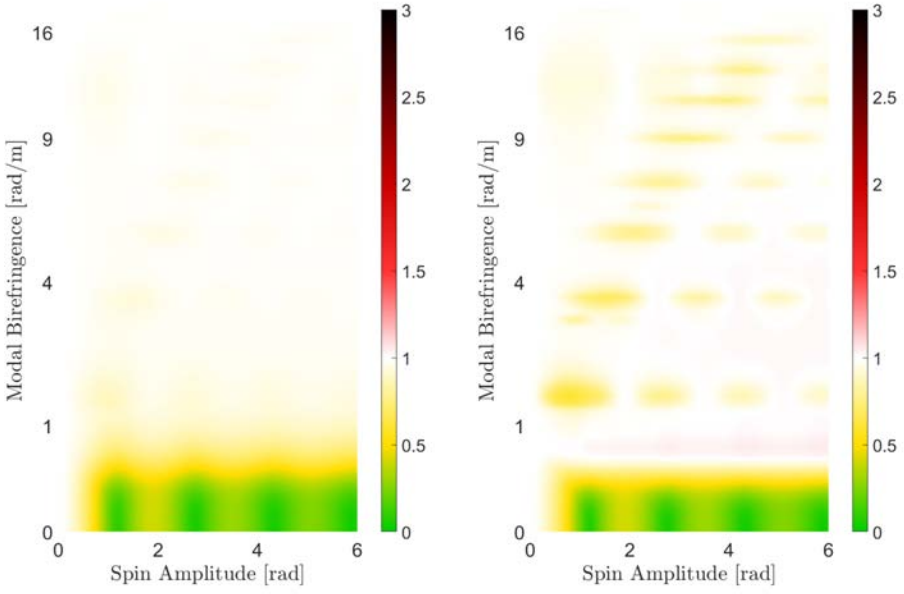

(a) 20 m.

(b) 100 m.

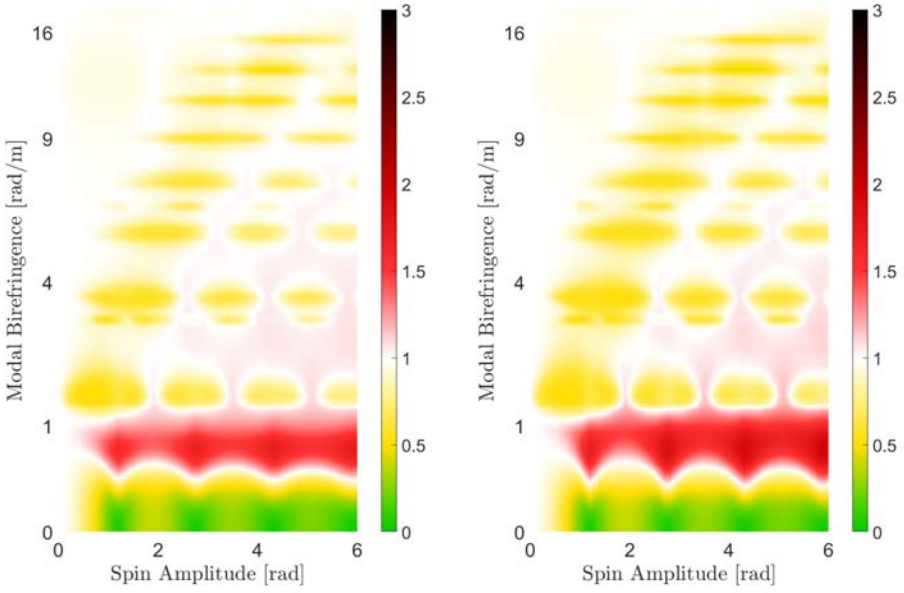

(c) 500 m.

(d) 1000 m.

Figure 5.10: SIRF as a function of the modal birefringence and the spin amplitude, in case of only core ellipticity.

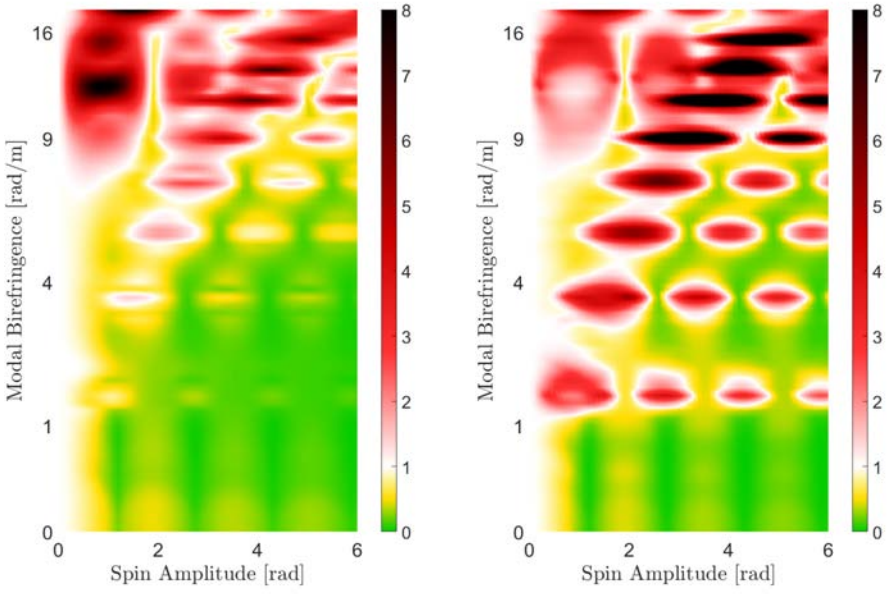

(a) 20 m.

(b) 100 m.

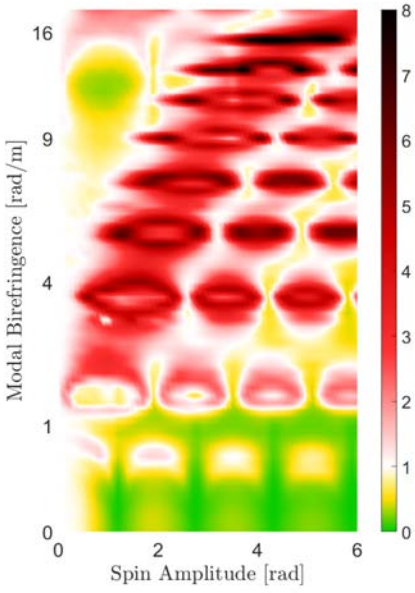

(c) 500 m.

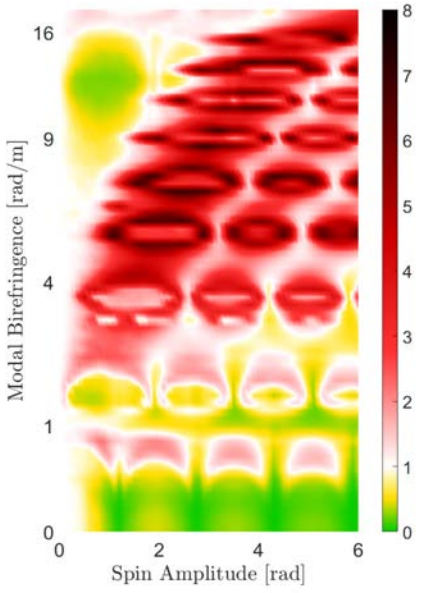

(d) 1000 m.

Figure 5.11: STD as a function of the modal birefringence and the spin amplitude, in case of only core ellipticity.

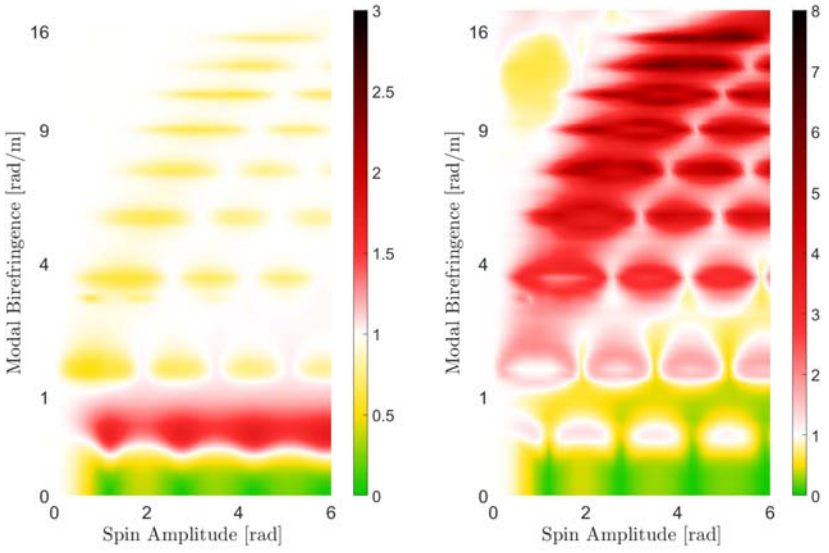

(a) $\mathrm{SIRF}_{\mathrm{rms}}$ (b) $\mathrm{SDR}_{\mathrm{rms}}$

Figure 5.12: $\mathrm{SIRF}_{\mathrm{rms}}$ and $\mathrm{SDR}_{\mathrm{rms}}$ at the end of the fiber, when stress birefringence and core ellipticity are present with the same intensity.

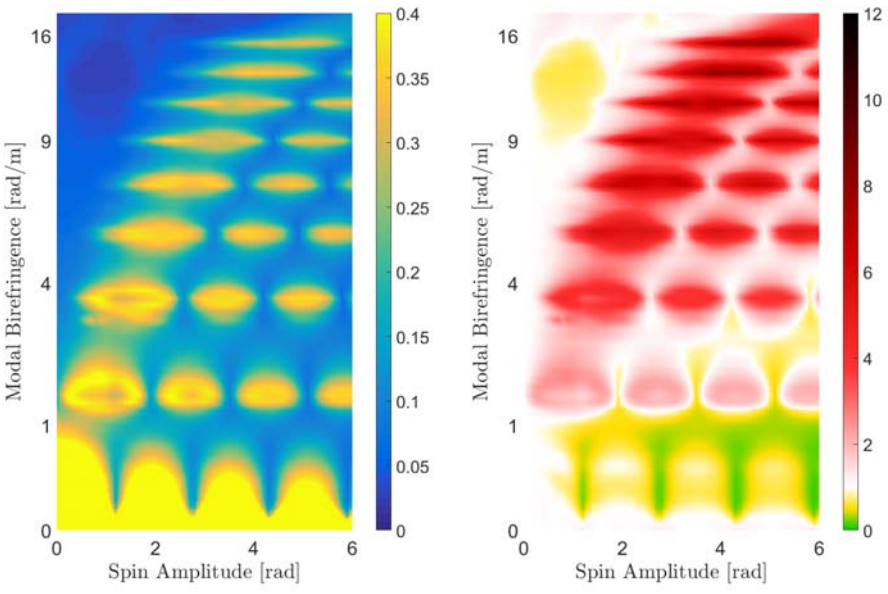

(a) (b)

Figure 5.13: (a): Ratio between the standard deviation and the mean rms-MD for the spun case. (b): Ratio between the standard deviation and the mean rms-MD for the spun case normalized over the unspun one.

5.3.3 Evolution of the Group Delays along the Fiber

Finally, it is interesting to see the comparison between the evolution along the fiber of the mean group delays, in case of spin and without it. In particular, the analysis has been carried out in two specific cases. The first is the one in which the spin is effective in increasing the coupling, resulting in a lower DGD (SIRF < 1) . Instead, the second is exactly the opposite and it concerns the case where the spin counters the effect of the coupling, increasing the DGD (SIRF > 1).

In Figure 5.14(a) the first case is proposed, where the group delays for each principal mode of propagation are represented with black and red lines, for the unspun and spun case respectively. It can be observed, that in the unspun case, the delays are packed in groups that correspond to the LP ones. In particular, from top to bottom they are the $LP_{0,1}$, $LP_{1,1}$, $LP_{2,1}$ and the $LP_{0,2}$. As the principal modes propagate, the group delays linearly widen increasing the overall DGD. However, if the spinning process is applied, the coupling among the LP groups is boosted and the group delays start to interweave one to each other, in according to the coupling mechanisms discussed in Section 3.2. This protracted behavior along the fiber results in a decreasing of the DGD. Moreover, it can be seen that the $LP_{1,1}$ group doesn't couple with the others. In fact, stress birefringence and core ellipticity induce only intra-coupling for this group (Figure 3.1 and Figure 3.2), and the red lines remain superposed to the black ones.

In Figure 5.14(b) is instead represented a case, in which the spin increases the DGD (SIRF > 1). In particular, the figure refers to a modal birefringence of 0.3 rad/m, then the modal beat length and the coupling one are comparable and they leads to a resonance situation. Indeed, the group delays in the unspun case (black lines) are interweaved underlining strong coupling among modes. In these settings, the spin breaks the matching condition between the modal and the coupling beat lengths and it deletes the effect of coupling, bringing back the situation in which the group delays grow linearly with the DGD.

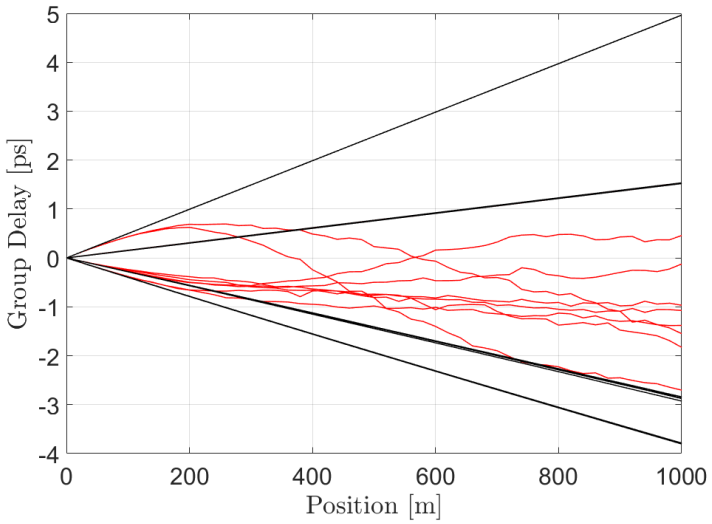

(a) Spin Amp. 4 rad, Modal Bire. 11 rad/m.

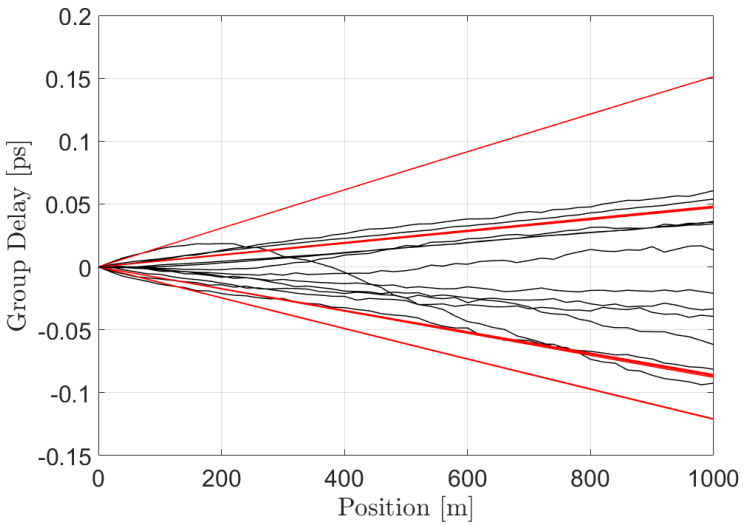

(b) Spin Amp. 2.8 rad, Modal Bire. 0.3 rad/m.

Figure 5.14: Behavior of the group delays for each principal state of propagation along the fiber. Black and red lines refer to the unspun and spun fiber respectively.

Chapter 6

Conclusion

This thesis has shed some light on the modal dispersion properties of multimode spun fiber. In particular, the design of multimode fibers with low differential group delay is required in order to keep a feasible complexity of the MIMO receivers. In this sense, the spinning process may help to mitigate the DGD.

Indeed, this work has focused on a numerical analysis, in order to discover the influence of the spinning process with respect to the modal dispersion. In particular, the numerical simulation has considered a few-mode fiber of 1 km length, working at a wavelength of 1550 nm, and supporting the propagation of the first 4 LP groups, that corresponds to a total of 12 spacial-polarization modes. The overall modal birefringence has been calculated using the hybrid modes and scaled to a range of values from 0 to 21 rad/m, corresponding to a minimum beat length of 0.3 m.

Moreover, only the intrinsic perturbations have been considered, because they are the only ones to be affected by the spin. In particular, the perturbation types were stress birefringence and core ellipticity, which coupling rate matrices were evaluated using the LP modes. Specifically, the numerical analysis has been carried out using a value of coupling strength $\Delta\kappa$ equals to 0.5, corresponding to a coupling beat length of $L_C = 12.5\,\mathrm{m}$, a common value in according to the majority of the experimental measurements. Moreover, the two perturbations have been considered aligned since their presence depends one to the other, and the orientation has been modeled as a Wiener process of correlation length equals to 10 m.

The considered spin has a sinusoidal profile with a spin period of 4 m. In particular, the spin amplitude has been varied from 0 to 6 rad, with a maximum spin rate of about 9.5 rad/m. Moreover, it has been supposed, that the only perturbation effect of the spin is a rigid rotation of the reference frame of the fiber, without any torsion stress.

In these settings, the simulation has been implemented using the wave-plate model approximation, where the length of each plate was of 1 cm, leading to a total number of $1 \cdot 10^5$ plates. Moreover, it has been assumed that $\partial \boldsymbol{B}/\partial\omega = \boldsymbol{B}/\omega$.

The results, based on an ensemble of 600 realizations, have shown that the spin can reduce the DGD of the fiber, for particular values of spin amplitude and modal birefringence. However, first of all it has been analyzed the case in which there are only stress birefringence. As theoretically discussed, in this case the

spinning process is completely ineffective. This is because stress birefringence induces coupling only within each LP group. However, this is not a real case, since stress birefringence is caused by core ellipticity. In this sense, considering the most likely case, in which the two perturbations act with the same intensity, the spin induces interesting effects. In particular, if the modal birefringence is very low, the spin causes a substantial reduction of the DGD. However, in the cases of practical interest the mitigation of the DGD is lower, and yields a SIRF of about 0.5. Moreover, there are regions where the spin is ineffective and others where it makes the DGD increasing. This last case occurs when the modal birefringence is comparable with the coupling strength, creating a resonance situation. The spin effect breaks this matching condition, countering the mode coupling and accentuating the modal dispersion.

In order to deepen the statistics of spun fiber DGD, also the standard deviation has been analyzed. The results highlight that for the practical regions in which the spin induces a reduction of the DGD, the latter presents a much more variant behavior. This means that, the DGD standard deviation of the spun case is greater than the one of the unspun fiber. However, in the cases in which the spin is ineffective, the standard deviation of the spun fiber DGD decreases and the statistics becomes more deterministic.

It has been also evaluated the ratio between the standard deviation and the mean of the DGD, for a spun fiber. The results have shown the the ratio is almost constant, but for the regions in which the spin decreases the DGD. Assuming in first approximation that the entire statistics can be defined by only the mean, then the underling DGD distribution changes depending on the specific values of spin amplitude and modal birefringence. The behavior is different from the unspun case, where the DGD has a Maxwellian distribution and therefore it is defined by only one parameter. To confirm this, the considered ratio has been normalized over the unspun correspondent one. The result show that the spinning process changes completely the underling statistics of the DGD, this is even more evident where the spin decreases the dispersion.

Finally, the statistics of the DGD have been compared with the ones of the square root modal dispersion. The results have shown that they present very similar behaviors. This is important because, from an analytical point of view, the latter parameter is much more simpler to deal with. Hopefully, this result would let the modal dispersion theory for multimode spun fiber easier to solve analytically.

Summing up, the spinning process can be a viable tool to further decrease the differential group delay in multimode fibers, even if its effectivess is lower than the single-mode case. Moreover, the same single-mode fiber spinning technology may be implemented in the multimode case, with the advantage that the SIRF local minima are wider and therefore they may be attainable using a simpler tuning system for the spin amplitudes.

Bibliography

[Mar74] D. Marcuse. "Coupled-Mode Theory for Anisotropic Optical Waveguides". In: *The Bell System Technical Journal* 54.6 (1974).

[PK74] G. C. Papanicolaou and W. Kohler. "Asymptotic theory of mixing stochastic ordinary differential equation". In: *Comm. Pure Appl. Math* 27 (1974), pp. 641–668.

[UR80] R. Ulrich and S. C. Rashleigh. "Bending-induce birefringence in single-mode fiber". In: *OSA Optics Letters* 5.6 (1980).

[WM96] P. Wai and C. Menyuk. "Polarization mode dispersion, decorrelation, and diffusion in optical fibers with randomly varying birefringence". In: *IEEE Journal of Lightwave Technology* 14.2 (1996).

[Cho00] Dipak Chowdhury. "Comparison Between Optical Fiber Birefringence Induced by Stress Anisotropy and Geometric Deformation". In: *IEEE Journal of Selected Topics in Quantum Electronics* 6.2 (2000).

[GK00] J. P. Gordon and H. Kogelnik. "PMD fundamentals: Polarization mode dispersion in optical fibers". In: *PNAS* 97.9 (2000).

[Gal+01] A. Galtarossa et al. "Measurement of birefringence correlation length in long, single-mode fibers". In: *Opt. Lett.* 26.13 (2001).

[MS01] Partha P. Mitra and Jason B. Stark. "Nonlinear limits to the information capacity of optical fibre communications". In: *Letters to nature* 411 (2001).

[FK05] Shanhui Fan and Joseph M. Kahn. "Principal modes in multimode waveguides". In: *OSA Optics Letters* 30.2 (2005).

[GM05] Andrea Galtarossa and Curtis R. Menyuk. *Polarization Mode Dispersion*. Springer, 2005.

[Pal06] Luca Palmieri. "Polarization Properties of Spun Single-Mode Fibers". In: *IEEE Journal of Lightwave Technology* 24.11 (2006).

[GPS08] Andrea Galtarossa, Luca Palmieri, and Luca Schenato. "About the Differential Group Delay of Spun Fibers". In: *IEEE Journal of Lightwave Technology* 26.2 (2008).

[AM12] Cristian Antonelli and Antonio Mecozzi. "Stokes-space analysis of modal dispersion in fibers with multiple mode transmission". In: *OSA Optics Express* 20.11 (2012).

[KW12] H. Kogelnik and P. J. Winzer. "Modal Birefringence in Weakly Guiding Fibers". In: *Journal of Lightwave Technology* 30.14 (2012).

[Win12] Peter J. Winzer. "Optical Networking Beyond WDM". In: *IEEE Photonics Journal* 4.2 (2012).

[Gui+14] Li Guifang et al. "Space-division multiplexing: the next frontier in optical communication". In: *OSA Advances in Optics and Photonics* 6 (2014).

[PG14] L. Palmieri and A. Galtarossa. "Coupling Effects Among Degenerate Modes in Multimode Optical Fibers". In: *IEEE Photonics Journal* 6.6 (2014).

[Pal14] Luca Palmieri. "Coupling mechanism in multimode fibers". In: *Next-Generation Optical Communication: Components, Sub-Systems, and System III* 9009 (2014).

[Pal15a] Luca Palmieri. "Mode Dispersion Properties of Few-Mode Spun Fibers". OFC, Los Angeles, 2015.

[Pal15b] Luca Palmieri. "Optical fiber systems lecture slides". 2015.

[PG16] Luca Palmieri and Andrea Galtarossa. "Intramodal Dispersion Properties of Step-Index Few-Mode Spun Fibers". In: *Journal of Lightwave Technology* 34.2 (2016).

[LCN] Ming-Jun Li, Xin Chen, and Daniel A. Nolan. *Fiber Spinning for Reducing Polarization Mode Dispersion in Single Mode Fibers: Theory and Application*. Tech. rep.

[PG] Luca Palmieri and Andrea Galtarossa. *A Preliminary Analysis of Spin in Few-Mode Optical Fibers*. Tech. rep.